A Parabolic Quadrilateral Finite Element for Compressible and Incompressible Flows

by

Dena Hendriana

Submitted to the Department of Mechanical Engineering
in partial fulfillment of the requirements for the degree of

Doctor of Science in Mechanical Engineering

at the

MASSACHUSETTS INSTITUTE OF TECHNOLOGY

May 1998 [June 1998]

Author . . . .
Department of Mechanical Engineering
May, 1998

Certified by . . . .
Klaus-Jürgen Bathe
Professor
Thesis Supervisor

Accepted by . . . .
Ain Ants Sonin
Chairman, Departmental Committee on Graduate Students

A Parabolic Quadrilateral Finite Element for Compressible and Incompressible Flows

by

Dena Hendriana

Submitted to the Department of Mechanical Engineering
on May, 1998, in partial fulfillment of the
requirements for the degree of
Doctor of Science in Mechanical Engineering

Abstract

A unified finite element solution scheme for incompressible and compressible flows would be most attractive in engineering practice. The objective in this thesis was to work toward this goal.

A 9-node finite element for compressible and incompressible 2-D flow solutions is presented. In the compressible flow formulation, a new high-order derivative artificial diffusion and a new shock capturing term are employed to stabilize the formulation. The new upwinding term is shown numerically to stabilize the formulation and an inf-sup test is performed assuming idealized 1-D conditions. The new shock capturing term performed well in the solutions of various judiciously selected numerical examples. Various flow problems in which the Mach numbers range from about 0.0005 to 6 are considered. The numerical results indicate that the element is applicable to a wide range of analysis problems.

For incompressible flows, the element must satisfy the relevant inf-sup condition, and an element is used with parabolic velocity and linear pressure interpolations (the 9/4c-element). An upwinding term in a similar form as for the compressible flow solution is introduced to stabilize the formulation. A convergence study with the formulation to estimate the order of convergence is performed. In addition, a new low order element is presented.

The new solution schemes for compressible and incompressible flows provide effective solution techniques and the study provides insight into the difficulties encountered in the development of a unified scheme for incompressible and compressible flows.

Thesis Supervisor: Klaus-Jürgen Bathe
Title: Professor

to my parents

Acknowledgments

I would like to express my deepest gratitude to my advisor, Prof. Klaus-Jürgen Bathe, for his invaluable guidance throughout my Doctorate Program at M.I.T. He has been both an excellent teacher and a good friend to me and has always shown great interest in my research work.

It is my pleasure to thank the Department of Mechanical Engineering for its hospitality. In particular, I would like to thank my colleagues in the Finite Element Research Group and the researchers at ADINA, R&D in Watertown, MA, for their encouragement, help and friendship.

My utmost gratitude is due to my parents, whom I have not been able to be with for the past many years, whose love and support during these long years of studying mean the most to me.

I would also like to thank to my sponsor, Indonesian Aircraft Company, PT. IPTN for funding my research and study at M.I.T.

Contents

List of Figures

Chapter 1

Introduction

1.1 Overview

During the past three decades, various numerical methods for fluid flow have been developed. These are catagorized into three major classes which are the finite difference, control volume and finite element methods. Although each of the methods has different basic assumptions and is derived differently, they are related to each other, see [1, 2, 3]. The finite difference method was mostly used in the early stages of solution; however, the method faces major difficulties when it is applied to problems with complex geometries. Some mapping functions can be introduced to remedy this difficulty, however the mapping functions become more complicated as the domain of the problem becomes more complex. The control volume method is mostly used to solve fluid flows. In the control volume method, the domain is discretized into finite volumes and the method assumes constant value of the variables within each volume. However, by assuming constant values of the variables, the method has low order accuracy. Some high order methods for the control volume have been proposed [4], but satisfactory results have not been obtained. In the finite element method, the domain is discretized into finite elements and the variables are prescribed in the elements by polynomial functions. The method has the advantages of being able to solve problems with complex geometries and to obtain higher order accuracy by choosing higher degree polynomial functions to prescribe the distribution of the variables in the elements.

The numerical solutions of compressible flows entail many difficulties due to the presence of shocks and viscous boundary layers. To solve compressible flow problems using the usual low-order control volume and finite difference methods, extremely fine meshes are needed, in particular, in the areas where boundary layers and shocks occur, to obtain reasonably accurate results. Similar fine meshes are also required when using the usually employed low-order finite element techniques, although of course the use of unstructured meshes allows the use of coarser meshes in some regions of the flow. The fine meshes are required because of the low-order convergence behavior of the finite elements, both for the diffusive and the convective terms in the Navier-Stokes equations. This observation motivates us to study the possibility of developing a parabolic quadrilateral element for compressible flows. The element would naturally provide a higher convergence behavior for the diffusive terms, and – provided effective upwinding and shock capturing schemes are embedded in the element – should also give a higher accuracy for the convective terms of the flow equations [5].

Many finite element methods have been proposed to obtain numerical solutions of compressible flow problems using a linear (that is, low-order) triangular element [6, 7, 8, 9, 10, 11, 12] and using a linear quadrilateral element [13, 14, 15]. Also, Shapiro endeavored to develop a parabolic quadrilateral element; however, the author did not entirely use parabolic functions since the convective term was discretized using linear interpolations [14]. Oden et al. developed *h-p* discretization schemes that include, of course, higher-order elements [16, 17, 18, 19]. These schemes are based upon the Taylor-Galerkin method, which has second order accuracy in time, to discretize the time and space variables, and to stabilize the convective term, an artificial diffusion is employed.

Oscillations might occur in the numerical solutions at the locations where the convective term is dominant and to eliminate these oscillations, an upwind method need be used. The SUPG method, proposed by Hughes et al. originally for incompressible flows [20], is a very popular upwind technique used in finite element discretizations since the method has no crosswind diffusion and a clear mathematical formulation.

The use of the SUPG technique and modifications for compressible flow problems have been proposed in several contributions [10, 13, 21] but only linear elements were used. Some authors extended the SUPG technique also for use with a quadratic element, but only the scalar, convective-diffusive problem and not the system of Navier-Stokes equations was considered [22, 23, 24, 25]. Jiang et al. [26] developed a method for compressible flow using a quadratic element which employs least squares finite element formulation. The solutions using this method do not contain oscillations but seem to be too diffusive.

A unified finite element solution scheme for incompressible and compressible flows would be most attractive in engineering practice. The objective in this thesis was to work toward this goal. To solve incompressible flows, it is well-known that the inf-sup condition for incompressible analysis should be satisfied by the element discretization. An effective element for incompressible analysis of solids is the parabolic element with four continuous pressure variables. The idea in this thesis was therefore to develop a parabolic element for incompressible and compressible flows, using for incompressible flows the same pressure discretization as for solids. We formulate the finite element solution scheme for incompressible flow based on the primitive variables, pressure, velocity and temperature, while for compressible flow, the conservative variables, density, mass flows and specific total energy are used.

We propose a new upwind method for the parabolic quadrilateral element to solve high-speed compressible flows. The upwinding is similar to what is used in the finite difference method.

In a quadratic element, the nodal connectivity is wider than in a linear element. This nodal connectivity makes it possible to design a higher order upwind method [27]. The upwind method that we propose contains second order derivatives, hence the numerical results using this technique are expected to have a higher order accuracy. The method is also simple and easy to implement.

In the presence of a shock, a stable numerical method still gives solutions with oscillations around the shock and to eliminate these oscillations, a shock capturing method is needed. We propose here a shock capturing procedure for the quadratic element compatible with the accuracy obtained using the new upwind term.

To extend the ideas used in the compressible flow analysis, we also consider incompressible flows. A finite element for incompressible flow analysis should satisfy the inf-sup condition for stability [5, 28, 29]. We use the 9/4c-element which satisfies the inf-sup condition and we apply a similar form of upwinding as in the compressible flow formulation. As a by-product, we also propose a low order element which satisfies the inf-sup condition.

1.2 Thesis outline

In chapter 2, we discuss the governing equations of fluid flow. The governing equations consist of the conservation of mass, momentum and energy equations which are written in conservative and nonconservative forms. In chapter 3, we introduce the constitutive relations for the compressible flow formulation. The finite element spaces are defined and the finite element discretization procedure for the compressible flow is discussed. Some numerical examples to confirm the effectiveness of the method are presented. The range of Mach number of the examples considered is from 0.0005 to 6, in which most engineering problems lie. In chapter 4, we introduce the constitutive relations for incompressible flow. The finite element procedure for incompressible flow is discussed. The 9/4c-element and a 5/1-element which satisfy the inf-sup condition are employed to discretize the domain. The results of some numerical examples are presented and a comparison of solutions using the compressible and incompressible flow formulations is given. In chapter 5, a discussion of an inf-sup test for upwind methods is presented. An inf-sup test similar to the test used in the incompressible formulation [30] is proposed. Various other upwind methods are also considered in the test for comparison purposes. Finally, in chapter 6, we give our conclusions drawn from this thesis and give recommendations for future research.

Chapter 2

Governing equations

In this chapter, we review the general governing equations of fluid flow. The detailed derivation of the equations is given in [1, 32] or other stardard textbooks and we only summarize the main ideas here. The equations are written in conservative and nonconservative forms. The equations in conservative form will be used in the compressible flow formulation and the equations in nonconservative form will be used in the incompressible flow formulation. The governing equations stated in this chapter are for any continuous medium since the constitutive relations for any specific medium are not yet introduced. The constitutive relations will be introduced in the next chapters.

2.1 Governing equations in conservative form

The governing equations for fluid flow contain the conditions of conservation of mass, momentum and energy. Consider a Cartesian control volume element which is fixed in space. The mass conservation principle expresses the fact that mass cannot disappear from the system nor be created. Here, we will not consider multiphase fluids, therefore no sources due to chemical reactions will be considered. The mass conservation then states that the rate of change of mass stored in the control volume element equals the net rate of mass inflow,

$$\frac{\partial}{\partial t}\int_{Vol}\rho\, dVol = -\int_S \rho\mathbf{V}\cdot d\mathbf{S}$$

where ρ is the density of the fluid; $\mathbf{V} = v_1\vec{i} + v_2\vec{j} + v_3\vec{k}$, (v_1, v_2, v_3) are velocity components. Applying the divergence rule to the mass inflow term, the equation, in differential form, becomes

$$\frac{\partial\rho}{\partial t} = -\frac{\partial(\rho v_1)}{\partial x_1} - \frac{\partial(\rho v_2)}{\partial x_2} - \frac{\partial(\rho v_3)}{\partial x_3} \tag{2.1}$$

The term on the left hand side of eqn. (2.1) is the rate of change of mass stored in the control volume, and the terms on the right hand side are the net rates of mass inflow for all directions. Using index notation, eqn (2.1) can be written as

$$\rho_{,t} + (\rho v_j)_{,j} = 0$$

where $()_{,t}$ and $()_{,j}$ denote differentiations with respect to time and the x_j-coordinate axis, respectively; v_j is the velocity in the x_j-direction.

Newton's law states that the rate of change of momentum stored in a fixed control volume element equals the net rate of momentum inflow plus the sum of the forces acting on the fluid. These forces consist of the body forces, such as gravity etc., and surface forces. The surface forces are the result of the internal deformations of the fluid.

$$\frac{\partial}{\partial t}\int_{Vol}\rho\,\mathbf{V}dVol = -\int_S \rho\mathbf{V}(\mathbf{V}\cdot d\mathbf{S}) + \int_S \boldsymbol{\tau}\, d\mathbf{S} + \int_{Vol}\rho\,\mathbf{f}^B dVol$$

where $\boldsymbol{\tau}$ are the internal stresses and $\mathbf{f}^B$ is the body force per unit mass. Applying the divergence rule to the momentum inflow and surface stress terms, the momentum conservation equation in the x_i-direction becomes, in differential form

$$\frac{\partial(\rho v_i)}{\partial t} = -\frac{\partial(\rho v_i v_1)}{\partial x_1} - \frac{\partial(\rho v_i v_2)}{\partial x_2} - \frac{\partial(\rho v_i v_3)}{\partial x_3} + \frac{\partial\tau_{1i}}{\partial x_1} + \frac{\partial\tau_{2i}}{\partial x_2} + \frac{\partial\tau_{3i}}{\partial x_3} + \rho f_i^B \tag{2.2}$$

where τ_{ji} is the component of the traction acting on the surface of the control volume element. The first subscript, j, denotes the plane onto which the traction is applied and the second subsript, i, denotes the direction of the traction. f_i^B is the volume force component per unit mass in the x_i-direction. Using index notation, the conservation of momentum equation (2.2) can be written as

$$(\rho v_i)_{,t} + (\rho v_i v_j)_{,j} - \tau_{ji,j} - \rho f_i^B = 0$$

The energy conservation principle states that the rate of change of the total energy stored in a fixed control volume element equals the net rate of energy inflow, plus the rate of heat transfer into the control volume across the boundary by conduction, plus the net rate of work done by the body force on the fluid in the control volume, plus the rate of energy generated in the control volume, plus the net rate of work done by the tractions on the surface of the control volume,

$$\frac{\partial}{\partial t}\int_{Vol} \rho E \; dVol = -\int_S \rho E \; \mathbf{V}\cdot d\mathbf{S} - \int_S \mathbf{q}\cdot d\mathbf{S} + \int_{Vol} (\rho \mathbf{f}^B \cdot \mathbf{V} + \rho q^B) dVol + \int_S (\boldsymbol{\tau}\; \mathbf{V})\cdot d\mathbf{S}$$

where $\mathbf{q}$ is the heat conduction; q^B is the heat source per unit mass. The total energy, E, is stored in the control volume as internal energy, e, and kinetic energy

$$E = e + \frac{1}{2}(v_1^2 + v_2^2 + v_3^2)$$

Applying the divergence rule to the energy inflow, heat transfer and surface work terms, the energy conservation equation can be written in differential form as

$$\begin{aligned} \frac{\partial(\rho E)}{\partial t} \quad = \quad & -\frac{\partial(\rho E v_1)}{\partial x_1} - \frac{\partial(\rho E v_2)}{\partial x_2} - \frac{\partial(\rho E v_3)}{\partial x_3} - \frac{\partial q_1}{\partial x_1} - \frac{\partial q_2}{\partial x_2} - \frac{\partial q_3}{\partial x_3} + \rho v_1 f_1^B \\ & + \rho v_2 f_2^B + \rho v_3 f_3^B + \frac{\partial(\tau_{11}v_1 + \tau_{12}v_2 + \tau_{13}v_3)}{\partial x_1} + \frac{\partial(\tau_{21}v_1 + \tau_{22}v_2 + \tau_{23}v_3)}{\partial x_2} \\ & + \frac{\partial(\tau_{31}v_1 + \tau_{32}v_2 + \tau_{33}v_3)}{\partial x_3} + \rho\, q^B \end{aligned} \tag{2.3}$$

where q_i is the heat conduction in the x_i-direction. Using index notation and summation convention, the conservation of energy equation (2.3) can be written as

$$(\rho E)_{,t} + (\rho E v_j - v_i \tau_{ji} + q_j)_{,j} - \rho v_i f_i^B - \rho\, q^B = 0$$

Summarizing, the complete governing equations for the fluid flow written in conservative form and using index notation are

$$\begin{aligned} \rho_{,t} + (\rho v_j)_{,j} &= 0 \\ (\rho v_i)_{,t} + (\rho v_i v_j)_{,j} - \tau_{ji,j} - \rho f_i^B &= 0 \\ (\rho E)_{,t} + (\rho E v_j - v_i \tau_{ji} + q_j)_{,j} - \rho v_i f_i^B - \rho\, q^B &= 0 \end{aligned} \tag{2.4}$$

2.2 Governing equations in nonconservative form

In the nonconservative form, the mass conservation equation (from eqn. (2.4)) is written as

$$\rho_{,t} + \rho_{,j} v_j + \rho v_{j,j} = 0$$

and the momentum conservation equation (from eqn. (2.4)) can be written as

$$v_i \rho_{,t} + \rho v_{i,t} + v_i (\rho v_j)_{,j} + \rho v_j v_{i,j} - \tau_{ji,j} - \rho f_i^B = 0 \tag{2.5}$$

Using the mass conservation equation, the first and third terms in eqn. (2.5) vanish, so we have

$$\rho v_{i,t} + \rho v_j v_{i,j} - \tau_{ji,j} - \rho f_i^B = 0 \tag{2.6}$$

The energy conservation equation (from eqn. (2.4)) can be written as

$$E \rho_{,t} + \rho E_{,t} + E(\rho v_j)_{,j} + \rho v_j E_{,j} - v_{i,j} \tau_{ji} - v_i \tau_{ji,j} + q_{j,j} - \rho v_i f_i^B - \rho\, q^B = 0 \tag{2.7}$$

Using the mass conservation equation, the first and third terms in eqn. (2.7) vanish. Inserting the definition $E = e + \frac{1}{2}v_i^2$, we have

$$\rho(e + \frac{1}{2}v_i^2)_{,t} + \rho v_j(e + \frac{1}{2}v_i^2)_{,j} - v_{i,j}\tau_{ji} - v_i\tau_{ji,j} + q_{j,j} - \rho v_i f_i^B - \rho\, q^B = 0 \qquad (2.8)$$

Multiplying the momentum conservation equation (eqn. (2.6)) by v_i and substracting the result from eqn. (2.8), we obtain

$$\rho e_{,t} + \rho v_j e_{,j} - v_{i,j}\tau_{ji} + q_{j,j} - \rho\, q^B = 0$$

The complete governing equations for fluid flow written in nonconservative form are

$$\begin{aligned} \rho_{,t} + \rho_{,j}v_j + \rho v_{j,j} &= 0 \\ \rho v_{i,t} + \rho v_j v_{i,j} - \tau_{ji,j} - \rho f_i^B &= 0 \\ \rho e_{,t} + \rho v_j e_{,j} - v_{i,j}\tau_{ji} + q_{j,j} - \rho\, q^B &= 0 \end{aligned} \qquad (2.9)$$

The entropy equation plays an important role in the solution of fluid flow; however, the equation is not independent of the energy equation. To derive the entropy equation, let us separate the stress into two parts

$$\tau_{ji} = -p\,\delta_{ij} + \tau'_{ji} \qquad (2.10)$$

and

$$p = -\frac{\tau_{ll}}{3}$$

where p is the pressure and τ'_{ji} is the deviatoric stress, δ_{ij} denotes the Kronecker delta (i.e. $\delta_{ij} = 1$ for $i = j$, and $\delta_{ij} = 0$ for $i \neq j$). We have the equation relating the Lagrangian description to the Eulerian description for the internal energy of fluid flow,

$$\rho\frac{de}{dt} = \rho\frac{\partial e}{\partial t} + \rho v_j\frac{\partial e}{\partial x_j}$$

In the Lagrangian coordinate system the fluid particle is followed whereas in the Eulerian coordinate system, a fixed location in space of the coordinate system is used. Using eqn. (2.10), the energy equation in eqns. (2.9) becomes

$$\rho \frac{de}{dt} = -p v_{j,j} + v_{i,j} \tau'_{ji} - q_{j,j} + \rho\, q^B \tag{2.11}$$

The first term on the right hand side of the above equation is the reversible work done by the pressure and this term vanishes in the limit of full incompressibility. The next term is the dissipation term acting as an irreversible heat source. Let us introduce the entropy per unit mass, s of the fluid through the thermodynamic relation

$$T\ ds = de + p\ d(\frac{1}{\rho})$$

where T is the temperature. Dividing the above equation by the increment of time to obtain the rate relation, we have

$$T \frac{ds}{dt} = \frac{de}{dt} + p \frac{d}{dt}(\frac{1}{\rho}) \tag{2.12}$$

Using the mass conservation equation, we can rewrite the last term in the above equation as

$$p \frac{d}{dt}(\frac{1}{\rho}) = -\frac{p}{\rho^2} \frac{d\rho}{dt} = -\frac{p}{\rho^2}(\frac{\partial \rho}{\partial t} + v_j \frac{\partial \rho}{\partial x_j}) = \frac{p}{\rho} v_{j,j}$$

Substituting eqn. (2.11) into (2.12) and using the above relation, we have the entropy equation

$$\rho T \frac{ds}{dt} = v_{i,j} \tau'_{ji} - q_{j,j} + \rho\, q^B \tag{2.13}$$

where $v_{i,j}\tau'_{ji}$ is a non-negative quantity and behaves as a source of non-reversible entropy generation. Note that the entropy variable is not a conserved quantity in the sense as the other quantities such as mass, momentum and energy. In the total system, the entropy must be non-decreasing to satisfy the second law of themodynamics.

For fluid flow analysis, one has a choice of choosing either the energy conservation equation or the entropy equation along with the mass and momentum conservation equations. In this thesis, we use the energy conservation equation in the formulation instead of the entropy equation since energy is a conserved quantity and is easier to use in analysis.

Chapter 3

Compressible flows

In this chapter, we start with a discussion of the constitutive relations for the fluid. The procedure for non-dimensionalization of the governing equations and the natural boundary conditions are discussed. The finite element formulation with upwinding and shock capturing for the space discretization is given. The time discretization using the finite difference method and the treatment of initial and boundary conditions are discussed. Finally, numerical examples to verify the effectiveness of the numerical method are presented. The work described in this chapter has been presented in [33].

3.1 Navier-Stokes equations for compressible flow

The governing equations (eqn. (2.4)) together with the constitutive relations compose the governing equations for compressible flow which are called the Navier-Stokes equations. The constitutive relations are the ideal gas relations, the stress-strain relation for Newtonian fluid flow and Fourier's law of heat conduction,

$$
\begin{aligned}
\theta &= \frac{E - \frac{1}{2}v_l^2}{c_v} \\
p &= (\gamma - 1)\rho(E - \frac{1}{2}v_l^2) \\
\tau_{ij} &= -p\,\delta_{ij} + \lambda v_{l,l}\delta_{ij} + \mu(v_{i,j} + v_{j,i}) \\
q_j &= -\frac{k}{c_v}(E - \frac{1}{2}v_l^2)_{,j}
\end{aligned}
$$

where $p, \theta, c_v, \mu, \lambda, k$ are pressure, absolute temperature, specific heat at constant volume, fluid viscosity, second viscosity coefficient, coefficient of thermal conductivity, respectively. δ_{ij} is the Kronecker delta (i.e. $\delta_{ij} = 1$ for $i = j$, and $\delta_{ij} = 0$ for $i \neq j$). γ is the ratio of specific heats, $\gamma = \frac{c_p}{c_v}$ and $c_p = c_v + R$, where c_p and R are the specific heat at constant pressure and the gas constant, respectively. Here, Stokes' hypothesis is used, $\lambda = -\frac{2}{3}\mu$. Substituting the constitutive relations into the conservation equations, we obtain the Navier-Stokes equations

$$
\begin{aligned}
\rho_{,t} + (\rho v_j)_{,j} &= 0 \\
(\rho v_i)_{,t} + \{\rho v_i v_j + (\gamma - 1)\rho(E - \frac{1}{2}v_l^2)\delta_{ij} - \lambda v_{l,l}\delta_{ij} - \mu(v_{i,j} + v_{j,i})\}_{,j} - \rho f_i^B &= 0 \\
(\rho E)_{,t} + \{\rho E v_j + v_j(\gamma - 1)\rho(E - \frac{1}{2}v_l^2) - v_j \lambda v_{l,l} - v_i \mu(v_{i,j} + v_{j,i}) & \\
- \frac{k}{c_v}(E - \frac{1}{2}v_l^2)_{,j}\}_{,j} - \rho v_i f_i^B - \rho q^B &= 0
\end{aligned}
$$

To avoid difficulties due to round-off errors caused by using too large or too small a value of the input data and to make solutions independent of any particular system of units, we perform a non-dimensionalization of the Navier-Stokes equations. The procedure of non-dimensionalization normalizes the working variables, density, momentum and total energy, so the variables are of the same order of magnitude. We define the non-dimensionalized variables,

$$
x_i^* = \frac{x_i}{L_o} \qquad v_i^* = \frac{v_i}{V_o} \qquad t^* = \frac{tV_o}{L_o} \qquad \theta^* = \frac{\theta}{\theta_o}
$$

$$
\rho^* = \frac{\rho}{\rho_o} \qquad p^* = \frac{p}{\rho_o V_o^2} \qquad E^* = \frac{E}{E_o}
$$

$$
c_v^* = \frac{c_v \theta_o}{E_o} \qquad R^* = \frac{R\theta_o}{E_o} \qquad \mu^* = \frac{\mu}{\rho_o V_o L_o} \qquad \lambda^* = \frac{\lambda}{\rho_o V_o L_o} \qquad k^* = \frac{k\theta_o}{\rho_o V_o L_o E_o}
$$

$$
f_i^{B*} = \frac{f_i^B L_o}{V_o^2} \qquad q^{B*} = \frac{q^B L_o}{V_o^3}
$$

where $L_o, V_o, \rho_o, \theta_o, E_o$ are characteristic values of length, velocity, density, temperature and total energy. Using these variables, the Navier-Stokes equations become

$$
\begin{aligned}
\rho^*_{,t^*} + (\rho^* v^*_j)_{,j^*} &= 0 \\
(\rho^* v^*_i)_{,t^*} + \{\rho^* v^*_i v^*_j + (\gamma - 1)\rho^*(\frac{E^*}{c} - \frac{1}{2} v^{*2}_l)\delta_{ij} - \lambda^* v^*_{l,l^*}\delta_{ij} - \mu^*(v^*_{i,j^*} + v^*_{j,i^*})\}_{,j^*} & \\
-\rho^* f^{B*}_i &= 0 \\
(\rho^* E^*)_{,t^*} + \{\rho^* E^* v^*_j + (\gamma - 1)\rho^* v^*_j(E^* - \frac{c}{2} v^{*2}_l) - c\lambda^* v^*_j v^*_{l,l^*} - c\mu^* v^*_i (v^*_{i,j^*} + v^*_{j,i^*}) & \\
-\frac{k^*}{c^*_v}(E^* - \frac{c}{2} v^{*2}_l)_{,j^*}\}_{,j^*} - c\rho^* v^*_i f^{B*}_i - c\rho^* q^{B*} &= 0
\end{aligned}
$$

where $c = \frac{V^2}{E_o}$ is a constant. The non-dimensionalized constitutive relations are

$$
\begin{aligned}
\theta^* &= \frac{E^* - \frac{c}{2} v^{*2}_l}{c^*_v} \\
p^* &= (\gamma - 1)\rho^*(\frac{E^*}{c} - \frac{1}{2} v^{*2}_l) \\
\tau^*_{ij} &= -p^*\delta_{ij} + \lambda^* v^*_{l,l^*}\delta_{ij} + \mu^*(v^*_{i,j^*} + v^*_{j,i^*}) \\
q^*_j &= -\frac{k^*}{c^*_v}(E^* - \frac{c}{2} v^{*2}_l)_{,j^*}
\end{aligned}
$$

The Navier-Stokes equations, after dropping the * superscripts to simplify the notation, can be written in vector form as

$$
\mathbf{U}_{,t} + \mathbf{F}_{j,j} - \mathbf{G}_{j,j} - \mathbf{R} = \mathbf{0} \tag{3.1}
$$

where $()_{,t}$ and $()_{,j}$ denote derivatives with respect to time and the x_j-coordinate. In this thesis, We shall only consider the two-dimensional case, for numerical solutions $(i, j, l = 1, 2)$ for which

$$
\mathbf{U} = \begin{bmatrix} \rho \\ \rho v_1 \\ \rho v_2 \\ \rho E \end{bmatrix} \tag{3.2}
$$

$$
\mathbf{F}_j = \begin{bmatrix} \rho v_j \\ \rho v_1 v_j + (\gamma-1)\rho(\frac{E}{c} - \frac{1}{2}v_l^2)\delta_{1j} \\ \rho v_2 v_j + (\gamma-1)\rho(\frac{E}{c} - \frac{1}{2}v_l^2)\delta_{2j} \\ \rho E v_j + (\gamma-1)\rho v_j (E - \frac{c}{2}v_l^2) \end{bmatrix} \tag{3.3}
$$

$$
\mathbf{G}_j = \begin{bmatrix} 0 \\ \lambda v_{l,l}\delta_{1j} + \mu(v_{1,j} + v_{j,1}) \\ \lambda v_{l,l}\delta_{2j} + \mu(v_{2,j} + v_{j,2}) \\ c\lambda v_j v_{l,l} + c\mu v_i(v_{i,j} + v_{j,i}) + \frac{k}{c_v}(E - \frac{c}{2}v_l^2)_{,j} \end{bmatrix} \tag{3.4}
$$

$$
\mathbf{R} = \begin{bmatrix} 0 \\ \rho f_1^B \\ \rho f_2^B \\ c\rho v_i f_i^B + c\rho q^B \end{bmatrix} \tag{3.5}
$$

Taking the quasi-linear form of the convective terms and rewriting the diffusive and source terms, the Navier-Stokes equations can be written as

$$
\mathbf{U}_{,t} + \mathbf{A}_j \mathbf{U}_{,j} - (\mathbf{K}_{ji}\mathbf{U}_{,i})_{,j} - \mathbf{S}\mathbf{U} = \mathbf{0} \tag{3.6}
$$

where the Jacobian matrices of $\mathbf{F}_j$ are

$$
\mathbf{A}_1 = \begin{bmatrix} 0 & 1 & 0 & 0 \\ \frac{(\gamma-3)}{2}v_1^2 + \frac{(\gamma-1)}{2}v_2^2 & (3-\gamma)v_1 & (1-\gamma)v_2 & \frac{1}{c}(\gamma-1) \\ -v_1 v_2 & v_2 & v_1 & 0 \\ -\gamma v_1 E + c(\gamma-1)v_1(v_1^2+v_2^2) & \gamma E - \frac{c(\gamma-1)}{2}(3v_1^2+v_2^2) & c(1-\gamma)v_1 v_2 & \gamma v_1 \end{bmatrix}
$$

$$
\mathbf{A}_2 = \begin{bmatrix} 0 & 0 & 1 & 0 \\ -v_1 v_2 & v_2 & v_1 & 0 \\ \frac{(\gamma-1)}{2}v_1^2 + \frac{(\gamma-3)}{2}v_2^2 & (1-\gamma)v_1 & (3-\gamma)v_2 & \frac{1}{c}(\gamma-1) \\ -\gamma v_2 E + c(\gamma-1)v_2(v_1^2+v_2^2) & c(1-\gamma)v_1 v_2 & \gamma E - \frac{c(\gamma-1)}{2}(v_1^2+3v_2^2) & \gamma v_2 \end{bmatrix}
$$

The matrices of the diffusive terms are

$$
\mathbf{K}_{11} = \begin{bmatrix} 0 & 0 & 0 & 0 \\ -\frac{\lambda v_1}{\rho} - \frac{2\mu v_1}{\rho} & \frac{\lambda}{\rho} + \frac{2\mu}{\rho} & 0 & 0 \\ -\frac{\mu v_2}{\rho} & 0 & \frac{\mu}{\rho} & 0 \\ c \cdot c_1 & \frac{c\lambda v_1}{\rho} + \frac{2c\mu v_1}{\rho} - \frac{ckv_1}{c_v\rho} & \frac{c\mu v_2}{\rho} - \frac{ckv_2}{c_v\rho} & \frac{k}{c_v\rho} \end{bmatrix}
$$

$$
\mathbf{K}_{12} = \begin{bmatrix} 0 & 0 & 0 & 0 \\ -\frac{\lambda v_2}{\rho} & 0 & \frac{\lambda}{\rho} & 0 \\ -\frac{\mu v_1}{\rho} & \frac{\mu}{\rho} & 0 & 0 \\ -\frac{c\lambda v_1 v_2}{\rho} - \frac{c\mu v_1 v_2}{\rho} & \frac{c\mu v_2}{\rho} & \frac{c\lambda v_1}{\rho} & 0 \end{bmatrix}
$$

$$
\mathbf{K}_{21} = \begin{bmatrix} 0 & 0 & 0 & 0 \\ -\frac{\mu v_2}{\rho} & 0 & \frac{\mu}{\rho} & 0 \\ -\frac{\lambda v_1}{\rho} & \frac{\lambda}{\rho} & 0 & 0 \\ -\frac{c\lambda v_1 v_2}{\rho} - \frac{c\mu v_1 v_2}{\rho} & \frac{c\lambda v_2}{\rho} & \frac{c\mu v_1}{\rho} & 0 \end{bmatrix}
$$

$$
\mathbf{K}_{22} = \begin{bmatrix} 0 & 0 & 0 & 0 \\ -\frac{\mu v_1}{\rho} & \frac{\mu}{\rho} & 0 & 0 \\ -\frac{\lambda v_2}{\rho} - \frac{2\mu v_2}{\rho} & 0 & \frac{\lambda}{\rho} + \frac{2\mu}{\rho} & 0 \\ c \cdot c_2 & \frac{c\mu v_1}{\rho} - \frac{ckv_1}{c_v\rho} & \frac{c\lambda v_2}{\rho} + \frac{2c\mu v_2}{\rho} - \frac{ckv_2}{c_v\rho} & \frac{k}{c_v\rho} \end{bmatrix}
$$

where

$$
\begin{aligned}
c_1 &= -\frac{\lambda v_1^2}{\rho} - \frac{2\mu v_1^2}{\rho} - \frac{\mu v_2^2}{\rho} - \frac{kE}{cc_v\rho} + \frac{kv_1^2}{c_v\rho} + \frac{kv_2^2}{c_v\rho} \\
c_2 &= -\frac{\lambda v_2^2}{\rho} - \frac{\mu v_1^2}{\rho} - \frac{2\mu v_2^2}{\rho} - \frac{kE}{cc_v\rho} + \frac{kv_1^2}{c_v\rho} + \frac{kv_2^2}{c_v\rho}
\end{aligned}
$$

and the matrix of the source terms is

$$\mathbf{S} = \begin{bmatrix} 0 & 0 & 0 & 0 \\ f_1^B & 0 & 0 & 0 \\ f_2^B & 0 & 0 & 0 \\ cq^B & cf_1^B & cf_2^B & 0 \end{bmatrix}$$

The Navier-Stokes equations written in terms of the conservative variables have the simplest form. Furthermore, due to the property of the convective terms being homogeneous functions of degree one of the conservative variables, we have the relation (see Appendix A, [2])

$$\mathbf{F}_j = \mathbf{A}_j \mathbf{U}$$

which is an important property to be used in an implicit method to evaluate the convective fluxes $\mathbf{F}_j(\mathbf{U})$.

The Euler equations are a special case of the Navier-Stokes equations when the diffusive and the source terms are zero. In matrix form, the Euler equations are simply

$$\mathbf{U}_{,t} + \mathbf{A}_j \mathbf{U}_{,j} = 0$$

The eigenvalues of A_j are real numbers, hence the Euler equations constitute a hyperbolic system of equations [34].

3.2 Finite element discretization

In this section, we discuss the finite-dimensional spaces used for the quadratic element and establish the finite element formulation. The artificial diffusion to stabilize the convective terms, and the shock capturing term to reduce oscillations around shocks and other discontinuities are presented. The treatment of the boundary conditions and initial conditions is discussed.

3.2.1 Finite element spaces

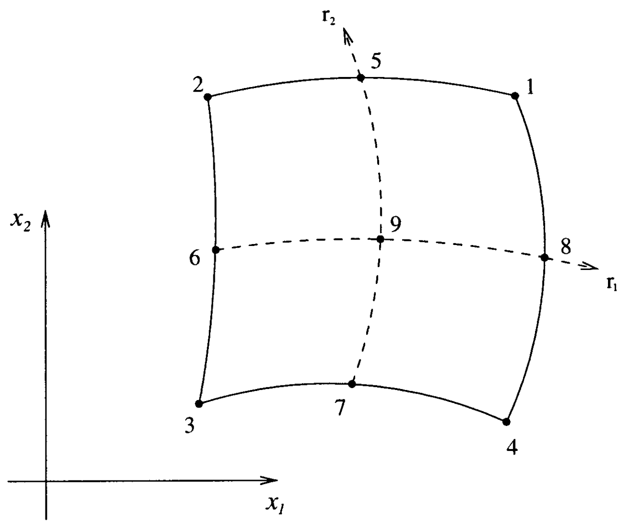

Figure 3-1: Nine-node quadrilateral element used for planar flows.

Consider a finite element discretization of the fluid domain Vol, into subdomains $Vol^{(m)}$, $m = 1, 2, ..., N$, where N is the number of elements [5]. A two-dimensional quadrilateral nine node element as shown in fig. 3-1 is considered. In the element, all variables are interpolated quadratically. Let the prescribed Dirichlet boundary conditions on the surface S_u be $\mathbf{g}(\mathrm{t})$ where the vector $\mathbf{g}(\mathrm{t})$ contains the specified function of the solution on the boundary S_u. Then the solution and weighting functional spaces for the discretization are

$$
\begin{aligned}
V_h &= \{\mathbf{v}_h | \mathbf{v}_h \in L^2(Vol); \frac{\partial (v_h)_i}{\partial x_j} \in L^2(Vol), (v_h)_i \in Q_2(Vol^{(m)}), i = 1, 2, 3, 4; \\
&\quad j = 1, 2; \mathbf{v}_h|_{S_u} = \mathbf{g}(t)\} \\
W_h &= \{\mathbf{w}_h | \mathbf{w}_h \in L^2(Vol); \frac{\partial (w_h)_i}{\partial x_j} \in L^2(Vol), (w_h)_i \in Q_2(Vol^{(m)}), i = 1, 2, 3, 4; \\
&\quad j = 1, 2; \mathbf{w}_h|_{S_u} = \mathbf{0}\}
\end{aligned}
$$

where $Q_2(Vol^{(m)})$ denotes the biquadratic function in the element m; and $L^2(Vol)$ is the space of square integrable functions in the volume, "Vol", of the body considered,

$$
L^2(Vol) = \{\mathbf{w} | \mathbf{w} \text{ is defined in } Vol \text{ and } \int_{Vol} (\sum_{i=1}^{4} (w_i)^2) dVol = \|\mathbf{w}\|^2_{L^2(Vol)} < +\infty\}
$$

3.2.2 Weighted residual formulation

Let us define a diagonal matrix $\mathbf{W}_h$

$$\mathbf{W}_h = \begin{bmatrix} \overline{\rho} & 0 & 0 & 0 \\ 0 & \overline{\rho v_1} & 0 & 0 \\ 0 & 0 & \overline{\rho v_2} & 0 \\ 0 & 0 & 0 & \overline{\rho E} \end{bmatrix}$$

where $\overline{\rho}, \overline{\rho v_1}, \overline{\rho v_2}, \overline{\rho E}$ are the virtual variables of density, mass flow in the x_1-direction, mass flow in the x_2-direction and total energy. The finite element formulation of the Navier-Stokes equations is :

Find $\mathbf{U}_h \in V_h$ such that for all Diag($\mathbf{W}_h$) $\in W_h$ the following variational equation is satisfied:

$$\begin{aligned} \int_{Vol} [\mathbf{W}_h\,(\mathbf{U}_{h,t} - \mathbf{S}\mathbf{U}_h) - \mathbf{W}_{h,j}\,\mathbf{A}_j\mathbf{U}_h + \mathbf{W}_{h,j}\,\mathbf{K}_{ji}\mathbf{U}_{h,i}\ ]\,dVol & \qquad (3.7) \\ + \sum_m \int_{Vol^{(m)}} \mathbf{W}_{h,kk}\,\mathbf{A}_k\boldsymbol{\tau}_k\mathbf{A}_k\mathbf{U}_{h,kk}\ dVol^{(m)} + \sum_m \int_{Vol^{(m)}} \nu_k\,\mathbf{W}_{h,k}\,\mathbf{U}_{h,k}\ dVol^{(m)} & \\ = \int_S \mathbf{W}_h^S\,(-\mathbf{F}_c + \mathbf{F}_d)\ dS & \end{aligned}$$

Here we have used that $\mathbf{F}_j = \mathbf{A}_j\mathbf{U}$. The matrix $\mathbf{W}_h^S$ contains the weighting functions evaluated on the surface S, where S is the entire boundary surface, and $\mathbf{F}_c$ and $\mathbf{F}_d$ are the natural boundary loading terms corresponding to the convective and diffusive terms, where for the convective natural boundary loading

$$\mathbf{F}_c = \mathbf{F}_j\ n_j = \begin{bmatrix} \rho v_j n_j \\ \rho v_1 v_j n_j + (\gamma-1)\rho(E - \frac{1}{2}v_l^2)\delta_{1j}n_j \\ \rho v_2 v_j n_j + (\gamma-1)\rho(E - \frac{1}{2}v_l^2)\delta_{2j}n_j \\ \rho E v_j n_j + (\gamma-1)\rho v_j(E - \frac{1}{2}v_l^2)n_j \end{bmatrix} \qquad (3.8)$$

and for the diffusive natural boundary loading

$$\mathbf{F}_d = \mathbf{G}_j\ n_j = \begin{bmatrix} 0 \\ \lambda v_{l,l}\delta_{1j}n_j + \mu(v_{1,j} + v_{j,1})n_j \\ \lambda v_{l,l}\delta_{2j}n_j + \mu(v_{2,j} + v_{j,2})n_j \\ \lambda v_j v_{l,l} n_j + \mu v_i(v_{i,j} + v_{j,i})n_j + \frac{k}{c_v}(E - \frac{1}{2}v_l^2)_{,j}n_j \end{bmatrix} \tag{3.9}$$

where n_j is the x_j-direction cosine of the unit (pointed outward) boundary normal vector.

The first integral term and the surface loading term correspond to the standard Galerkin procedure applied to the compressible flow governing equations. The second integral term is the artificial diffusion term and the third integral term is the shock capturing term.

3.2.3 Artificial diffusion

The purpose of the artificial diffusion is to stabilize the unstable convective terms in the standard Galerkin procedure. Although the quadratic element is "more stable" than the linear element, it still requires artificial diffusion (that is, upwinding) to eliminate oscillations. Oden et al. used an artificial diffusion of the form $-(c\ \Delta t\ h^2|\frac{\partial v_i}{\partial x_i}|\mathbf{U}_{,x_i})_{,x_i}$ for their h-p discretization schemes where $c, \Delta t, h$ are a problem-adjustable parameter, the time increment and the element size, respectively. This artificial diffusion is applicable for transient analysis only since Δt is used in the definition of the the artificial diffusion term. In our work, the artificial diffusion term for the quadratic element is given by

$$\sum_m \int_{Vol^{(m)}} \mathbf{W}_{h,kk}\ (\mathbf{A}_k \boldsymbol{\tau}_k \mathbf{A}_k)\mathbf{U}_{h,kk}\ \ dVol^{(m)} \tag{3.10}$$

The motivation for the upwind term in eqn. (3.10) is given in Appendix B. Note that high-order derivatives are used in order to achieve a higher order accuracy in the upwind method. Using a higher order element results in a wider nodal connectivity and so a higher order upwind method can be employed [27].

The above upwind technique applies an artificial diffusion in all directions instead of only in the streamline direction as in the SUPG technique, but the magnitude of upwinding in the k-direction depends on the convective matrix $\mathbf{A}_k$. Our numerical experiments have shown that applying the artificial diffusion in all directions gives a more stable numerical result than when the artificial diffusion is only applied in the streamline direction, and crosswind diffusion is insignificant. This is because a high-order derivative upwind method is employed which has negligible crosswind diffusion in the solution.

The value of $\boldsymbol{\tau}_k$ for the artificial diffusion is of the form used in finite difference solutions,

$$\boldsymbol{\tau}_k = \frac{1}{9}(|\frac{\partial x_k}{\partial \mathbf{r}}|)^3|\mathbf{A}_k|^{-1} \tag{3.11}$$

where $\mathbf{r}$ denotes the coordinates in the natural coordinate system of the element. For the two-dimensional case

$$|\frac{\partial x_k}{\partial \mathbf{r}}| = \sqrt{(\frac{\partial x_k}{\partial r_1})^2 + (\frac{\partial x_k}{\partial r_2})^2} \tag{3.12}$$

The factor $\frac{1}{9}$ is obtained by considering the 1-D convection-diffusion problem. With the factor $\frac{1}{9}$, the artificial diffusion results into full upwinding corresponding to the corner nodes of the elements (see Appendix D). We define

$$|\mathbf{A}_k|^{-1} = \mathbf{X}_k|\boldsymbol{\Lambda}_k|^{-1}\mathbf{X}_k^{-1}$$

where $\mathbf{X}_k$ is a matrix whose its columns are the eigenvectors of the matrix $\mathbf{A}_k$ and $\boldsymbol{\Lambda}$ is a diagonal matrix whose its components are the eigenvalues of the matrix $\mathbf{A}_k$ corresponding to the eigenvectors $\mathbf{X}_k$ (we describe the eigenvalues and eigenvectors of the matrix $\mathbf{A}_k$ later).

To obtain an understanding of how the artificial diffusion term affects the Galerkin formulation, we consider the finite element method applied to the one-dimensional steady-state Euler equation,

$$-\int_{Vol}\mathbf{W}_{h,1}\ \mathbf{A}_1\mathbf{U}_h\ \ dVol+\sum_m\int_{Vol^{(m)}}\mathbf{W}_{h,11}\ \mathbf{A}_1\boldsymbol{\tau}_1\mathbf{A}_1\mathbf{U}_{h,11}\ \ dVol^{(m)}=-\int_S\mathbf{W}_h^S\ \mathbf{F}_c\ \ dS \tag{3.13}$$

For a uniform mesh, Δx is constant so that for each element

$$\boldsymbol{\tau}_1=\frac{1}{9}(\frac{\Delta x}{2})^3|\mathbf{A}_1|^{-1} \tag{3.14}$$

Combining equations (3.13) and (3.14), we obtain

$$\sum_m\int_{Vol^{(m)}}\{-\mathbf{W}_{h,1}\ \mathbf{A}_1\mathbf{U}_h+\mathbf{W}_{h,11}\ \frac{1}{9}(\frac{\Delta x}{2})^3|\mathbf{A}_1|\mathbf{U}_{h,11}\}\ \ dVol^{(m)}=-\int_S\mathbf{W}_h^S\ \mathbf{F}_c\ \ dS \tag{3.15}$$

where for a smooth function $\mathbf{U}$, the second term (the artificial diffusion term) approaches zero with third order as $\Delta x\to 0$.

3.2.4 Shock capturing

The shock capturing term is designed to eliminate oscillations in the vicinity of shocks and other discontinuities. In the formulation considered, the shock capturing term is

$$\sum_m\int_{Vol^{(m)}}\nu_k\mathbf{W}_{h,k}\ \mathbf{U}_{h,k}\ \ dVol^{(m)} \tag{3.16}$$

where ν_k is a tuned variable. This shock capturing term applies an artificial diffusion in all directions with the magnitude in the x_k-direction proportional to ν_k. We wish to have a value of ν_k that is small at a reasonable distance from the shock and sufficiently large in the vicinity of the shock, and use

$$\nu_k=\frac{1}{4}\frac{h_k||h_j^2\mathbf{A}_j\mathbf{U}_{h,jj}||}{||\mathbf{U}_h||} \tag{3.17}$$

where h_l is the x_l-direction "length" of the element,

$$h_l = \frac{1}{\sqrt{(\frac{1}{2}\frac{\partial r_1}{\partial x_l})^2 + (\frac{1}{2}\frac{\partial r_2}{\partial x_l})^2}} \tag{3.18}$$

The value $\frac{1}{4}$ is obtained by choosing the factor that gives the best shock solution of the test problem considered at the end of this section. If, instead, the factors $\frac{1}{3}$ or $\frac{1}{6}$ are used, only a slightly different shock solution is observed. This shock capturing term has the form given by Beau et al. [13] (derived from the shock capturing term proposed by Hughes et al. [21, 35]) for linear elements, but the difference lies in the definition of ν_k.

Away from the shock where the finite element solution is smooth, $\mathbf{U}_{h,jj}$ is not large (the magnitude depends of course on the problem considered) and ν_k is small for a small element size. In those regions, the shock capturing term gives third-order accuracy since $\mathbf{U}_{h,jj}$ weakly depends on the mesh size. On the other hand, in the vicinity of a shock, the finite element solution gives a large value $\mathbf{U}_{h,jj}$, hence ν_k is large and the shock capturing term stabilizes the solution. Near a shock, the shock capturing term gives first-order accuracy because on the shock $\mathbf{U}_{h,jj}$ is a function of the mesh size which cancels the h_j^2 term in the ν_k definition.

To show the capability of the shock capturing method, consider the usually employed test problem in fig. 3-2 [11, 36]. The two-dimensional steady-state problem contains an oblique shock. At the inlet on the left and upper boundaries, the convective fluxes are prescribed corresponding to the condition

$$M = 2,\ \rho = 1,\ v_1 = \cos 10^0,\ v_2 = -\sin 10^0$$

The convective fluxes are imposed at the left and upper boundaries instead of imposing the Dirichlet boundary condition in order to avoid the inconsistency in the boundary conditions at the lower-left corner where the slip-wall condition is imposed. On the right boundary, no variable is prescribed. The fluid properties are $\gamma = 1.4, c_v = 715, k = \mu = 0$. Solutions using the uniform and distorted meshes

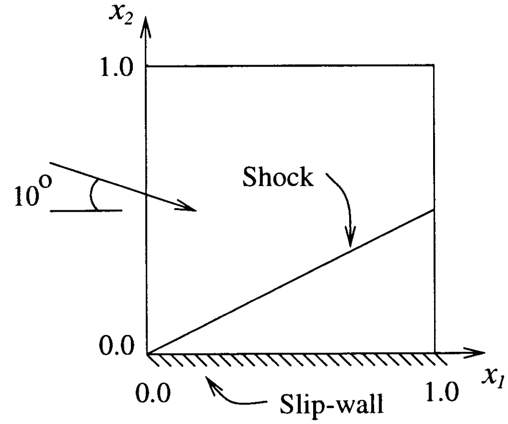

Figure 3-2: Two dimensional shock problem.

shown in fig. 3-3 have been obtained. The finite element solutions are shown in fig. 3-4. The finite element method using the quadratic element gives reasonable results for both meshes.

The plots of density distributions along $x_1 = 1$ using both meshes are shown in fig. 3-5. This figure shows that the shock is captured within at most four elements with two elements containing the high gradient of the jump variable and the other two elements giving a smooth transition of the solution.

Fig. 3-4 shows that the mesh with distorted elements gives a better solution. This is the case, because the element distribution is favorable to the shock in the lower-left corner where the shock starts. Namely, the mesh is finer in this corner, and of course the smaller the elements used to capture the shock, the better is the solution.

Another problem, a reflecting shock problem, is also considered to test the shock capturing method. The domain consists of three flow regions which are separated by shocks, see fig. 3-6. In the numerical experiment, all variables are imposed on the left and top boundaries. On the bottom, the slip wall condition is imposed. No condition is applied on the right boundary. The fluid properties are $\gamma = 1.4, c_v = 715, k = \mu = 0$. The mesh is of 60×20 elements and the domain is $0 \leq x_1 \leq 3.5$ and $0 \leq x_2 \leq 1$.

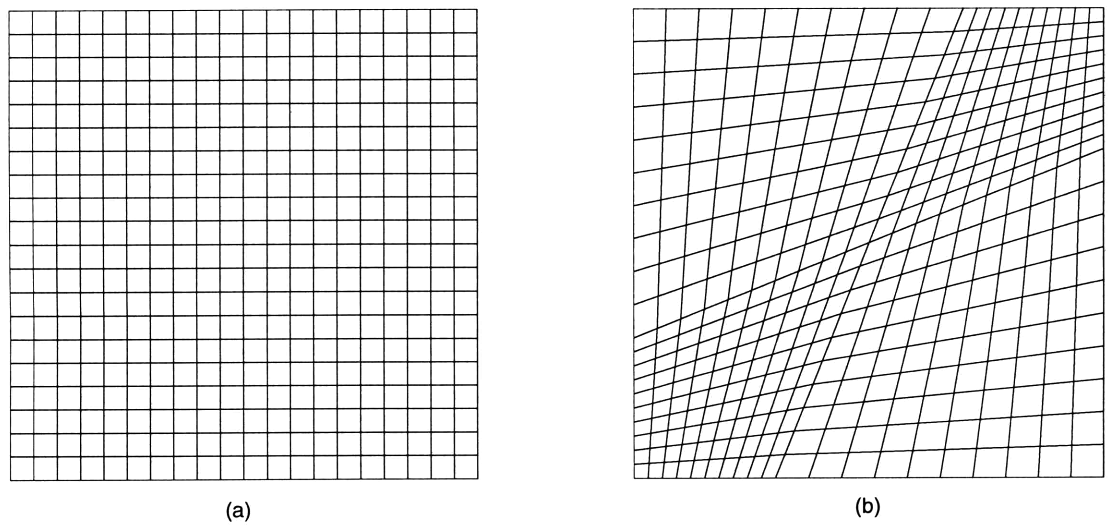

Figure 3-3: Meshes used for the two-dimensional shock problem (a) Uniform mesh, (b) Distorted mesh.

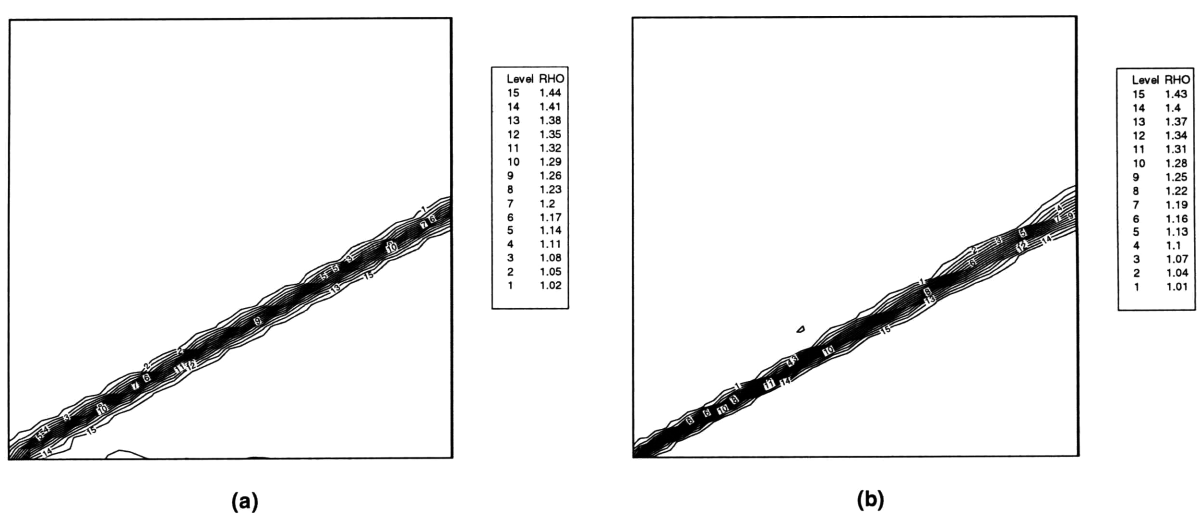

Figure 3-4: Contour plot of density of the finite element solution using (a) uniform mesh (b) distorted mesh.

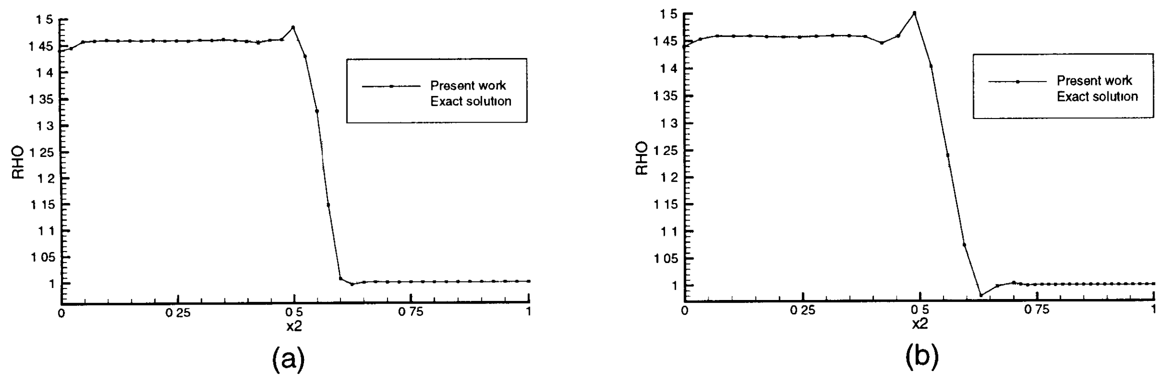

Figure 3-5: Density distribution along $x_1 = 1.0$ using (a) uniform mesh (b) distorted mesh.

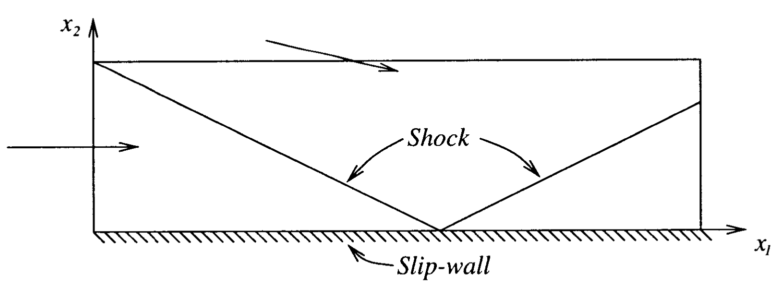

Figure 3-6: Two dimensional reflecting shock problem.

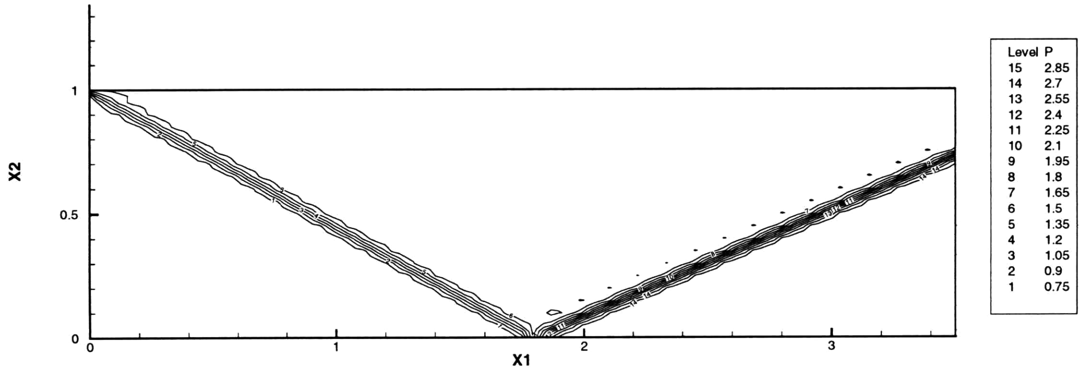

Figure 3-7: Solution of the two dimensional reflecting shock problem.

The boundary conditions are

$$
\begin{aligned}
\text{left}: &\quad M = 2.9, \rho = 1, v_1 = 2.9, v_2 = 0 \\
\text{top}: &\quad M = 2.3781, \rho = 1.7, v_1 = 2.61934, v_2 = -0.50632 \\
\text{bottom}: &\quad v_2 = 0
\end{aligned}
$$

Note that the boundary condition corresponding to the top boundary is imposed to the upper left corner. The numerical result is shown is fig. 3-7. Fig. 3-7 shows that the shock developed at the left upper corner due to the jump in the imposed boundary conditions is reflected by the lower boundary.

3.2.5 Time discretization

The result of the finite element space discretization of a fluid flow problem gives

$$\mathbf{M}\mathbf{U}_{,t} + \mathcal{K}\mathbf{U} = \mathbf{R}$$

where $\mathbf{M}$ is the mass matrix, $\mathcal{K}$ is the coefficient matrix and $\mathbf{R}$ is the loading vector. Many researchers [16, 17, 18, 19, 41, 42, 43] used the Taylor expansion for the time discretization; but here, the Euler backward method, which is an implicit method, is used for the time discretization so that a relatively large time step can be used without loss of stability. In an implicit method, the size of the time step does not depend on a stability consideration, but only depends on accuracy considerations (and convergence in the iterations) [5]. When we calculate the steady state solution of a problem, the solution can be obtained with fewer time step iterations using an implicit method than using an explicit method. Using the Euler backward method, we have

$$\mathbf{M}\frac{1}{\Delta t}({}^{t+\Delta t}\mathbf{U} - {}^{t}\mathbf{U}) + {}^{t+\Delta t}\mathcal{K}^{t+\Delta t}\mathbf{U} = {}^{t+\Delta t}\mathbf{R}$$

Note that the $\mathbf{M}$ matrix does not depend on the solution, while the $\mathcal{K}$ matrix is a nonlinear matrix which depends on the solution at time $t + \Delta t$.

The Euler backward method is theoretically stable, regardless of the size of the time step. However, iteration is required to obtain the solution of the nonlinear problem for each time step. A large time step which is still acceptable for the implicit method might result into iteration convergence difficulties. For practical problems, too large a time step makes the iteration process diverge, hence a resonable size time step is required.

3.2.6 Initial and boundary condition treatment

Well-posedness of initial and boundary conditions is very crucial for the problem considered. The treatment of boundary conditions is very important for a reliable solution. If the boundary conditions are treated explicitly, the limitations on the CFL[1] make the algorithm inefficient; therefore the boundary conditions have to be evaluated implicitly in order for the implicit scheme to be stable at high CFL numbers.

The boundary conditions require that $\Gamma_u + \Gamma_f = \Gamma$ and $\Gamma_u \cap \Gamma_f = \emptyset$, where Γ_u is the surface boundary where the essential boundary condition is applied, Γ_f is the surface boundary where the natural boundary condition is applied and Γ is the complete boundary surface. Here, we will discuss some boundary conditions which are commonly used in practice.

[1]Courant, Friedrichs, Lewy number; CFL=$\frac{V\Delta t}{h}$

Natural boundary conditions

Using integration by parts for the diffusive terms results into the diffusive boundary loading term, $\mathbf{F}_d$. The boundary loading term $\mathbf{F}_d$ is

$$\mathbf{F}_d = \begin{bmatrix} 0 \\ f_1^s \\ f_2^s \\ cf_1^s v_1 + cf_2^s v_2 - cq^s \end{bmatrix}$$

where c is the constant obtained by the non-dimensionalization, see section 3.1; f_i^s is the surface traction excluding the pressure term, v_i is the velocity in the x_i-direction and q^s is the heat flux. The surface traction f_i^s is defined as

$$f_i^s = [\lambda v_{l,l}\delta_{ij} + \mu(v_{i,j} + v_{j,i})]\ n_j \tag{3.19}$$

where n_j is the component of the normal vector on the boundary surface S pointing outward the domain. The last element in $\mathbf{F}_d$ consists of the work done by the surface tractions and the surface heat transfer. The heat transfer on the boundary S is

$$q^s = -k\theta_{,j}\ n_j \tag{3.20}$$

Revisiting the non-dimensionalized variables, the non-dimensional boundary surface traction in the x_i-direction is

$$\begin{aligned} f_i^{s*} &= (\lambda^* v^*_{k,k^*}\delta_{ij} + \mu^*(v^*_{i,j^*} + v^*_{j,i^*}))\ n_j \\ &= (\lambda v_{k,k}\delta_{ij} + \mu(v_{i,j} + v_{j,i}))\ n_j \frac{1}{\rho_o V_o^2} \\ &= \frac{f_i^s}{\rho_o V_o^2} \end{aligned}$$

and the non-dimensional boundary surface heat transfer is

$$q^{s*} = -k^*\theta^*_{,j^*}\ n_j$$

$$
\begin{aligned}
&= -k\theta_{,j}\, n_j \frac{1}{\rho_o V_o E_o} \\
&= \frac{q^s}{\rho_o V_o E_o}
\end{aligned}
$$

A problem contains the following natural boundary conditions:

- surface traction $f_i^s = h_i$
- heat flux $q^s = h_t$

where h_i and h_t are the given informations. If h_i and/or h_t are unknown, we can calculate their values using eqns. (3.19) and (3.20) from the current solution $\mathbf{U}_h$ on the boundary.

Some problems have a symmetry condition in which case, $u_n = 0$ and $\frac{\partial \theta}{\partial n} = 0$, resulting into $h_1 = h_2 = 0$ and $h_t = 0$.

Essential boundary conditions

The essential boundary conditions on the surface S_u are applied when all, or some of the solution variables which are density, mass flow in the x_1-direction, mass flow in the x_2-direction, and the total energy are prescribed. These boundary conditions can be applied using the penalty method, or just setting the variables to their prescribed values and eliminating the corresponding unknown equations from the solution process. The latter method is recommended because it is more efficient. It reduces the number of global equations to be solved.

No-slip wall with prescribed temperature condition

The no-slip wall condition with precribed temperature is a common boundary condition in physical problems. For the incompressible flow formulation with temperature as one of the solution variables, the prescribed temperature condition is an essential boundary condition. However, for the compressible flow formulation, temperature is not one of the solution variables. A special procedure should be used to prescribe temperature in the compressible flow formulation.

Consider the constitutive relation for temperature,

$$\theta = \frac{E - \frac{1}{2}(v_1^2 + v_2^2)}{c_v}$$

When the temperature is prescribed, $\theta = \theta_c$, the constraint equation to be satisfied by the solution variables is

$$c_v\theta_c(\rho) + \frac{v_1}{2}(\rho v_1) + \frac{v_2}{2}(\rho v_2) - (\rho E) = 0$$

The velocity is zero on the wall, therefore the constraint equation to prescribe the temperature becomes

$$c_v\theta_c(\rho) - (\rho E) = 0 \tag{3.21}$$

Now consider the energy conservation equation,

$$\begin{aligned}(\rho E)_{,t} + \{\rho E v_j + v_j(\gamma - 1)\rho(E - \frac{1}{2}v_l^2) - v_j\lambda v_{l,l} - v_i\mu(v_{i,j} + v_{j,i}) \\ -\frac{k}{c_v}(E - \frac{1}{2}v_l^2)_{,j}\}_{,j} - \rho v_i f_i^B - \rho q^B &= 0 \quad (3.22)\end{aligned}$$

Applying the Galerkin procedure to eqn. (3.22) weighted with virtual total energy and using integration by parts on the convective and diffusive terms, we obtain

$$\begin{aligned}\int_{Vol}(\overline{\rho E})\{(\rho E)_{,t} - \rho v_i f_i^B - \rho q^B\} + (\overline{\rho E})_{,j}\{-\rho E v_j - v_j(\gamma - 1)\rho(E - \frac{1}{2}v_l^2) + v_j\lambda v_{l,l} \\ +v_i\mu(v_{i,j} + v_{j,i}) + \frac{k}{c_v}(E - \frac{1}{2}v_l^2)_{,j}\}\, dVol = \int_S(\overline{\rho E})^s\{-F_{c4} + F_{d4}\}\, dS\end{aligned}$$

where $\overline{\rho E}$ is the virtual total energy and F_{c4} is the convective boundary condition,

$$F_{c4} = \left[\rho E v_j + v_j(\gamma - 1)\rho(E - \frac{1}{2}v_l^2)\right] n_j$$

where n_j is component of the boundary surface normal vector. F_{d4} is the diffusive boundary term,

$$F_{d4} = \left[-v_j \lambda v_{l,l} - v_i \mu (v_{i,j} + v_{j,i}) - \frac{k}{c_v}(E - \frac{1}{2}v_l^2)_{,j} \right] n_j$$

F_{d4} consists of heat transfer and the work done by the surface tractions on the boundary. On the wall, the velocity is zero so that $F_{c4} = 0$ and

$$F_{d4} = -\frac{k}{c_v}(E - \frac{1}{2}v_l^2)_{,j} n_j = q^s$$

which is the heat transfer on the surface. As in the incompressible flow formulation, when the temperature is prescribed, the heat transfer on the boundary is unknown. The procedure for the no-slip wall boundary condition with prescribed temperature is to calculate the unknown surface heat transfer q^s and apply the Galerkin procedure on the constraint equation (eqn. (3.21)) weighted with the virtual surface heat transfer $\overline{q^s}$. Hence, we have

$$\begin{aligned} \int_{Vol} (\overline{\rho E}) \{ (\rho E)_{,t} - \rho v_i f_i^B - \rho q^B \} + (\overline{\rho E})_{,j} \{ -\rho E v_j - v_j(\gamma - 1)\rho(E - \frac{1}{2}v_l^2) \\ + v_j \lambda v_{l,l} + v_i \mu (v_{i,j} + v_{j,i}) + \frac{k}{c_v}(E - \frac{1}{2}v_l^2)_{,j} \} \, dVol - \int_S (\overline{\rho E})^s \, q^s \, dS &= 0 \end{aligned}$$

and

$$\int_S (\overline{q^s}) \{ c_v \theta_c(\rho) - (\rho E) \} dS = 0$$

When upwinding and shock capturing terms are considered, we modify the energy conservation equation expressed in the above equation by adding these additional terms.

Note that the Lagrange multiplier method should not be used to prescribed the temperature in the compressible flow formulation because the method will affect the mass conservation equation and will create mass a source on the wall, see Appendix C for more details.

Impermeable slip-wall boundary condition

The slip-wall boundary condition on surface S_w requires that there is no net mass flow going through the boundary. This boundary condition specifies that the integral of the mass flow in the normal direction in the surface S_w to be zero which will result in no net mass flow pass through the boundary [38]. For example, at node k on surface S_w as shown in fig. 3-8, the slip-wall boundary condition gives the following constraint equation

$$\int_{S_a+S_b} (\widehat{\rho v_n})^k dS = \int_{S_a} (\widehat{\rho v_j})^k \, n_{aj} \, dS + \int_{S_b} (\widehat{\rho v_j})^k \, n_{bj} \, dS = 0 \tag{3.23}$$

where v_n is the velocity in the normal direction of the boundary surface; $(\widehat{\rho v_1})^k$, $(\widehat{\rho v_2})^k$ are the unknown mass flow variables at the node k; n_{ja}, n_{jb} are the normal vector components of element boundaries a and b; S_a, S_b are the surfaces of elements a and b. We define r_a, r_b to be the local coordinate systems for the surface elements a and b, see respectively fig. 3-8. For a linear element, the interpolation functions for $(\rho v_j)^k$ of elements a and b are

$$h_a = \frac{1}{2}(1 + r_a) \qquad\qquad h_b = \frac{1}{2}(1 - r_b)$$

The normal vector of the boundary surface is defined as

$$\vec{n} dS = (\frac{\partial y}{\partial r} dr, -\frac{\partial x}{\partial r} dr)$$

where x and y are the coordinates of the boundary surface and r is the surface local coordinate system. Using the interpolation functions and the normal vector definition, eqn. (3.23) becomes

$$\int_{Sa} \{h_a \frac{\partial y_a}{\partial r_a} (\widehat{\rho v_1})^k - h_a \frac{\partial x_a}{\partial r_a} (\widehat{\rho v_2})^k\} dr_a + \int_{Sb} \{h_b \frac{\partial y_b}{\partial r_b} (\widehat{\rho v_1})^k - h_b \frac{\partial x_b}{\partial r_b} (\widehat{\rho v_2})^k\} dr_b = 0$$

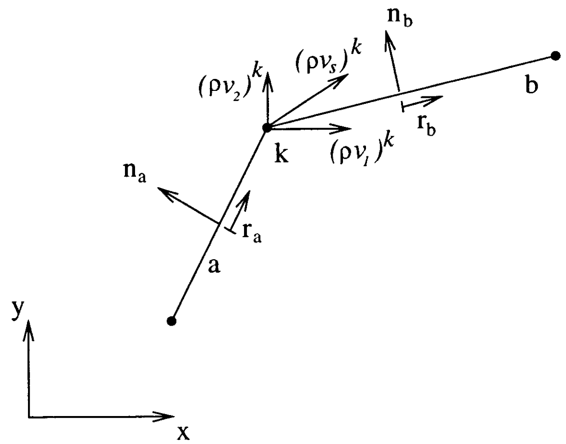

Figure 3-8: Node k of linear element on the surface S_w.

Collecting the terms, the constraint equation becomes

$$\left[\int_{Sa} h_a \frac{\partial y_a}{\partial r_a}\, dr_a + \int_{Sb} h_b \frac{\partial y_b}{\partial r_b}\, dr_b\right] (\widehat{\rho v_1})^k - \left[\int_{Sa} h_a \frac{\partial x_a}{\partial r_a}\, dr_a + \int_{Sb} h_b \frac{\partial x_b}{\partial r_b}\, dr_b\right] (\widehat{\rho v_2})^k = 0 \tag{3.24}$$

The terms in the brackets can be calculated since the geometry of the boundary surface is known.

The constraint equation is imposed using the Lagrange multiplier method [5]. Writing eqn. (3.24) in matrix form, we have

$$\mathbf{B}\mathbf{U}_k = 0$$

where $\mathbf{U}_k^T = \left[(\widehat{\rho v_1})^k, (\widehat{\rho v_2})^k\right]$. let $\mathbf{K}$ be the global coefficient matrix and $\mathbf{R}$ be the global load vector corresponding to the nodal variables $\mathbf{U}_k$. The Lagrange multiplier method to impose the constraint equation (3.24) is

$$\begin{bmatrix} \mathbf{K} & \mathbf{B}^T \\ \mathbf{B} & 0 \end{bmatrix} \begin{bmatrix} \mathbf{U}_k \\ \lambda_k \end{bmatrix} = \begin{bmatrix} \mathbf{R} \\ 0 \end{bmatrix}$$

where λ_k is an additional variable corresponding to node k.

The procedure explained above is performed for all nodes on the slip-wall boundary

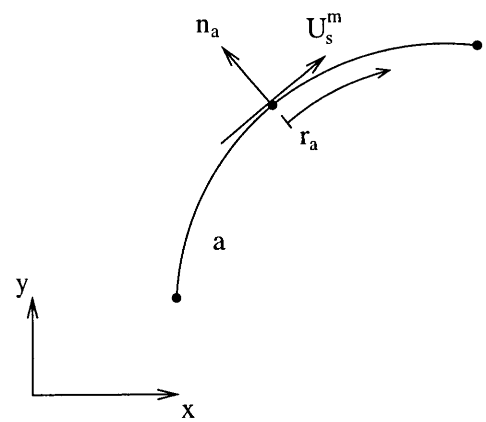

Figure 3-9: Middle node m of a quadratic element on the surface S_w.

surface S_w. For each node, the Lagrange multiplier method introduces an additional variable to be calculated; hence the total number of additional variables equals the number of nodes on the boundary surface S_w.

For the quadratic element, the same procedure is applied with different interpolation functions

$$h_a = \frac{1}{2} r_a (1 + r_a) \qquad\qquad h_b = \frac{-1}{2} r_b (1 - r_b)$$

Also for the quadratic element, there is an element middle node, see fig. 3-9. The constraint equation for the middle node m is

$$\int_{Sa} h_m \frac{\partial y_a}{\partial r_a}\, dr_a \;\; (\widehat{\rho v_1})^m - \int_{Sa} h_m \frac{\partial x_a}{\partial r_a}\, dr_a \;\; (\widehat{\rho v_2})^m = 0 \tag{3.25}$$

where h_m is the interpolation function

$$h_m = 1 - r_a^2$$

The Lagrange multiplier method is also used to impose this constraint equation (eqn. (3.25)).

Open-flow boundary condition

Applying integration by parts to the convective terms results in the convective boundary loading term $\mathbf{F}_c$. The boundary where we need to prescribe $\mathbf{F}_c$ is often called an open-flow boundary. The treatment of the open-flow boundary condition should be consistent with the theory of characteristics [2] to correctly impose the required wave propagations. For this, it is necessary to use the eigenvalues and eigenvectors of the convective matrix $\mathbf{A}_j$. Consider the following eigenproblem of $\mathbf{A}_j$,

$$\mathbf{A}_j \mathbf{x}_{ji} = \lambda_{ji} \mathbf{x}_{ji} \tag{3.26}$$

where $\mathbf{x}_{ji}$ is the i^{th} eigenvector of the matrix $\mathbf{A}_j$ and λ_{ji} is the corresponding eigenvalue. The solution of the eigenproblem (3.26) yields the eigenpairs $(\lambda_{ji}, \mathbf{x}_{ji})$, $i = 1, .., 4$, and the complete eigenproblem solution can be written as

$$\mathbf{A}_j \mathbf{X}_j = \mathbf{X}_j \boldsymbol{\Lambda}_j$$

where $\mathbf{X}_j$ is the matrix of the eigenvectors, $\mathbf{X}_j = [\mathbf{x}_{j1}, .., \mathbf{x}_{j4}]$, and $\boldsymbol{\Lambda}_j$ is a diagonal matrix of the corresponding eigenvalues, $\boldsymbol{\Lambda}_j = \text{diag}(\lambda_{j1}, \lambda_{j2}, \lambda_{j3}, \lambda_{j4})$. The eigenvectors are associated with the transformation of the wave quantities into the original variables and the eigenvalues are associated with the velocity of wave propagations.

The eigenvalues and eigenvectors of the Jacobian matrix $\mathbf{A}_1$ are

$$\boldsymbol{\Lambda}_1 = \begin{bmatrix} v_1 & 0 & 0 & 0 \\ 0 & v_1 & 0 & 0 \\ 0 & 0 & v_1 + a & 0 \\ 0 & 0 & 0 & v_1 - a \end{bmatrix}$$

$$\mathbf{X}_1 = \begin{bmatrix} 0 & 1 & 1 & 1 \\ 0 & v_1 & v_1 + a & v_1 - a \\ 1 & 0 & v_2 & v_2 \\ v_2 & \frac{1}{2}(v_1^2 - v_2^2) & H + v_1 a & H - v_1 a \end{bmatrix}$$

and for $\mathbf{A}_2$ are

$$\mathit{\Lambda}_2 = \begin{bmatrix} v_2 & 0 & 0 & 0 \\ 0 & v_2 & 0 & 0 \\ 0 & 0 & v_2 + a & 0 \\ 0 & 0 & 0 & v_2 - a \end{bmatrix}$$

$$\mathbf{X}_2 = \begin{bmatrix} 0 & 1 & 1 & 1 \\ 1 & 0 & v_1 & v_1 \\ 0 & v_2 & v_2 + a & v_2 - a \\ v_1 & \frac{1}{2}(-v_1^2 + v_2^2) & H + v_2 a & H - v_2 a \end{bmatrix}$$

where a and H are the sound speed and the total enthalpy; $a = \sqrt{(\gamma - 1)\gamma(E - \frac{1}{2}(v_1^2 + v_2^2))}$, $H = \gamma E - (\gamma - 1)\frac{1}{2}(v_1^2 + v_2^2)$.

Consider the convective boundary loading term

$$\mathbf{F}_c = \vec{\mathbf{F}} \cdot \vec{n} = \mathbf{F}_1 n_1 + \mathbf{F}_2 n_2$$

where n_1 and n_2 are the components of the normal vector of the boundary surface pointing outward of the domain. Introducing (n, s) as a local coordinate system at the boundary surface where n is in the normal direction and s is in the tangential direction, the convective boundary flux can be written as

$$\mathbf{F}^n = \begin{bmatrix} \rho v_n \\ \rho v_n^2 + p \\ \rho v_n v_s \\ \rho v_n H \end{bmatrix}$$

Here v_n is the velocity component in the normal direction (positive when its direction is pointing outward of the domain) and v_s is the velocity component in the tangential direction. The convective boundary loading $\mathbf{F}_c$ can be related to the boundary flux

$\mathbf{F}^n$ by a transformation coordinates such that

$$\mathbf{F}^n = \mathbf{T}\mathbf{F}_c$$

where $\mathbf{T}$ is the transformation matrix

$$\mathbf{T} = \begin{bmatrix} 1 & 0 & 0 & 0 \\ 0 & n_1 & n_2 & 0 \\ 0 & s_1 & s_2 & 0 \\ 0 & 0 & 0 & 1 \end{bmatrix}$$

with s_1, s_2 to be the components of the tangential vector of the boundary surface. Note that $\mathbf{T}^{-1} = \mathbf{T}^T$ which is coming from the fact that $\vec{n}$ is perpendicular to $\vec{s}$. We also have

$$\mathbf{U}^n = \mathbf{T}\mathbf{U}$$

where $\mathbf{U}^{nT} = [\rho, \rho v_n, \rho v_s, \rho E]$. The characteristic wave propagation at the boundary can be analyzed by considering the one-dimensional Euler equations in the normal direction,

$$\frac{\partial \mathbf{U}^n}{\partial t} + \frac{\partial \mathbf{F}^n}{\partial n} = 0$$

and the quasi-linear form of the above equation can be written as

$$\frac{\partial \mathbf{U}^n}{\partial t} + \mathbf{A}_n \frac{\partial \mathbf{U}^n}{\partial n} = 0$$

where $\mathbf{A}_n = \frac{\partial \mathbf{F}^n}{\partial \mathbf{U}^n}$. The eigenvalues and eigenvectors of the Jacobian matrix $\mathbf{A}_n$ are

$$\boldsymbol{\Lambda}_n = \begin{bmatrix} v_n & 0 & 0 & 0 \\ 0 & v_n & 0 & 0 \\ 0 & 0 & v_n + a & 0 \\ 0 & 0 & 0 & v_n - a \end{bmatrix}$$

$$\mathbf{X}_n = \begin{bmatrix} 0 & 1 & 1 & 1 \\ 0 & v_n & v_n + a & v_n - a \\ 1 & 0 & v_s & v_s \\ v_s & \frac{1}{2}(v_n^2 - v_s^2) & H + v_n a & H - v_n a \end{bmatrix}$$

Decomposing $\mathbf{A}_n$ ($\mathbf{A}_n = \mathbf{X}_n \boldsymbol{\Lambda}_n \mathbf{X}_n^{-1}$) and multiplying the equation by $\mathbf{X}_n^{-1}$, we have

$$\mathbf{X}_n^{-1} \frac{\partial \mathbf{U}^n}{\partial t} + \boldsymbol{\Lambda}_n \mathbf{X}_n^{-1} \frac{\partial \mathbf{U}^n}{\partial n} = 0$$

Defining $\mathbf{W} = \mathbf{W}(\mathbf{U}^n)$ such that

$$\frac{\partial \mathbf{W}}{\partial \mathbf{U}^n} = \mathbf{X}_n^{-1}$$

we obtain

$$\frac{\partial \mathbf{W}}{\partial t} + \boldsymbol{\Lambda}_n \frac{\partial \mathbf{W}}{\partial n} = 0$$

Note that $\boldsymbol{\Lambda}_n$ is $\mathrm{diag}(\lambda_1, \lambda_2, \lambda_3, \lambda_4)$ where $\lambda_{1,2} = v_n, \lambda_3 = v_n + a, \lambda_4 = v_n - a$, and a is the sonic speed; $\mathbf{W}^T = [w_1, w_2, w_3, w_4]$ is the vector containing the wave quantities. The direction of the wave corresponding to w_i at the boundary is indicated by the value of λ_i. When $\lambda_i < 0$, the wave is entering the domain and when $\lambda_i > 0$, the wave is leaving the domain. For a well-posed problem, the entering wave quantity needs to be specified, whereas the leaving wave quantity should not be specified. Some cases of the openflow boundary conditions are

- on supersonic inflow, all λ_is are less than zero, so all w_is need to be specified.
- on supersonic outflow, all λ_is are greater than zero, so no w_i should be specified.
- on subsonic inflow, three λ_is are less than zero and another one is greater than zero, therefore the three w_i corresponding to $\lambda_i < 0$ need to be specified.
- on subsonic outflow, three λ_i are greater than zero and another one is less than zero, therefore the one w_i corresponding to $\lambda_i < 0$ needs to be specified.

The flux splitting method can be used to impose an openflow boundary condition. The method correctly specifies the entering waves calculated from a specified farfield boundary condition $\mathbf{U}_\infty$ and does not modify the leaving waves. The convective boundary flux using the flux splitting method is

$$\begin{aligned}\mathbf{F}^n &= \mathbf{F}_{in}(\mathbf{U}^n_\infty) + \mathbf{F}_{out}(\mathbf{U}^n) \\ &= \frac{1}{2}\left[\mathbf{F}^n(\mathbf{U}^n_\infty) + \mathbf{F}^n(\mathbf{U}^n)\right] - \frac{1}{2}|\mathbf{A}_n|(\mathbf{U}^n_\infty - \mathbf{U}^n)\end{aligned}$$

where $\mathbf{U}^{nT}_\infty = [\rho_\infty, \rho v_{n\infty}, \rho v_{s\infty}, \rho E_\infty]$ is the specified farfield boundary condition and $\mathbf{U}^{nT} = [\rho, \rho v_n, \rho v_s, \rho E]$ is the solution to be calculated at the boundary. The flux splitting method relies on the absolute value of the matrix $\mathbf{A}_n$ which will automatically select the entering waves and specify them by the given farfield condition $\mathbf{U}^n_\infty$. This can be shown by linearizing the problem such that $\mathbf{F}^n(\mathbf{U}^n_\infty) = \mathbf{A}_n\mathbf{U}^n_\infty$ and $\mathbf{F}^n(\mathbf{U}^n) = \mathbf{A}_n\mathbf{U}^n$ and decomposing the matrix $\mathbf{A}_n$. Hence we have

$$\begin{aligned}\mathbf{F}^n &= \frac{1}{2}\{\mathbf{X}_n\boldsymbol{\Lambda}_n\mathbf{X}_n^{-1}\mathbf{U}^n_\infty + \mathbf{X}_n\boldsymbol{\Lambda}_n\mathbf{X}_n^{-1}\mathbf{U}^n - \mathbf{X}_n|\boldsymbol{\Lambda}_n|\mathbf{X}_n^{-1}(\mathbf{U}^n_\infty - \mathbf{U}^n)\} \\ &= \frac{1}{2}\mathbf{X}_n(\boldsymbol{\Lambda}_n - |\boldsymbol{\Lambda}_n|)\mathbf{X}_n^{-1}\mathbf{U}^n_\infty + \frac{1}{2}\mathbf{X}_n(\boldsymbol{\Lambda}_n + |\boldsymbol{\Lambda}_n|)\mathbf{X}_n^{-1}\mathbf{U}^n \qquad (3.27)\end{aligned}$$

When λ_i is positive, which corresponds to a leaving wave, the first term in eqn. (3.27) is zero, therefore w_i is only a function of $\mathbf{U}^n$. On the other hand, when λ_i is negative which corresponds to an entering wave, the second term in eqn. (3.27) is zero, therefore w_i is only a function of $\mathbf{U}^n_\infty$.

To obtain better convergence for an implicit method, Luo et al. [12] proposed to use Roe's flux-difference splitting [39] to evaluate the convective boundary fluxes,

$$\mathbf{F}^n = \frac{1}{2}\left[\mathbf{F}^n(\mathbf{U}^n_\infty) + \mathbf{F}^n(\mathbf{U}^n)\right] - \frac{1}{2}|\mathbf{A}_n(\mathbf{U}^n_R)|(\mathbf{U}^n_\infty - \mathbf{U}^n)$$

where $\mathbf{U}^n_R$ is the Roe's average value of $\mathbf{U}^n$ [39, 40] on the boundary. The important property of the matrix $\mathbf{A}_n(\mathbf{U}^n_R)$ is that

$$\mathbf{A}_n(\mathbf{U}^n_R)\{\mathbf{U}^n_\infty - \mathbf{U}^n\} = \mathbf{F}^n(\mathbf{U}^n_\infty) - \mathbf{F}^n(\mathbf{U}^n)$$

where $\mathbf{U}_R^{nT} = [\rho_R, \rho_R v_{nR}, \rho_R v_{sR}, \rho_R E_R]$ and from [39, 40], we have

$$
\begin{aligned}
\rho_R &= \sqrt{\rho_\infty \rho} \\
v_{nR} &= \frac{v_{n\infty}\sqrt{\rho_\infty} + v_n\sqrt{\rho}}{\sqrt{\rho_\infty} + \sqrt{\rho}} \\
v_{sR} &= \frac{v_{s\infty}\sqrt{\rho_\infty} + v_s\sqrt{\rho}}{\sqrt{\rho_\infty} + \sqrt{\rho}} \\
H_R &= \frac{H_\infty\sqrt{\rho_\infty} + H\sqrt{\rho}}{\sqrt{\rho_\infty} + \sqrt{\rho}}
\end{aligned}
$$

and we also have the relation $a_R^2 = (\gamma - 1)\{H_R - \frac{1}{2}(v_{nR}^2 + v_{sR}^2)\}$. Relating the characteristic wave propagation analysis at the boundary to the convective boundary loading $\mathbf{F}_c$, we have the following equation

$$
\begin{aligned}
\mathbf{F}_c &= \mathbf{T}^T\mathbf{F}^n \\
&= \mathbf{T}^T\left[\frac{1}{2}\{\mathbf{F}^n(\mathbf{U}_\infty^n) + \mathbf{F}^n(\mathbf{U}^n)\} - \frac{1}{2}|\mathbf{A}_n(\mathbf{U}_R^n)|(\mathbf{U}_\infty^n - \mathbf{U}^n)\right] \\
&= \mathbf{T}^T\left[\frac{1}{2}\{\mathbf{T}\mathbf{F}_c(\mathbf{U}_\infty) + \mathbf{T}\mathbf{F}_c(\mathbf{U})\} - \frac{1}{2}|\mathbf{A}_n(\mathbf{U}_R^n)|\mathbf{T}(\mathbf{U}_\infty - \mathbf{U})\right] \\
&= \frac{1}{2}\{\mathbf{F}_c(\mathbf{U}_\infty) + \mathbf{F}_c(\mathbf{U})\} - \frac{1}{2}\mathbf{T}^T|\mathbf{A}_n(\mathbf{U}_R^n)|\mathbf{T}(\mathbf{U}_\infty - \mathbf{U}) \\
&= \frac{1}{2}\{\mathbf{F}_1(\mathbf{U}_\infty)n_1 + \mathbf{F}_2(\mathbf{U}_\infty)n_2 + \mathbf{A}_1(\mathbf{U})n_1\mathbf{U} + \mathbf{A}_2(\mathbf{U})n_2\mathbf{U} \\
&\quad -\mathbf{T}^T|\mathbf{A}_n(\mathbf{U}_R^n)|\mathbf{T}(\mathbf{U}_\infty - \mathbf{U})\}
\end{aligned}
$$

Note that $|\mathbf{A}_n(\mathbf{U}_R^n)| = \mathbf{X}_n(\mathbf{U}_R^n)|\boldsymbol{\Lambda}_n(\mathbf{U}_R^n)|\mathbf{X}_n^{-1}(\mathbf{U}_R^n)$. Here, $\mathbf{U}_\infty^T = [\rho_\infty, \rho v_{1\infty}, \rho v_{2\infty}, \rho E_\infty]$

The finite element boundary condition for the convective boundary load term using Roe's flux-difference splitting method is

$$
\begin{aligned}
\int_S \mathbf{W}^s\,\mathbf{F}_c\,dS &= \int_S \mathbf{W}^s\,\frac{1}{2}\{\mathbf{F}_1(\mathbf{U}_\infty)n_1 + \mathbf{F}_2(\mathbf{U}_\infty)n_2 - \mathbf{T}^T|\mathbf{A}_n(\mathbf{U}_R^n)|\mathbf{T}\mathbf{U}_\infty\}\,dS \\
&\quad + \int_S \mathbf{W}^s\,\frac{1}{2}\{\mathbf{A}_1(\mathbf{U}_h)n_1 + \mathbf{A}_2(\mathbf{U}_h)n_2 + \mathbf{T}^T|\mathbf{A}_n(\mathbf{U}_R^n)|\mathbf{T}\}\mathbf{U}_h\,dS
\end{aligned}
$$

To incorporate these terms in the implicit method, we include the first integral term in the load vector and the second integral term in the coefficient matrix. Note that the first integral term is also a function of $\mathbf{U}_h$, through $\mathbf{U}_R$, but for simplicity, we include the first integral term in the load vector.

When all the farfield conditions are known, such as density, velocity and pressure, we can evaluate $\mathbf{U}_\infty$ from the given values. However, when we are only given a partial farfield condition, such as only pressure, or temperature, we need to evaluate $\mathbf{U}_\infty$ based on the characteristic theory. For example, for the subsonic outlet, three waves are leaving the domain and only one (corresponding to w_4) is entering the domain. Therefore we need to specify w_4 to have a well-posed problem. To calculate the correct value for w_4, we need to use the given constraint variable such as pressure or temperature.

For the subsonic outlet with prescribed pressure, we have

$$\begin{bmatrix} \rho_\infty \\ \rho v_{n\infty} \\ \rho v_{s\infty} \\ \rho E_\infty \end{bmatrix} = \begin{bmatrix} \rho \\ \rho v_n \\ \rho v_s \\ \rho E \end{bmatrix} + \begin{bmatrix} 1 \\ v_n - a \\ v_s \\ H - v_n a \end{bmatrix} w_4 \tag{3.28}$$

The right hand side terms of the above equation are evaluated from the solution $\mathbf{U}_h$ at the boundary except w_4 which is the variable to be calculated. The vector coefficient in front of w_4 in the above equation is the eigenvector corresponding to w_4. When the pressure at the farfield condition is prescribed, we have from the constitutive relation

$$p_\infty = (\gamma - 1)\{\rho E_\infty - \frac{1}{2}\frac{(\rho v_{l\infty})^2}{\rho_\infty}\}$$

or,

$$\frac{p_\infty}{(\gamma-1)} = \rho E + (H - v_n a) w_4 - \frac{1}{2}\left[\frac{\{\rho v_n + (v_n - a) w_4\}^2 + \{\rho v_s + v_s w_4\}^2}{\rho + w_4}\right]$$

We can solve the above equation for w_4 analytically. The above equation has two w_4 solutions and we take the one of smaller magnitude. With given w_4, we can then calculate the farfield condition corresponding to the subsonic outlet with prescribed pressure by using eqn. (3.28). This boundary condition has to be imposed iteratively.

For the subsonic outlet with prescribed temperature, the procedure is similar to the one with prescribed pressure; however, we use the temperature constitutive relation to calculate w_4. We have

$$
\begin{aligned}
c_v\theta_\infty &= E_\infty - \frac{1}{2}v_{l\infty}^2 \\
&= \frac{\rho E_\infty}{\rho_\infty} - \frac{1}{2}\frac{(\rho v_{l\infty})^2}{\rho_\infty^2} \\
&= \frac{\rho E + (H - v_n a)w_4}{\rho + w_4} - \frac{1}{2}\left[\frac{\{\rho v_n + (v_n - a)w_4\}^2 + \{\rho v_s + v_s w_4\}^2}{(\rho + w_4)^2}\right]
\end{aligned}
$$

We solve the above equation for w_4 analytically. As in the case of the prescribed pressure, the above equation has two solutions for w_4 and we take the one of smaller magnitude. With this value of w_4, we can calculate the farfield condition corresponding to the subsonic outlet with prescribed temperature using eqn. (3.28).

At the subsonic inlet, there are three waves entering the domain which need to be specified in order to have a well-posed problem. Therefore, we can specify only three variables of the farfield condition. Let us consider two sets of variables specified on this boundary,

- prescribing: $\rho v_{n\infty}, \rho v_{s\infty}$ and temperature θ_∞, or
- prescribing: $\rho v_{n\infty}, \rho v_{s\infty}$ and pressure

It would be complicated to use the same procedure as for the subsonic outlet condition since for the subsonic inlet, we prescribe three variables. Instead, we proceed as follows. From observation, the density distribution does not change significantly close to the boundary. Therefore it is reasonable to assume that the density at the farfield condition is the same as the density of the solution, $\rho_\infty = \rho$. Hence, the farfield condition with prescribed $\rho v_n, \rho v_s$ and temperature θ_∞ is

$$
\begin{aligned}
\rho_\infty &= \rho \\
\rho v_{n\infty} &= \rho v_n \text{ (given)} \\
\rho v_{s\infty} &= \rho v_s \text{ (given)}
\end{aligned}
$$

$$\rho E_{\infty} = \rho c_v \theta_{\infty} + \frac{1}{2}\{\frac{(\rho v_{n\infty})^2 + (\rho v_{s\infty})^2}{\rho}\}$$

If the pressure is prescribed instead of the temperature, we calculate the total energy of the farfield condition as

$$\rho E_{\infty} = \frac{p_{\infty}}{(\gamma - 1)} + \frac{1}{2}\{\frac{(\rho v_{n\infty})^2 + (\rho v_{s\infty})^2}{\rho}\}$$

Based upon our numerical experiments, the procedure of prescribing three variables for the subsonic inlet given above performs well. For other combinations of specified variables, a similar procedure can be used.

Note that the procedure used here is similar to the procedure of the boundary treatment in the control volume method. In the control volume method, extra nodes outside the domain are used to calculate correct convective boundary fluxes. The farfield condition $\mathbf{U}_{\infty}$ is the condition at the "outside nodes" in the control volume method.

3.2.7 Numerical convergence study

The purpose of this numerical convergence study is to determine in an example solution the order of accuracy of the scheme proposed in this thesis.

Consider the problem described in fig. 3-10. The problem describes an inviscid supersonic flow over a slip-wall with controlled body forces and heat generation. The fluid properties are assumed to be constant, $R = 286, c_v = 715, k = \mu = 0$. The exact solution for this problem is

$$\begin{aligned}
\rho &= 1 - \frac{1}{2}x_1 x_2 \\
\rho v_1 &= 1 - x_1^4 \\
\rho v_2 &= 2 + 4x_1^3 x_2 \\
\rho E &= (6 + 12x_1^4 x_2)/(1 - \frac{1}{2}x_1 x_2)^2
\end{aligned}$$

The required body forces in x_1 and x_2-directions to satisfy the exact solutions can be

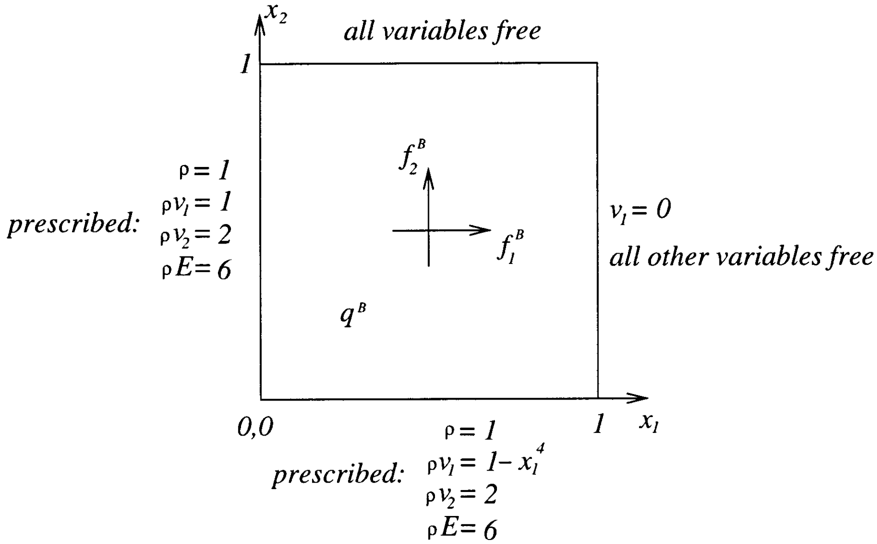

Figure 3-10: Convergence study problem.

calculated from the conservation of momentum equations. The heat generation, q^B, can be calculated from the conservation of energy equation.

We perform the convergence study using $8 \times 8, 16 \times 16$ and 32×32 uniform meshes. The errors measured are : $||\mathbf{U} - \mathbf{U}_h||_{L^2}$ and $||\mathbf{U} - \mathbf{U}_h||_{H^1}$. The result is shown in fig. 3-11. Fig. 3-11 shows that the slope of the solution error in the L^2-norm is 2.23 and in the H^1-norm is 1.03.

The solutions of this problem using 16×16 mesh are shown in fig. 3-12.

3.2.8 Conservation of flux

Conservation of flux means that the discrete formulation will not produce any spurious contributions to the quantities in the interior region. The conservation property is important to capture shocks. Consider our finite element formulation in eqn. (3.7). In order to investigate the global conservation of flux, consider the case when we set $\mathbf{W}_h = \mathbf{I}$ (we set all the virtual functions, density, mass flows and total energy, to be a constant 1), therefore we have [45]

$$\int_{Vol} (\mathbf{U}_{h,t} - \mathbf{S}\mathbf{U}_h) dVol = \int_S (-\mathbf{F}_c + \mathbf{F}_d) dS$$

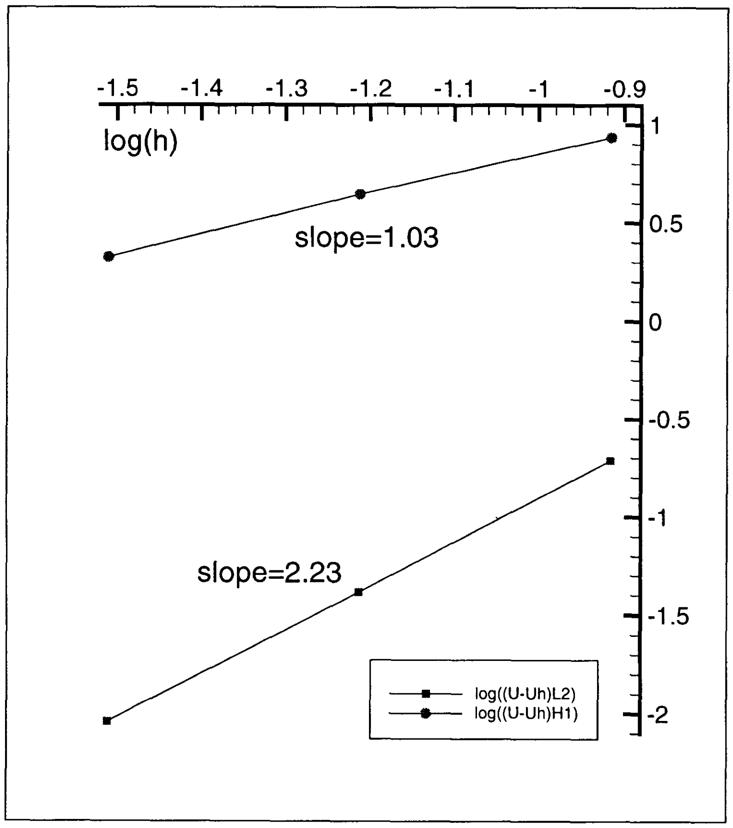

Figure 3-11: Error convergence for the problem.

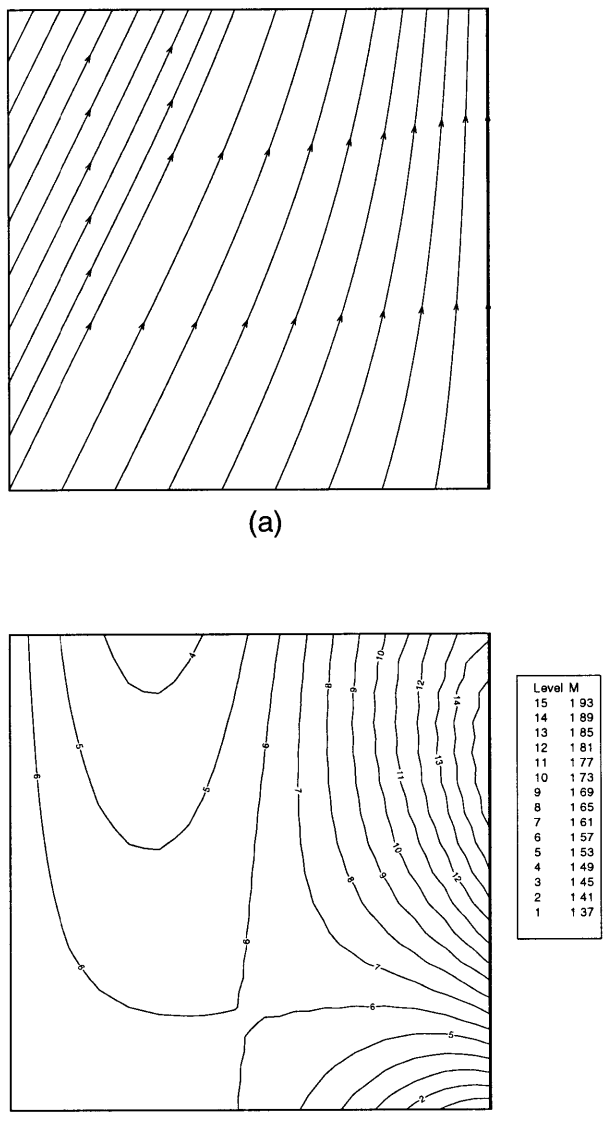

Figure 3-12: Solution of the convergence study problem, (a) streamline, (b) Mach number.

and if we consider a steady-state condition with no sources, we obtain

$$0 = \int_S (-\mathbf{F}_c + \mathbf{F}_d) dS$$

This confirms the conservation property for the case assumed.

Considering an individual element, the conservation of flux can be proved by the following argument. Let us define

$$\mathbf{W}_h = \begin{bmatrix} \overline{\rho} & 0 & 0 & 0 \\ 0 & \overline{\rho v_1} & 0 & 0 \\ 0 & 0 & \overline{\rho v_2} & 0 \\ 0 & 0 & 0 & \overline{\rho E} \end{bmatrix} = \widehat{\overline{\mathbf{U}}}^T \mathbf{H}^T$$

where $\widehat{\overline{\mathbf{U}}}$ is a vector containing the nodal values of the virtual variables and $\mathbf{H}$ is the interpolation matrix,

$$\widehat{\overline{\mathbf{U}}}^T = \begin{bmatrix} (\overline{\rho})_1 & \ldots & (\overline{\rho})_9 & 0 & \ldots & 0 & 0 & \ldots & 0 & 0 & \ldots & 0 \\ 0 & \ldots & 0 & (\overline{\rho v_1})_1 & \ldots & (\overline{\rho v_1})_9 & 0 & \ldots & 0 & 0 & \ldots & 0 \\ 0 & \ldots & 0 & 0 & \ldots & 0 & (\overline{\rho v_2})_1 & \ldots & (\overline{\rho v_2})_9 & 0 & \ldots & 0 \\ 0 & \ldots & 0 & 0 & \ldots & 0 & 0 & \ldots & 0 & (\overline{\rho E})_1 & \ldots & (\overline{\rho E})_9 \end{bmatrix}$$

and $(\overline{\rho})_k$, $(\overline{\rho v_1})_k$, $(\overline{\rho v_2})_k$, $(\overline{\rho E})_k$ are the nodal values of the virtual density, mass flow in x_1-direction, mass flow in x_2-direction and total energy at the node k. The matrix $\mathbf{H}$ is the matrix containing the interpolation functions for the virtual variables

$$\mathbf{H} = \begin{bmatrix} \mathbf{h} & \mathbf{0} & \mathbf{0} & \mathbf{0} \\ \mathbf{0} & \mathbf{h} & \mathbf{0} & \mathbf{0} \\ \mathbf{0} & \mathbf{0} & \mathbf{h} & \mathbf{0} \\ \mathbf{0} & \mathbf{0} & \mathbf{0} & \mathbf{h} \end{bmatrix}$$

and $\mathbf{h}$ is a vector of nodal interpolations

$$\mathbf{h} = [h_1, h_2, h_3, h_4, h_5, h_6, h_7, h_8, h_9]$$

where h_k is the interpolation function for node k.

Consider $\mathbf{U}_h$ to be the finite element solution obtained by solving eqn. (3.7). For element m, the nodal fluxes $\tilde{\mathbf{F}}_m$ obtained from the convective term are defined as follows

$$\tilde{\mathbf{F}}_m = \int_{Vol^{(m)}} \mathbf{H}^T_{,j}\, \mathbf{F}_j(\mathbf{U}_h) dVol^{(m)}$$

where $\mathbf{F}_j(\mathbf{U}_h)$ is the convective flux and its value is calculated from the known values $\mathbf{U}_h$. The sum of the nodal mass flows in the element m are obtained by adding all the mass flow components in the vector $\tilde{\mathbf{F}}_m$ therefore we have

Sum of nodal mass flows $\tilde{\mathbf{F}}_m$ in element m

$$\begin{aligned} &= [1, ..., 1, 0, ..., 0, 0, ..., 0, 0, ..., 0]\, \tilde{\mathbf{F}}_m \\ &= [1, ..., 1, 0, ..., 0, 0, ..., 0, 0, ..., 0] \int_{Vol^{(m)}} \mathbf{H}^T_{,j}\, \mathbf{F}_j(\mathbf{U}_h) dVol^{(m)} \\ &= 0 \end{aligned}$$

The sum of the mass flow $\tilde{\mathbf{F}}_m$ in the element m is zero therefore we can conclude that the convective term discretization in the element m does not give any spurious contribution of mass flows. With a similar procedure, we can also prove that the convective term discretization in the element m does not give any spurious contribution to the x_1-momentum, x_2-momentum, and energy fluxes. These results confirm the flux conservation on the element level. Also, let us define the nodal fluxes from the upwinding and shock capturing contribution $\tilde{\mathbf{D}}_m$ in the element m such that

$$\tilde{\mathbf{D}}_m = \int_{Vol^{(m)}} \mathbf{H}^T_{,jj}\, \mathbf{A}_j \boldsymbol{\tau}_j \mathbf{A}_j \mathbf{U}_{h,jj} dVol^{(m)} + \int_{Vol^{(m)}} \nu_j \mathbf{H}^T_{,j}\, \mathbf{U}_{h,j} dVol^{(m)}$$

The vector $(\mathbf{A}_j \boldsymbol{\tau}_j \mathbf{A}_j \mathbf{U}_{h,jj})$ in the upwinding term is a known function calculated from $\mathbf{U}_h$. The sum of the nodal fluxes from the contributions of upwinding and shock capturing in the element m is obtained by summing all the components of the vector $\tilde{\mathbf{D}}_m$ therefore we have

$$
\begin{aligned}
&\text{Sum of nodal mass flows } \tilde{\mathbf{D}}_m \text{ in element } m \\
&\quad = [1,...,1,0,...,0,0,...,0,0,...,0]\,\tilde{\mathbf{D}}_m \\
&\quad = \int_{Vol^{(m)}}[1,...,1,0,...,0,0,...,0,0,...,0]\,\mathbf{H}^T_{,jj}\;\mathbf{A}_j\boldsymbol{\tau}_j\mathbf{A}_j\mathbf{U}_{h,jj}dVol^{(m)} \\
&\quad\quad + \int_{Vol^{(m)}}\nu_j\,[1,...,1,0,...,0,0,...,0,0,...,0]\,\mathbf{H}^T_{,j}\;\mathbf{U}_{h,j}dVol^{(m)} \\
&\quad = 0
\end{aligned}
$$

The same results are obtained for the x_1-momentum, x_2-momentum and energy nodal fluxes. These results also confirm that the upwinding and shock capturing terms do not give a spurious contribution to the flux.

If we define a different convective term discretization with nodal fluxes $\bar{\mathbf{F}}_m$ as follows

$$
\bar{\mathbf{F}}_m = \int_{S^{(m)}} \mathbf{H}^{ST}\;\mathbf{F}_j(\mathbf{U}_h)\;n_j dS^{(m)}
$$

where $S^{(m)}$ contains all the sides of the element surface. The vector $\bar{\mathbf{F}}_m$ contains the total outflow of the fluxes at the element m and it is obtained by integrating the outflow of the fluxes around the element boundaries. We can ask: do we have the conservation of flux $\bar{\mathbf{F}}_m$ for element m? Let us consider the following identity,

$$
\begin{aligned}
\int_{S^{(m)}} \mathbf{H}^{ST}\;\mathbf{F}_j(\mathbf{U}_h)\;n_j dS^{(m)} &= \int_{Vol^{(m)}}\{\mathbf{H}^T\;\mathbf{F}_j(\mathbf{U}_h)\}_{,j}dVol^{(m)} \\
&= \int_{Vol^{(m)}}\mathbf{H}^T\;\mathbf{F}_{j,j}(\mathbf{U}_h)dVol^{(m)} + \int_{Vol^{(m)}}\mathbf{H}^T_{,j}\;\mathbf{F}_j(\mathbf{U}_h)dVol^{(m)}
\end{aligned}
$$

The sum of the nodal fluxes $\bar{\mathbf{F}}_m$ in element m obtained by summing all the components in $\bar{\mathbf{F}}_m$ is given by

$$
\begin{aligned}
\text{Sum of nodal fluxes } \bar{\mathbf{F}}_m \text{ in element } m &= [1,1,1....1]\;\bar{\mathbf{F}}_m \\
&= \int_{Vol^{(m)}}[1,1,1....1]\;\mathbf{H}^T\;\mathbf{F}_{j,j}(\mathbf{U}_h)dVol^{(m)} \\
&\quad + \int_{Vol^{(m)}}[1,1,1....1]\;\mathbf{H}^T_{,j}\;\mathbf{F}_j(\mathbf{U}_h)dVol^{(m)}
\end{aligned}
$$

$$= \int_{Vol^{(m)}} [1,1,1,1]\, \mathbf{F}_{j,j}(\mathbf{U}_h) dVol^{(m)}$$

When the solution $\mathbf{U}_h$ in the element m is constant, $\mathbf{F}_{j,j} = 0$, and therefore the sum of the nodal fluxes in $\bar{\mathbf{F}}_m$ will be zero. When the solution $\mathbf{U}_h$ in the element m is not constant, the sum of the nodal fluxes in $\bar{\mathbf{F}}_m$ will not be zero, and the sum value will be larger when the gradient of the convective flux is large. In the finite element formulation for the steady state Euler problem, the sum of the nodal fluxes defined in $\bar{\mathbf{F}}_m$ can be used as an error measure since this quantity represents a discretization error.

Note that in the control volume method, variables are assumed to be constant within each of the volume therefore always $\mathbf{F}_{j,j} = 0$. Hence, for the control volume method, the summation of the nodal fluxes as defined for $\bar{\mathbf{F}}_m$ will be zero which indicates that the control volume method conserves fluxes in the integral sense used for $\bar{\mathbf{F}}_m$.

3.3 Numerical examples

In this section, we present numerical examples to study the performance of the finite element formulation that we propose in this thesis. In the absense of a mathematical analysis, while might even require simplifying assumptions, it is prudent to solve judiciously chosen test problems: these test problems should contain the numerical difficulties that finite element methods encounter in solving compressible flows (see, for example, ref. [46] for such an approach related to shell analysis). The numerical difficulties are due to shocks, boundary layers, interaction between shock and boundary layer and low Mach number. Other difficulties are also encountered when we try to apply correct boundary conditions such as pressure, temperature, etc.

3.3.1 Supersonic flow over a bump

This problem is considered to study the performance of the proposed method in solving a problem with a complex shock solution. The problem of supersonic flow

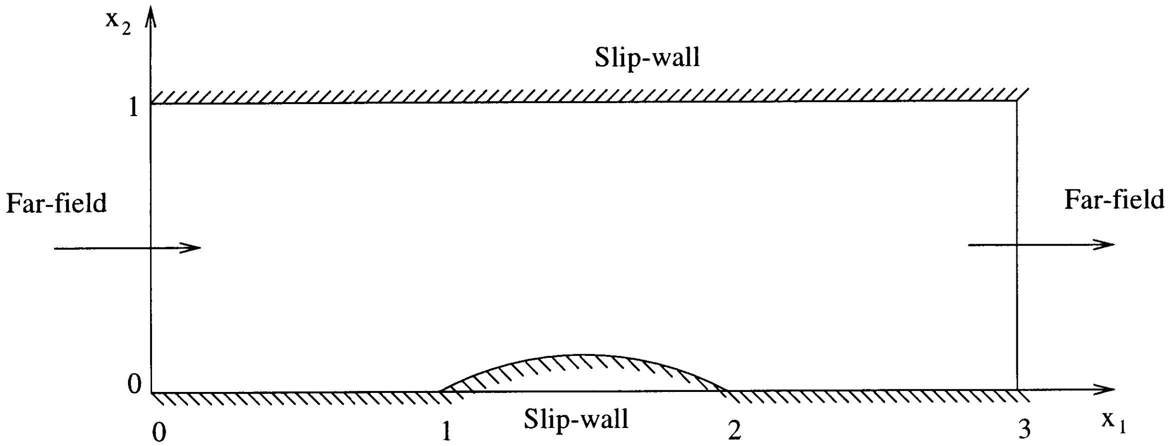

Figure 3-13: Supersonic flow over a bump problem.

over a bump is described in fig. 3-13. In this problem, a bump is placed in a 2D channel and the flow is assumed to be frictionless. The bump arc is described by

$$x_2 = 0.04(1 - 4(x_1 - 1.5)^2) \qquad\qquad 1 \leq x_1 \leq 2$$

The domain is descretized into a mesh of 15×46 elements. The upper and lower boundaries are assumed to be slip-wall boundary conditions. On the left and right boundaries, openflow boundary conditions are applied and the free-stream flow has the following condition

$$M = 1.4,\ \rho = 1,\ v_1 = 1,\ v_2 = 0$$

The fluid properties are assumed to be constant with $\gamma = 1.4, c_v = 715, k = \mu = 0$. The calculated nodal pressure distribution using our proposed finite element is shown in fig. 3-14. For comparison, the ADINA-F solution for this problem is shown in fig. 3-15 [47].

The solution shows that a shock is developed to originate from the leading edge of the bump. As the shock reaches the upper boundary where the slip-wall condition is applied, the shock is reflected and then as the reflected shock hits the lower boundary, to the right of the trailing edge of the bump, it is reflected again. The reflected shock

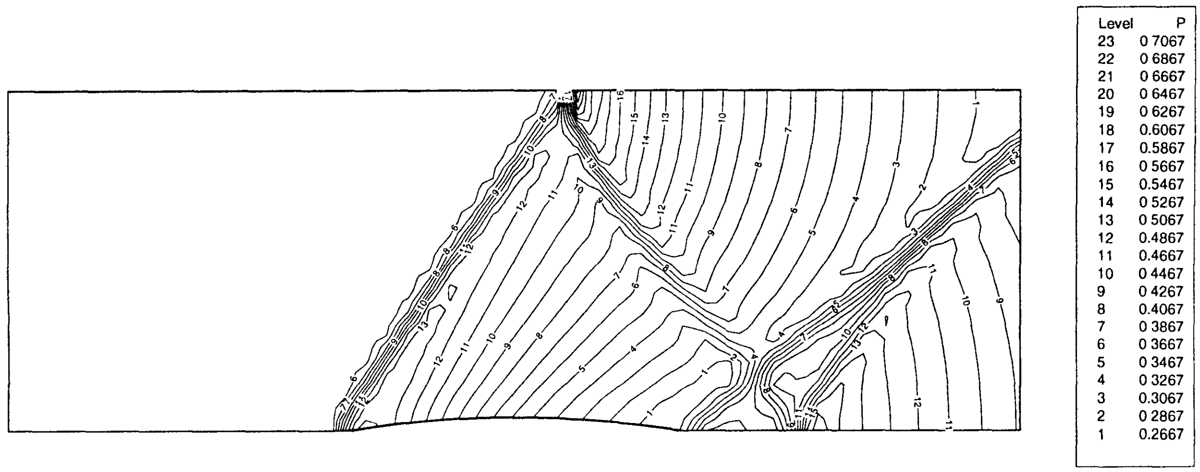

Figure 3-14: Nodal pressure solution of the supersonic flow over a bump problem.

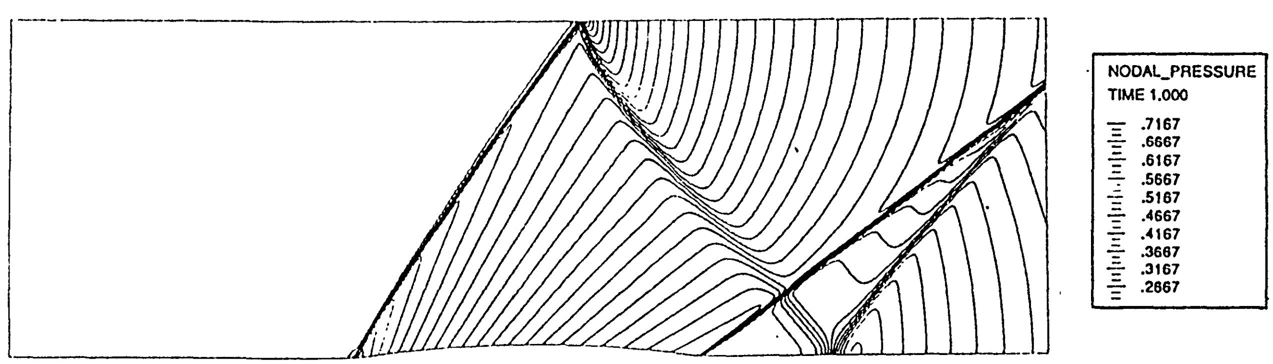

Figure 3-15: Nodal pressure solution of the supersonic flow over a bump problem using ADINA-F.

is interacting with the shock developed at the trailing edge of the bump.

The density distributions along $x_2 = 1$ and along the center of the channel are shown in fig. 3-16. The solution by Beau et al. [13] using a fine mesh, 60×184, and the solution using ADINA-F with a very fine mesh are also shown for comparison. From fig. 3-16, we see that our finite element solution is close to the prediction presented by Beau et al. and the ADINA-F solution. Our finite element solution for the shock originating from the leading edge is close to the comparison solutions in terms of the shock magnitude and location, and the same holds for the predictions of the reflected shock. However, considering the solutions for the trailing edge shock, a difference in location is observed, with our finite element solution being closer to the ADINA-F solution than is Beau's solution. Note that in fig. 3-16 (b), the ADINA-F solution gives distinct shock locations for the doubly reflected leading edge shock and the trailing edge shock (around $x_1 = 2.7$) due to a sufficiently small element size being used.

3.3.2 Natural convection problem.

To show the ability of our finite element formulation to solve a very low Mach number problem, we consider the natural convection problem described in fig. 3-17. To obtain the steady state solution, we used a transient analysis and iterated the solution from the initial condition to the time when the changes in the variables are small. The initial condition is given as: pressure $p = 10^5$, temperature $\theta = 300$ and velocity $v_1 = v_2 = 0$. The fluid properties are assumed to be constant, $R = 286, c_v = 715, k = 1.0, \mu = 0.001$. We discretized the domain into a mesh of 20×20 elements with smaller elements close to the boundary to capture the boundary layers, see fig. 3-18. The results of the problem using the proposed finite element formulation are shown in figs. 3-19 and 3-20. Considering fig. 3-19, we see that the boundary layers have been captured using the mesh. The maximum Mach number in the solution is about 0.0005 which is reached by the fluid located at $x_2 = 0.5$ and right outside the boundary layer of the left and right side walls.

For comparison, we solve the natural convection problem using ADINA-F with

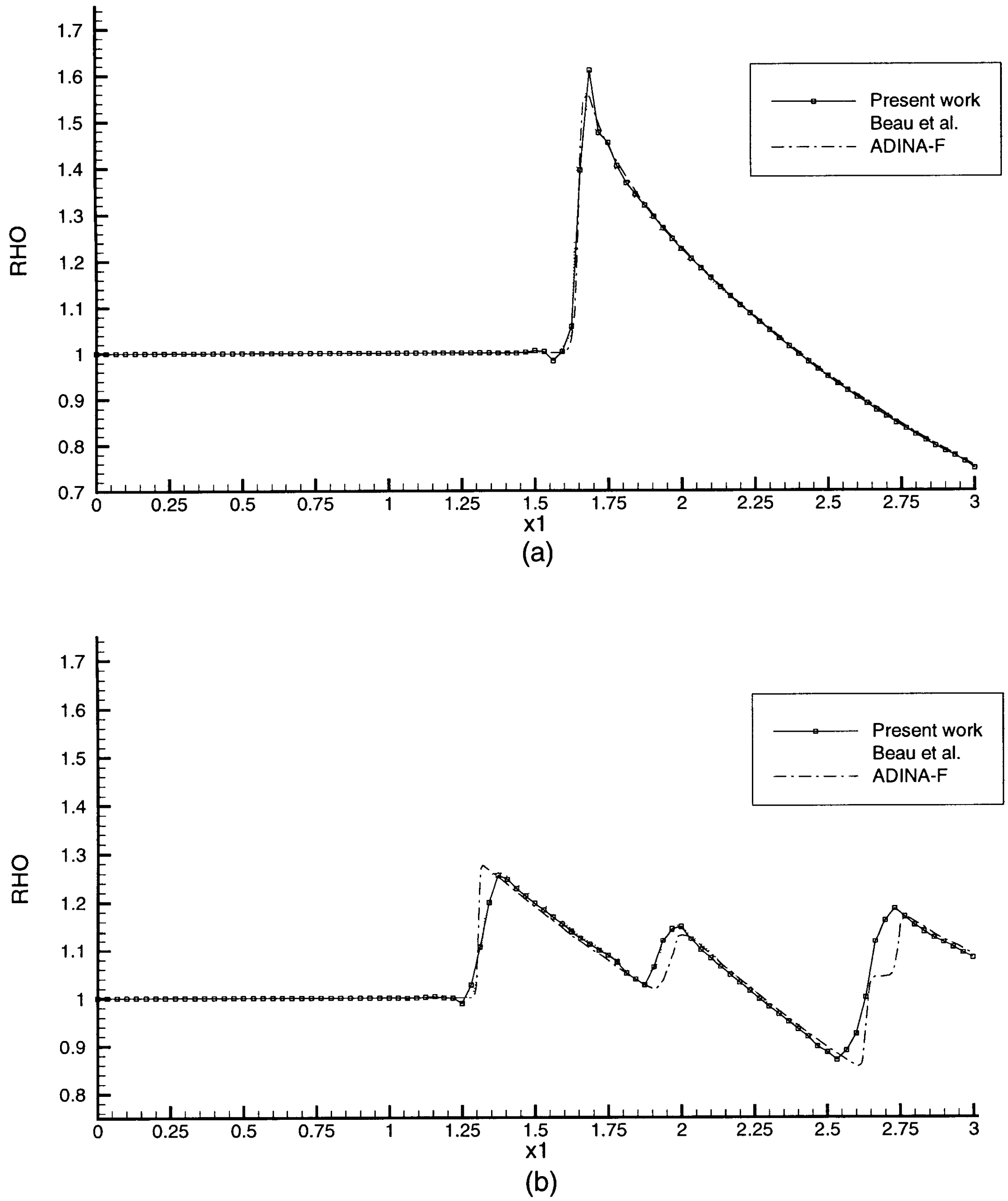

Figure 3-16: Density distribution (a) along x_2=1.0 (b) along the center of the channel.

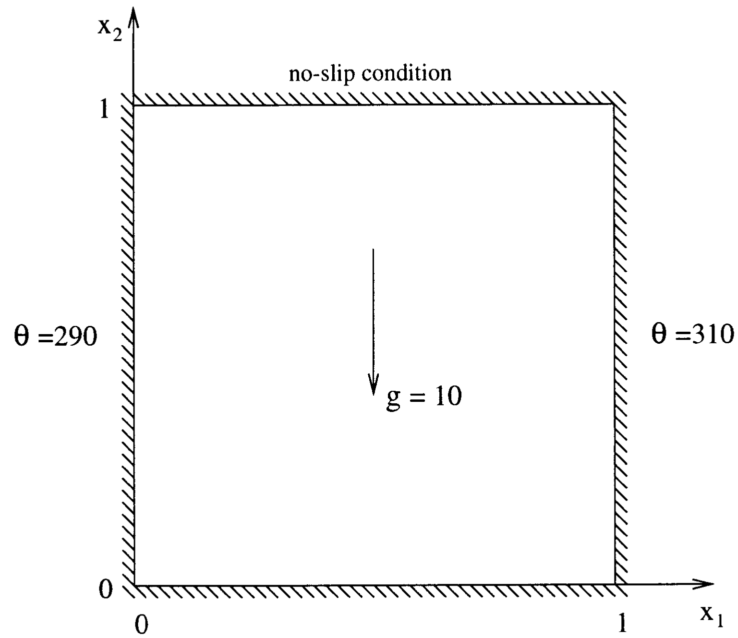

Figure 3-17: Natural convection problem.

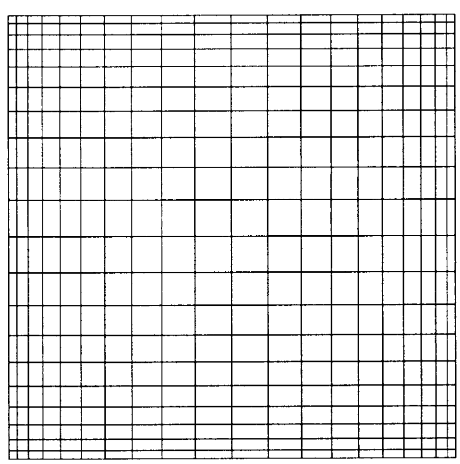

Figure 3-18: The mesh used for the natural convection problem.

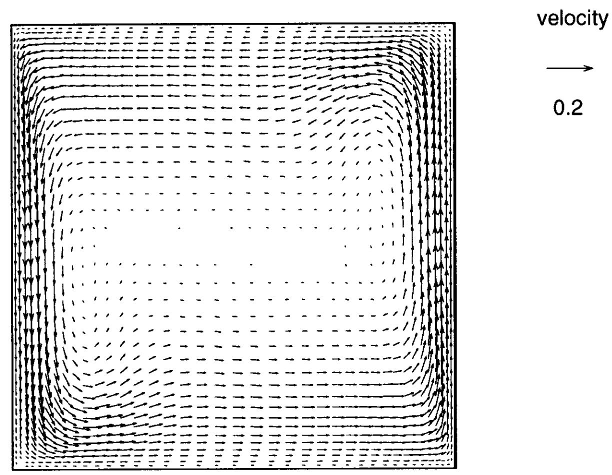

Figure 3-19: The velocity vector solution of the natural convection problem.

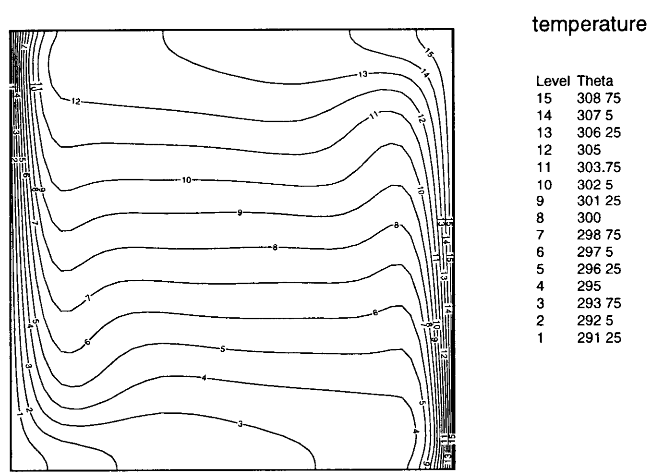

Figure 3-20: The temperature distribution solution of the natural convection problem.

the incompressible formulation and the Boussinesq approximation [32] to calculate the body force due to the density change. The calculated x_2-direction velocity and temperature distributions along $x_2 = 0.5$ are plotted in fig. 3-21 for our finite element solution and the ADINA-F solution. The results are close to each other, especially the calculated temperature distributions.

The predicted heat flux distributions on the left and right side boundaries are plotted in fig. 3-22. The solution using our finite element formulation is reasonably close to the solution obtained with ADINA-F. In plotting the heat flux for our finite element results, the values have been calculated by averaging at the corner nodes and interpolating linearly over the elements.

3.3.3 Supersonic flow over a flat plate

The flow over a flat plate is considered to study the performance of the proposed method to solve for a boundary layer and shock. The domain and boundary conditions of the 2D Navier-Stokes flow problem are shown in fig. 3-23. In this problem, a Mach three flow is passing over an infinitely thin plate at zero angle of attack and a curved shock and a boundary layer are developed. The Reynolds number is 10^3 based on the free stream values and the length of the plate, L. The fluid properties are $\gamma = 1.4$, $R = 286.62$, $\mu = 0.0906\ \theta^{1.5}/(\theta + 0.0001406)$ and $k = \frac{\gamma c_v \mu}{Pr}$, where Pr is the Prandtl number, $Pr = 0.72$.

The area of the computational domain is given by $-0.2 \leq x_1 \leq 1.2$, $0 \leq x_2 \leq 0.8$, and the leading edge of the plate is placed at $x_1 = 0$. The domain is discretized into a mesh of 24×42 elements with smaller elements close to the leading edge of the plate. At the inflow boundary ($x_1 = -0.2$) and top boundary ($x_2 = 0.8$), all four variables are prescribed with the condition $\rho = 1, v_1 = 1, v_2 = 0, \theta = 2.769E-4$. On the symmetry line ($x_2 = 0$ and $x_1 < 0$), the symmetric conditions $v_2 = \tau_{12} = q_2 = 0$ are imposed. On the plate ($x_2 = 0$ and $x_1 \geq 0$), the no-slip condition, $v_1 = v_2 = 0$, and the stagnation temperature, $\theta_s = 7.754E{-4}$, are prescribed. At the outflow boundary ($x_1 = 1.2$), no variable is prescribed except the shear stress term to accomodate the

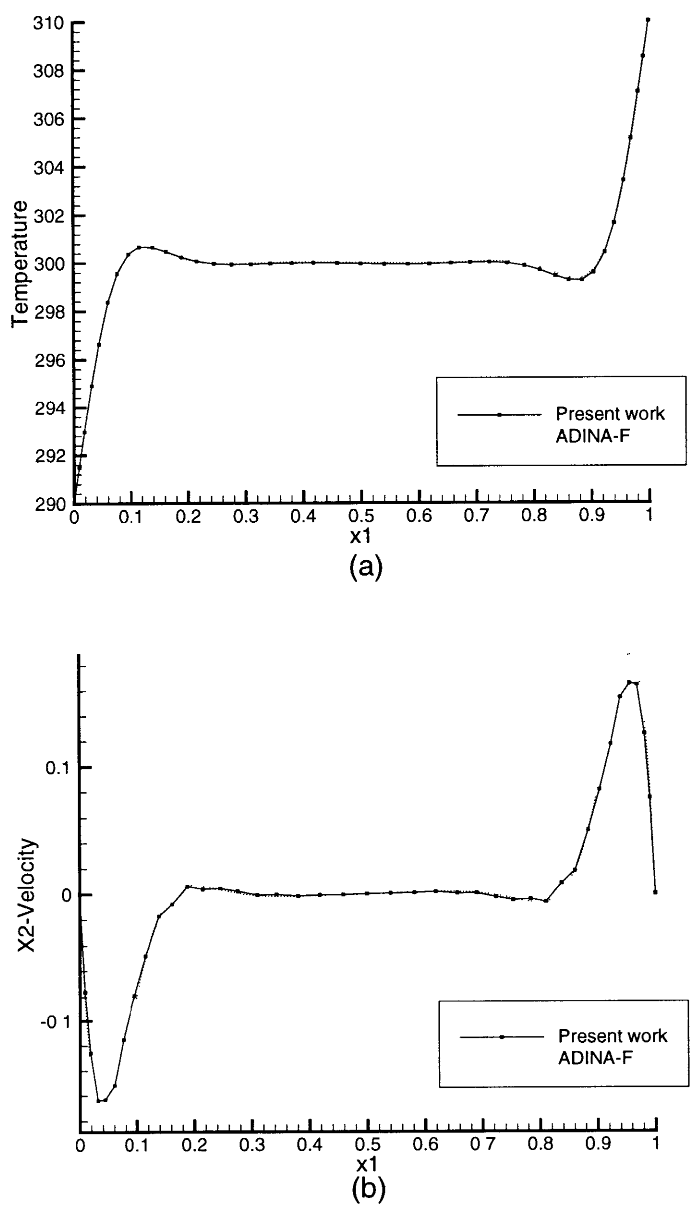

Figure 3-21: The solution along $x_2 = 0.5$ (a) temperature (b) velocity component in x_2-direction.

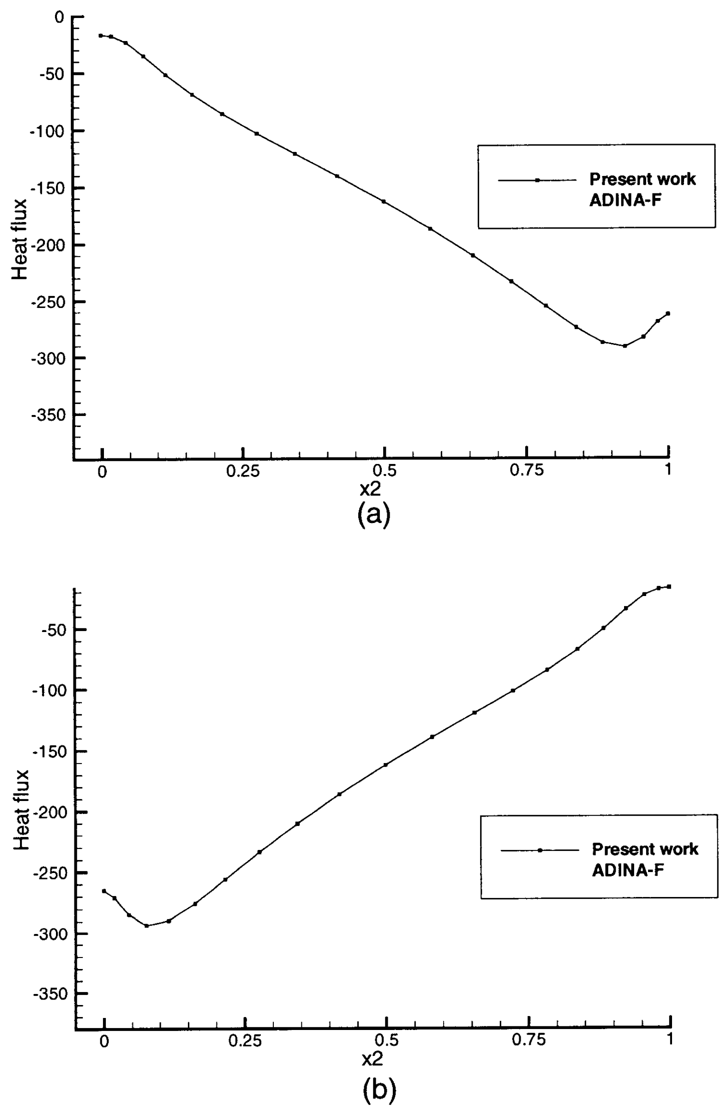

Figure 3-22: The heat flux in x_1-direction on the wall (a) left side (b) right side.

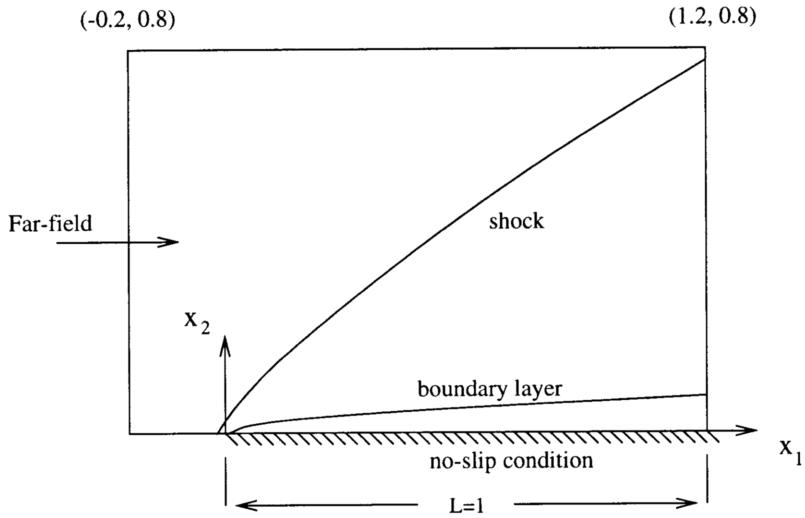

Figure 3-23: Supersonic flow over a flat plate problem.

boundary layer velocity profile at the right boundary, $\tau_{12} = \mu(\frac{\partial v_1}{\partial x_2} + \frac{\partial v_2}{\partial x_1})$. The shear stress is calculated iteratively from the solution.

The calculated solution for the problem is shown in fig. 3-24. A shock originating from the leading edge of the plate and the development of a boundary layer are shown in the solution. Across the shock, the density increases and the Mach number decreases (the density has a maximum value at the leading edge point where there is a singularity.) To give a comparison, fig. 3-25 shows the plot of the coefficient of skin friction (defined as $C_f = \frac{\tau_{wall}}{\frac{1}{2}\rho_\infty V_\infty^2}$, where ρ_∞ and V_∞ are the far-field fluid density and velocity, and τ_{wall} is the wall shear stress) along the plate and compares the computed result with the result published by Shakib et al. [36] using a very fine mesh (28,672 linear elements). Although a rather coarse mesh was used, the skin friction coefficient obtained using our finite element formulation is very close to the result given in ref. [36].

3.3.4 Mach 6.06 compression corner

This problem is considered to study the performance of the proposed method in solving the interaction of a boundary layer and a shock. A Mach 6.06, Reynolds

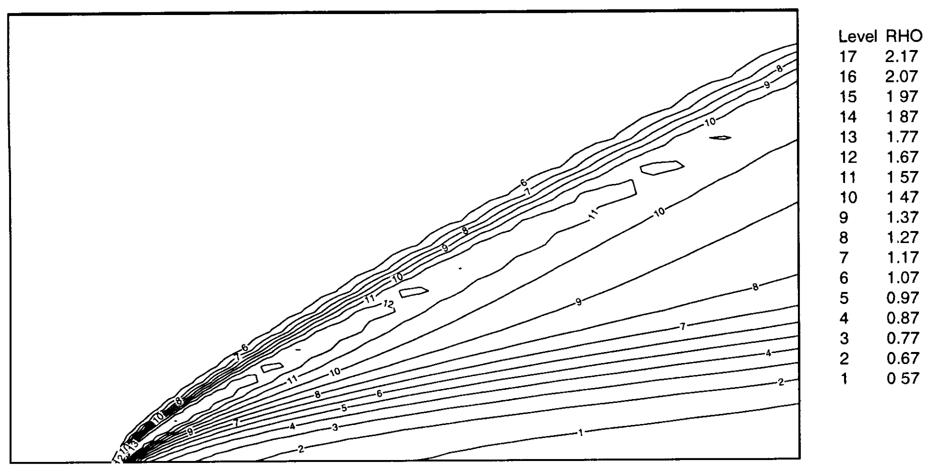
Level RHO
17 2.17
16 2.07
15 1 97
14 1 87
13 1.77
12 1.67
11 1 57
10 1 47
9 1.37
8 1.27
7 1.17
6 1.07
5 0.97
4 0.87
3 0.77
2 0.67
1 0 57

(a)

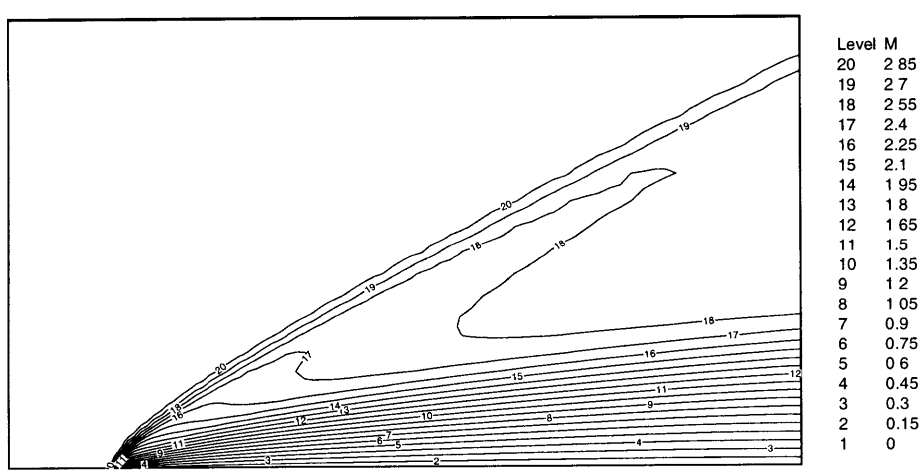
Level M
20 2 85
19 2 7
18 2 55
17 2.4
16 2.25
15 2.1
14 1 95
13 1 8
12 1 65
11 1.5
10 1.35
9 1 2
8 1 05
7 0.9
6 0.75
5 0 6
4 0.45
3 0.3
2 0.15
1 0

(b)

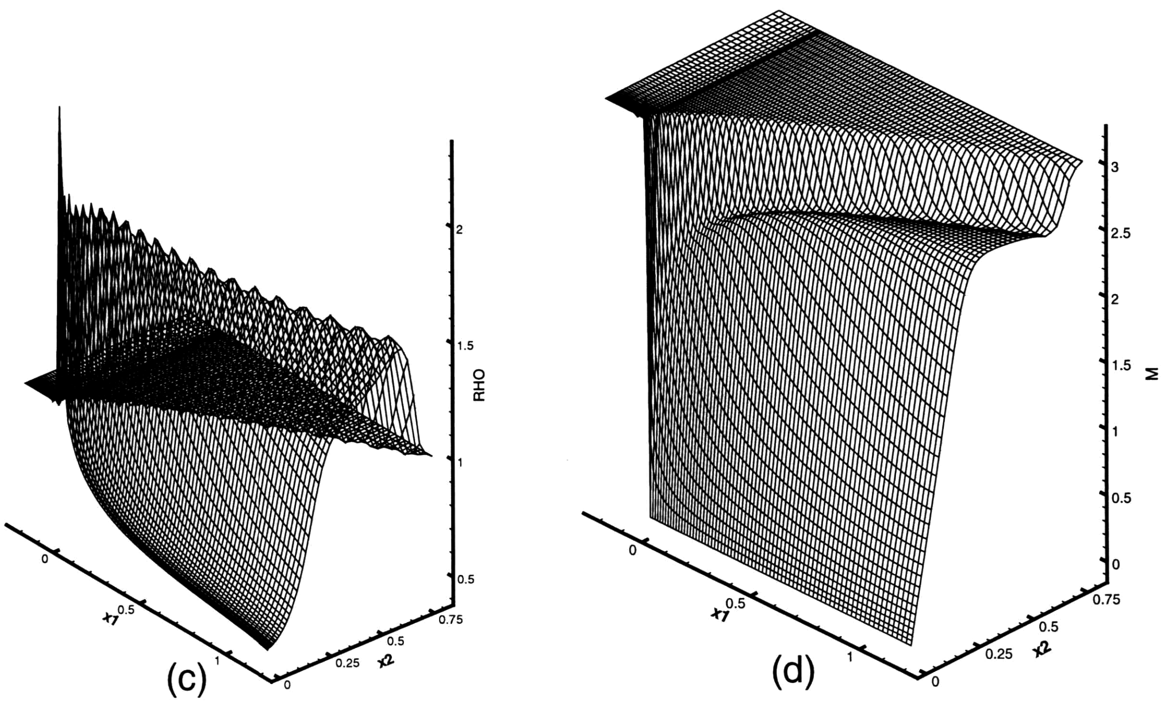

Figure 3-24: Solution of the flow over a flat plate problem (a) density (b) Mach number (c) density distribution in 3D representation (d) Mach number distribution in 3D representation.

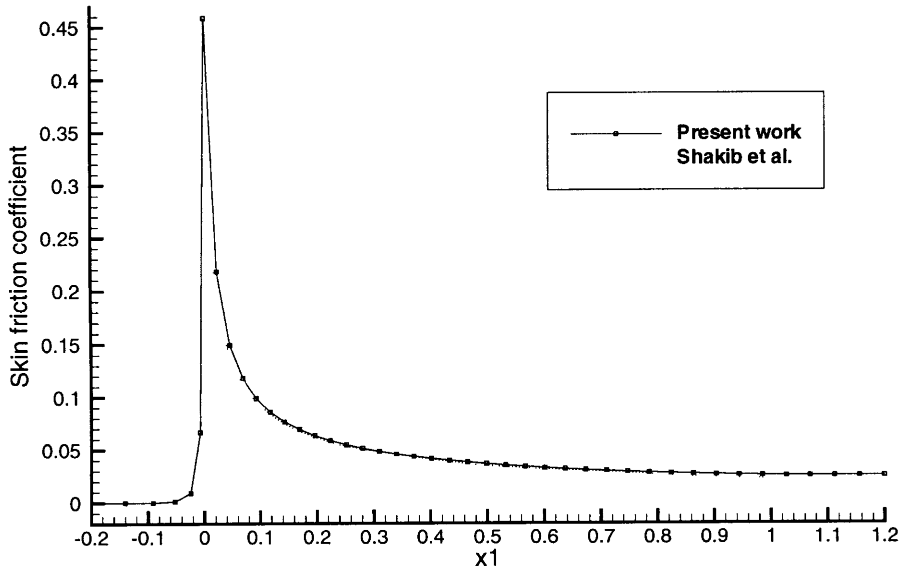

Figure 3-25: Skin friction coefficient distribution along the plate.

number 150,000, flow over a compression corner at an angle of 10.25^o is considered, see fig.3-26. The Reynolds number is calculated based on the free stream conditions and the distance from the leading edge of the plate to the corner. The fluid properties are $\gamma = 1.4$, $R = 286.62$, $\mu = 0.002637\ \theta^{1.5}/(\theta + 0.00015324)$, and $k = \frac{\gamma c_v \mu}{Pr}$, where Pr is the Prandtl number, $Pr = 0.72$.

At the inflow, we impose convective fluxes with the farfield condition $\rho = 1, v_1 = 1, v_2 = 0, \theta = 6.7861E-5$. At the upper boundaries, all four variables are prescribed with the farfield condition. On the plate, the no-slip condition, $v_1 = v_2 = 0$, and the adiabatic condition are prescribed. A rather long computational domain is employed to avoid boundary effects due to the inflow and outflow conditions. The computational domain is discretized into 21×46 quadratic elements. The mesh used is shown in fig. 3-27. We put many elements close to the wall to capture the boundary layer.

The solution of this problem using our finite element formulation is shown in fig. 3-28. A shock develops from the leading edge of the plate and propagates through the whole domain. At the corner, a compression shock develops due to the change

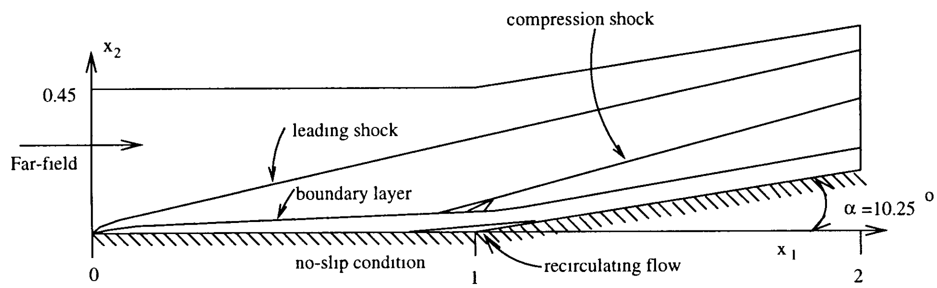

Figure 3-26: Flow over a compression corner.

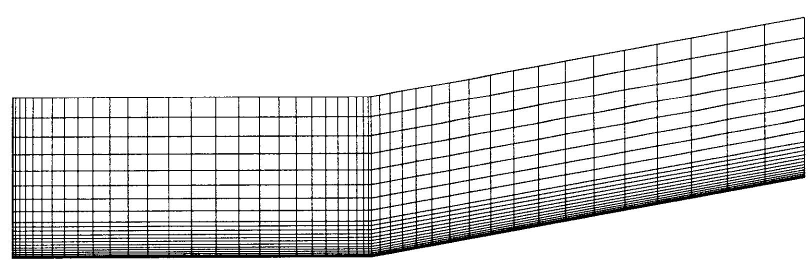

Figure 3-27: The mesh used for the flow over a compression corner problem.

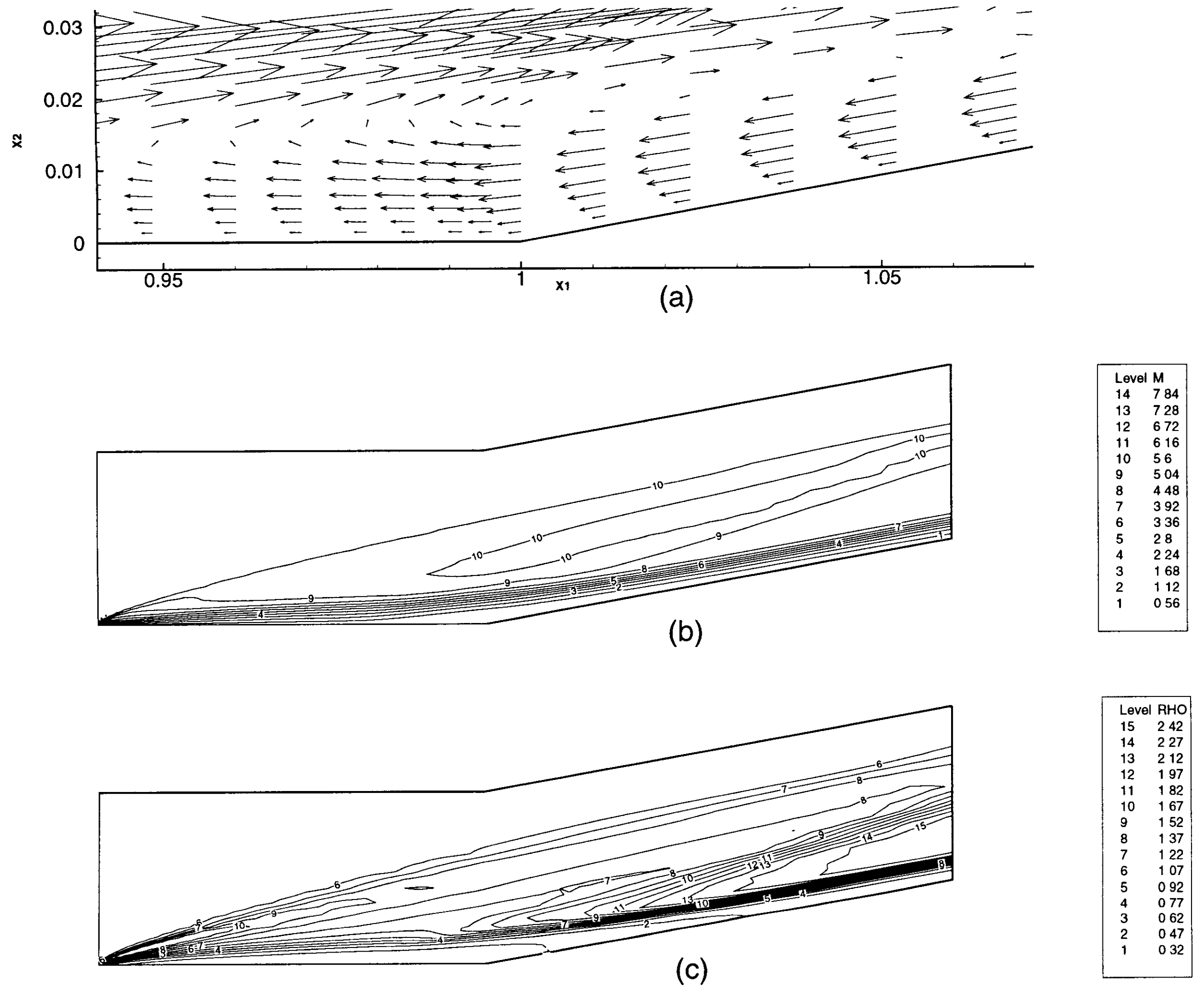

Figure 3-28: Solution of the flow over a compression corner (a) backflow in the corner (b) Mach number distribution (c) density distribution.

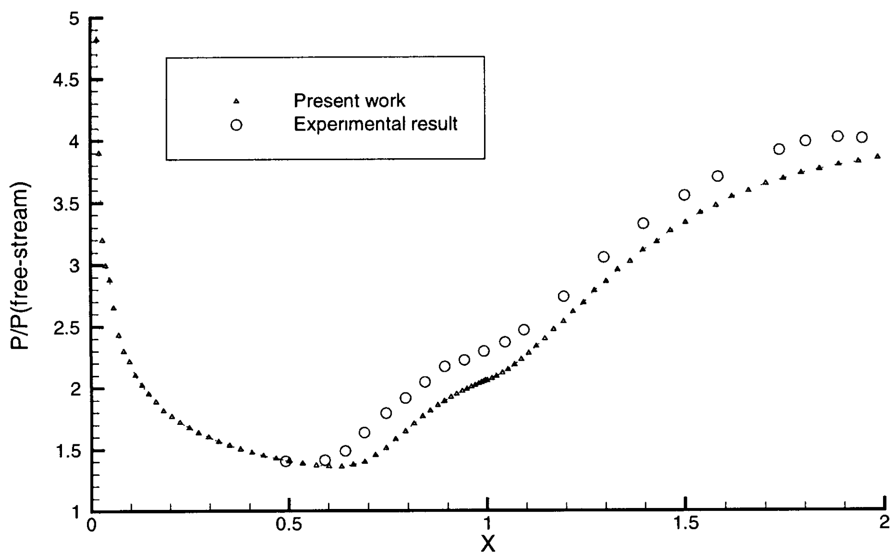

Figure 3-29: Normalized pressure distribution along the plate.

of angle of the wall and the shock is interacting with the boundary layer at this location. To obtain a reasonably good solution, the mesh in the corner area should be fine enough to capture the boundary layer and the compression shock. In our solution, the compression shock is clearly seen in fig. 3-28 (c).

The back flow in the corner area is observed because there is an increase in pressure along the wall due to the inclination of the wall with the angle α. The larger the angle α, the more significant is the effect of the pressure increase in the corner, and the larger the back flow in the solution. In our solution, the back flow is shown in fig. 3-28 (a).

Fig. 3-29 shows the calculated pressure distribution normalized by the free-stream pressure along the plate and also the experimental result [48]. Reasonably good agreement is observed.

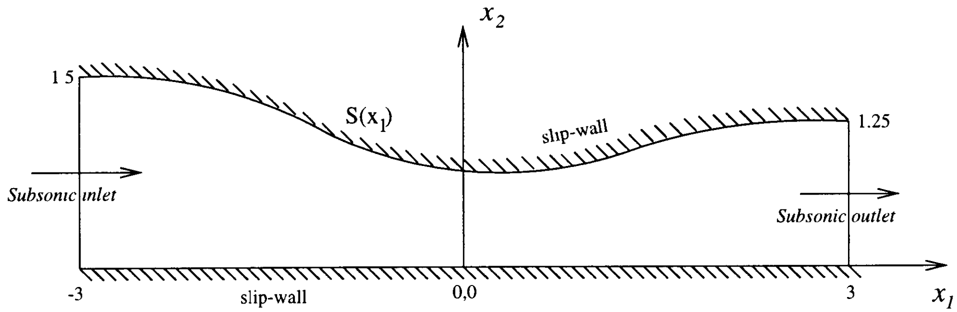

Figure 3-30: Transonic flow in a converging-diverging nozzle problem.

3.3.5 Shock in a converging-diverging nozzle

This problem is considered to study the performance of the openflow boundary conditions described in section 3.2.6 and to study whether the location of the shock is properly predicted even with a coarse mesh. The problem is described in fig. 3-30. The geometry of the nozzle is described by

$$S(x_1) = \begin{cases} 0.196875 - 0.86875\,x_1 - 0.144792\,x_1^2 & -3 \leq x_1 < -1 \\ 0.6 - 0.0625\,x_1 + 0.258333\,x_1^2 & -1 \leq x_1 < 1 \\ 0.228125 + 0.68125\,x_1 - 0.113542\,x_1^2 & 1 \leq x_1 \leq -1 \end{cases}$$

The slip-wall boundary conditions are imposed to the upper and lower boundaries. The subsonic inlet flow is prescribed at the left boundary with the condition :

$$\theta = 300, \rho v_1 = 150, \rho v_2 = \text{free}$$

and the subsonic outlet flow is prescribed at the right boundary with the condition :

$$p = 10^5$$

The fluid properties are assumed to be constant, $R = 286, \gamma = 1.4, k = \mu = 0$. The meshes used are : $4 \times 24, 8 \times 48$, and 16×96 elements and the coarsest mesh is shown in fig. 3-31. The pressure solutions for the sequence of meshes are shown in fig. 3-32.

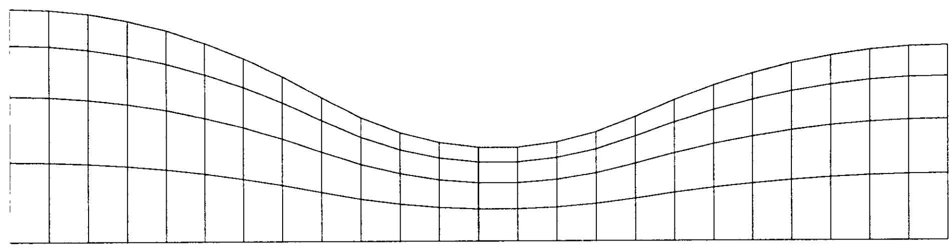

Figure 3-31: Coarsest mesh used for the transonic flow in a converging-diverging nozzle problem.

Fig. 3-32 shows that as the mesh is refined, the location of the shock does not change, therefore the location of the shock is independent of the mesh. However, of course, the quality of the shock solution depends on the mesh. The pressure solutions along the symmetry line using different meshes are plotted in fig. 3-33 and an ADINA-F solution is also shown for comparison.

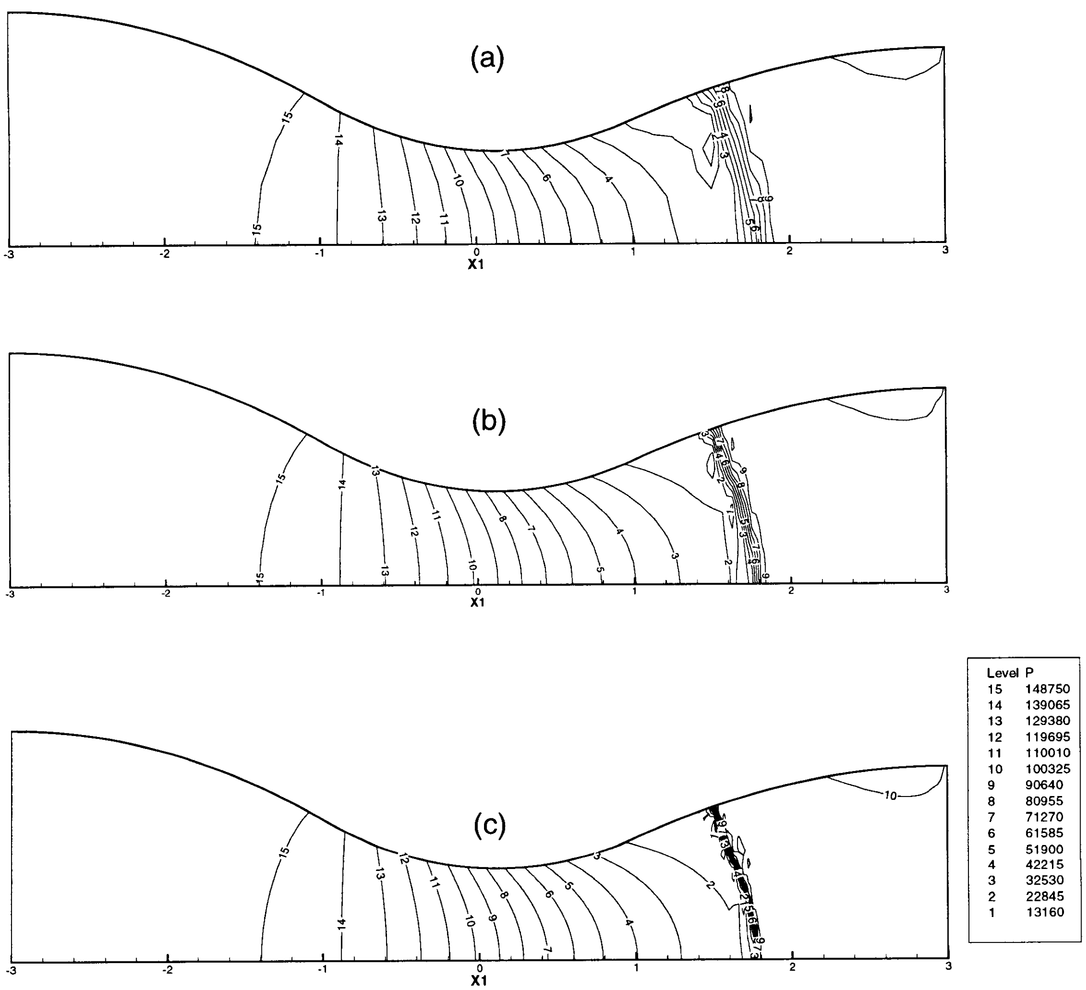

Figure 3-32: Pressure solutions of the transonic flow in a converging-diverging nozzle problem using different meshes, (a) coarse mesh, (b) fine mesh, (c) finest mesh.

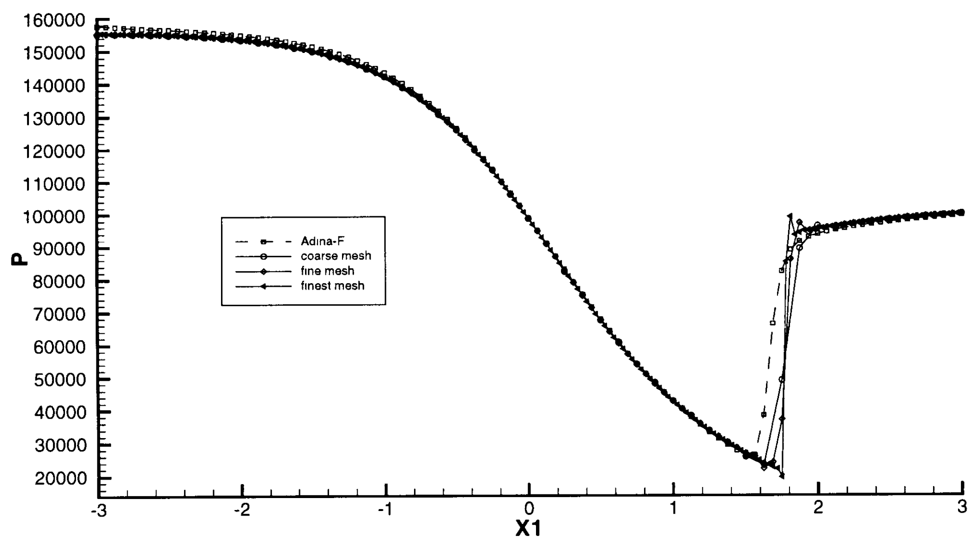

Figure 3-33: Pressure distribution solutions of the transonic flow in a converging-diverging nozzle problem along the symmetric line.

Chapter 4

Incompressible flows

Our objective is to use the incompressible flow formulation and compare with the compressible flow formulation in solving very low Mach number problems. We give emphasis to study the performance of an upwind method for the incompressible flow formulation which has the same form as the upwind term for the compressible flow formulation. In this chapter, we start with the discussion of the constitutive relations for the fluid under the assumption of incompressibility. Then the procedure for non-dimensionalization of the governing equations is discussed. The finite element discretization with upwinding is formulated. The necessity of satisfying the inf-sup condition is explained. Finally, numerical examples to verify the effectiveness of the numerical method are presented.

4.1 Navier-Stokes equations for incompressible flow

The conservation law equations (eqn. (2.9)) together with the constitutive relations and the assumption of incompressibility compose the Navier-Stokes equations for incompressible flow. The constitutive relations are the Newtonian fluid stress relation, Fourier's law of heat conduction and the internal energy relation for the incompressible fluid

$$\tau_{ji} = -p\,\delta_{ij} + \mu(v_{i,j} + v_{j,i})$$

$$q_j = -k\theta_{,j}$$
$$e = c_p\theta$$

where p, θ, c_p, μ, k are pressure, temperature, specific heat, fluid viscosity, coefficient of thermal conductivity, respectively. δ_{ij} is the Kronecker delta (i.e. $\delta_{ij} = 1$ for $i = j$, and $\delta_{ij} = 0$ for $i \neq j$). Note that in incompressible flow, the specific heat at constant volume is equal to the specific heat at constant pressure [49]. Substituting the constitutive relations into the conservation equations and using the incompressibility assumption, we obtain the Navier-Stokes equations for incompressible flow

$$\begin{aligned} v_{j,j} &= 0 \\ \rho v_{i,t} + \rho v_j v_{i,j} + p_{,i} - \mu(v_{i,j} + v_{j,i})_{,j} - f_i^B &= 0 \\ \rho c_p \theta_{,t} + \rho c_p v_j \theta_{,j} - \frac{\mu}{2}(v_{i,j} + v_{j,i})^2 - (k\theta_{,j})_{,j} - q^B &= 0 \end{aligned}$$

Note that the body force f_i^B is written in the unit force per volume and the heat source q^B is written in the unit energy per volume. The term $pv_{i,i}$ in the dissipation term of the energy equation vanishes by using the mass conservation equation, $v_{j,j} = 0$.

To avoid difficulty due to round-off errors caused by using too large or too small a value of the input data and to render solutions independent of any particular system of units, we non-dimensionalize of the Navier-Stokes equations. The procedure of non-dimensionalization normalizes the working variables, pressure, velocity and temperature in order that these variables are of the same order of magnitude. Defining the non-dimensionalized variables,

$$x_i^* = \frac{x_i}{L_o} \qquad v_i^* = \frac{v_i}{V_o} \qquad p^* = \frac{p}{\rho V_o^2} \qquad \theta^* = \frac{\theta}{\Delta\theta_o} \qquad t^* = \frac{tV_o}{L_o}$$

$$\mu^* = \frac{\mu}{\rho V_o L_o} = \frac{1}{Re} \qquad \mu^{**} = \frac{\mu V_o}{2\rho c_p \Delta\theta_o L_o} = \frac{Ec}{Re} \qquad k^* = \frac{k}{\rho c_p V_o L_o} = \frac{1}{Pe}$$

$$f_i^{B*} = \frac{f_i^B L_o}{\rho V_o^2} \qquad q^{B*} = \frac{q^B L_o}{\rho c_p \Delta\theta_o V_o}$$

where L_o, V_o, $\Delta\theta_o$ are characteristic values of length, velocity and temperature. Re, Pe, Ec are Reynolds, Peclet and Eckert non-dimensional numbers. The Eckert number, $Ec = \frac{\frac{1}{2}V_o^2}{c_p \Delta\theta_o}$, is the ratio of the kinetic energy to the internal energy. Using these variables, the Navier-Stokes equations become

$$\begin{aligned} v^*_{j,j^*} &= 0 \\ v^*_{i,t^*} + v^*_j v^*_{i,j^*} + p^*_{,i^*} - \mu^*(v^*_{i,j^*} + v^*_{j,i^*})_{,j^*} - f_i^{B*} &= 0 \\ \theta^*_{,t^*} + v^*_j \theta^*_{,j^*} - \mu^{**}(v^*_{i,j^*} + v^*_{j,i^*})^2 - (k^* \theta^*_{,j^*})_{,j^*} - q^{B*} &= 0 \end{aligned}$$

The Navier-Stokes equations, after dropping the * superscripts to simplify the notation, can be written as

$$\begin{aligned} v_{j,j} &= 0 \\ v_{i,t} + v_j v_{i,j} + p_{,i} - \frac{1}{Re}(v_{i,j} + v_{j,i})_{,j} - f_i^B &= 0 \\ \theta_{,t} + v_j \theta_{,j} - \frac{Ec}{Re}(v_{i,j} + v_{j,i})^2 - (\frac{1}{Pe}\theta_{,j})_{,j} - q^B &= 0 \end{aligned} \tag{4.1}$$

From eqns. (4.1), we see that the Reynolds number inversely scales the diffusive term in the momentum equation and Peclet number inversely scales the diffusive term in the energy equation. The larger the Reynolds and Peclet numbers, the smaller are the diffusive terms. The Eckert number scales the contribution of the dissipative term in the energy equation.

4.2 Finite element spaces

Consider a finite element discretization of the fluid domain Vol, into subdomains $Vol^{(m)}$, $m = 1, 2, ..., N$, where N is the number of elements [5]. The two-dimensional quadrilateral 5/1-element and 9/4c-element, as shown in fig. 4-1 and 4-2, are employed to discretize the domain.

In the 5/1-element, the velocity variables and x_1, x_2 coordinates are interpolated using 5-node interpolations [5]; hence quadratically along the side with three nodes and linearly along the other sides, see fig. 4-1. The temperature is interpolated

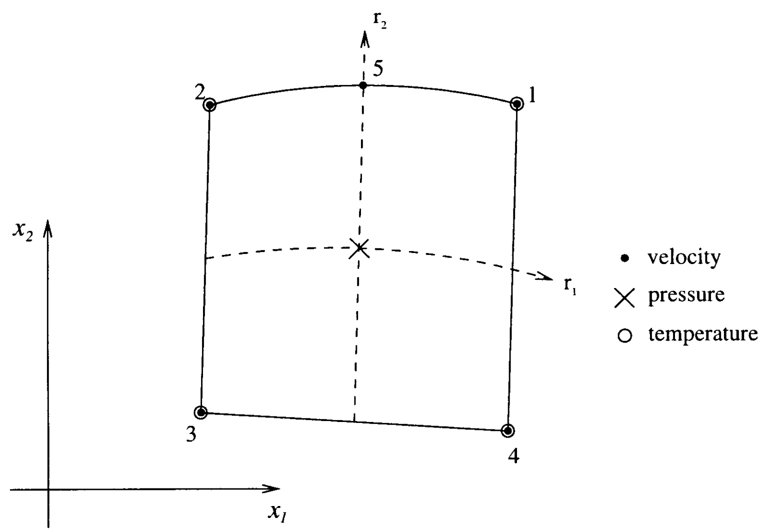

Figure 4-1: Five-node quadrilateral element used for planar flows.

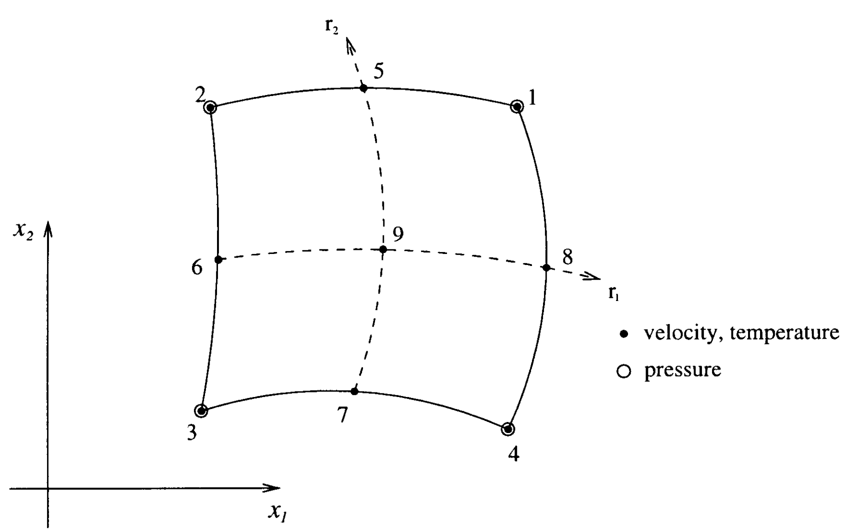

Figure 4-2: 9/4c quadrilateral element used for planar flows.

bilinearly and the pressure is assumed to be constant in the element and discontinuous across elements.

In the 9/4c-element, the velocity variables, temperature and x_1, x_2 coordinates are interpolated quadratically and the pressure is interpolated bilinearly [5].

Let the prescribed Dirichlet boundary conditions on the surface S_u be $\mathbf{g}(\mathrm{t})$ where the vector $\mathbf{g}(\mathrm{t})$ contains the specified function of the solution on the boundary S_u. Then the solution and weighting functional spaces for the discretization using the 5/1-element are

$$\begin{aligned} V_h^5 &= \{\mathbf{v}_h | \mathbf{v}_h \in L^2(Vol); \frac{\partial (v_h)_i}{\partial x_j} \in L^2(Vol), i = 2,3,4; j = 1,2; (v_h)_1 \in Q_0(Vol^{(m)}), \\ &\quad (v_h)_{2,3} \in Q_1^+(Vol^{(m)}), (v_h)_4 \in Q_1(Vol^{(m)}), \mathbf{v}_h|_{S_u} = \mathbf{g}(t)\} \end{aligned}$$

$$\begin{aligned} W_h^5 &= \{\mathbf{w}_h | \mathbf{w}_h \in L^2(Vol); \frac{\partial (w_h)_i}{\partial x_j} \in L^2(Vol), i = 2,3,4; j = 1,2; (w_h)_1 \in Q_0(Vol^{(m)}), \\ &\quad (w_h)_{2,3} \in Q_1^+(Vol^{(m)}), (w_h)_4 \in Q_1(Vol^{(m)}), \mathbf{w}_h|_{S_u} = \mathbf{0}\} \end{aligned}$$

where $Q_0(Vol^{(m)}), Q_1(Vol^{(m)}), Q_1^+(Vol^{(m)})$ denote constant, bilinear, and 5-node interpolation functions respectively, in the element m; and $L^2(Vol)$ is the space of square integrable functions in the volume, "Vol", of the body considered,

$$L^2(Vol) = \{\mathbf{w} | \mathbf{w} \text{ is defined in } Vol \text{ and } \int_{Vol} (\sum_{i=1}^{4} (w_i)^2) dVol = \|\mathbf{w}\|^2_{L^2(Vol)} < +\infty\}$$

The solution and weighting functional spaces for the discretization using the 9/4c-element are

$$\begin{aligned} V_h^9 &= \{\mathbf{v}_h | \mathbf{v}_h \in L^2(Vol); \frac{\partial (v_h)_i}{\partial x_j} \in L^2(Vol), i = 1,2,3,4; j = 1,2; (v_h)_1 \in Q_1(Vol^{(m)}), \\ &\quad (v_h)_{2,3,4} \in Q_2(Vol^{(m)}), \mathbf{v}_h|_{S_u} = \mathbf{g}(t)\} \end{aligned}$$

$$W_h^9 = \{\mathbf{w}_h | \mathbf{w}_h \in L^2(Vol); \frac{\partial (w_h)_i}{\partial x_j} \in L^2(Vol), i = 1,2,3,4; j = 1,2; (w_h)_1 \in Q_1(Vol^{(m)}),$$

$$(w_h)_{2,3,4} \in Q_2(Vol^{(m)}), \mathbf{w}_h|_{S_u} = \mathbf{0}\}$$

where $Q_2(Vol^{(m)})$ denotes the biquadratic function in the element m.

4.3 Weighted residual formulation

The finite element formulation for the incompressible flow using the 5/1-element is:

Find $(p_h, v_{h1}, v_{h2}, \theta_h) \in V_h^5$ such that for all $(\overline{p}_h, \overline{v}_{h1}, \overline{v}_{h2}, \overline{\theta}_h) \in W_h^5$ we have

$$\begin{aligned}
-\int_{Vol} \overline{p}_h \, v_{hj,j} \, dVol &= 0 \\
\int_{Vol} \{\overline{v}_{hi}(\rho v_{hi,t} + \rho v_{hj} v_{hi,j}) - \overline{v}_{hi,i}\, p_h + \overline{v}_{hi,j}\, \mu(v_{hi,j} + v_{hj,i})\}\, dVol & \\
+\sum_m \int_{Vol^{(m)}} \overline{v}_{hi,k}\, (v_{hk} \tau v_{hj}) v_{hi,j} \; dVol^{(m)} &= \int_{Vol} \overline{v}_{hi}\, f_i^B \, dVol + \int_S \overline{v}_{hi}^s f_i^s \, dS \\
\int_{Vol} \{\overline{\theta}_h(\rho c_p \theta_{h,t} + \rho c_p v_{hj} \theta_{h,j} - \frac{\mu}{2}(v_{hi,j} + v_{hj,i})^2) + \overline{\theta}_{h,j}\, k \theta_{h,j}\}\, dVol & \\
+\sum_m \int_{Vol^{(m)}} \overline{\theta}_{h,k}\, (v_{hk} \tau v_{hj}) \theta_{h,j} \; dVol^{(m)} &= \int_{Vol} \overline{\theta}_h\, q^B \, dVol + \int_S \overline{\theta}_h^s q^s \, dS
\end{aligned} \tag{4.2}$$

Here we already have introduced the artificial diffusion terms which are the second integral terms on the left hand side of the momentum and energy conservation equations.

The finite element formulation for the incompressible flow using the 9/4c-element is:

Find $(p_h, v_{h1}, v_{h2}, \theta_h) \in V_h^9$ such that for all $(\overline{p}_h, \overline{v}_{h1}, \overline{v}_{h2}, \overline{\theta}_h) \in W_h^9$ we have

$$\begin{aligned}
-\int_{Vol} \overline{p}_h \, v_{hj,j} \, dVol &= 0 \\
\int_{Vol} \{\overline{v}_{hi}(\rho v_{hi,t} + \rho v_{hj} v_{hi,j}) - \overline{v}_{hi,i}\, p_h + \overline{v}_{hi,j}\, \mu(v_{hi,j} + v_{hj,i})\}\, dVol & \\
+\sum_m \int_{Vol^{(m)}} \overline{v}_{hi,jj}\, \tau_j |v_{hj}|\, v_{hi,jj} \; dVol^{(m)} &= \int_{Vol} \overline{v}_{hi}\, f_i^B \, dVol + \int_S \overline{v}_{hi}^s f_i^s \, dS \\
\int_{Vol} \{\overline{\theta}_h(\rho c_p \theta_{h,t} + \rho c_p v_{hj} \theta_{h,j} - \frac{\mu}{2}(v_{hi,j} + v_{hj,i})^2) + \overline{\theta}_{h,j}\, k \theta_{h,j}\}\, dVol & \\
+\sum_m \int_{Vol^{(m)}} \overline{\theta}_{h,jj}\, \tau_j |v_{hj}|\, \theta_{h,jj} \; dVol^{(m)} &= \int_{Vol} \overline{\theta}_h\, q^B \, dVol + \int_S \overline{\theta}_h^s q^s \, dS
\end{aligned} \tag{4.3}$$

where $\overline{p}_h, \overline{v}_{hi}, \overline{\theta}_h$ are virtual pressure, velocity and temperature, respectively. The boundary terms are :

$$f_i^s = [-p\ \delta_{ij} + \mu(v_{i,j} + v_{j,i})]\ n_j$$

and

$$q^s = -k\theta_{,j}\ n_j$$

where n_j is the x_j-direction cosine of the unit (pointed outward) boundary normal vector.

The second integral terms in the momentum and energy equations are the artificial diffusion terms.

4.4 Artificial diffusion

The purpose of the artificial diffusion is to stabilize the unstable convective discretization using the Galerkin procedure. For the 5/1-element, the artificial diffusion term is given by

$$\sum_m \int_{Vol^{(m)}} \overline{\phi}_{h,k}\ (v_{hk}\tau v_{hj})\ \phi_{h,j}\ \ dVol^{(m)}$$

where ϕ_h can be v_{hi} or θ_h. The value of τ is defined as

$$\tau = |\frac{\partial \mathbf{x}}{\partial \mathbf{r}}| \frac{\xi(Re_h)}{|\mathbf{V}|}$$

where $\mathbf{r}$ denotes the coordinates in the natural coordinate system of the element. For the two-dimensional case, the "characteristic length" of the element is defined as

$$|\frac{\partial \mathbf{x}}{\partial \mathbf{r}}| = \sqrt{(\frac{\partial x_1}{\partial r_1})^2 + (\frac{\partial x_1}{\partial r_2})^2 + (\frac{\partial x_2}{\partial r_1})^2 + (\frac{\partial x_2}{\partial r_2})^2}$$

and the speed is defined as

$$|\mathbf{V}| = \sqrt{v_{h1}^2 + v_{h2}^2}$$

and

$$\xi(Re_h) = \begin{cases} \frac{Re_h}{3} & Re_h \leq 3 \\ 1 & Re_h > 3 \end{cases}$$

$$Re_h = \frac{2\rho|\mathbf{V}||\frac{\partial \mathbf{x}}{\partial \mathbf{r}}|}{\mu}$$

The artificial diffusion given here is only applied in the streamline direction. This can be shown by writing the artificial diffusion term in the following form :

$$\sum_m \int_{Vol^{(m)}} \begin{bmatrix} \overline{\phi}_{h,1} & \overline{\phi}_{h,2} \end{bmatrix} \begin{bmatrix} \tau v_{h1}^2 & \tau v_{h1} v_{h2} \\ \tau v_{h1} v_{h2} & \tau v_{h2}^2 \end{bmatrix} \begin{bmatrix} \phi_{h,1} \\ \phi_{h,2} \end{bmatrix} \; dVol$$

The characteristic behavior of the artificial diffusion can then be analyzed by considering the eigenproblem

$$\{ \begin{bmatrix} \tau v_{h1}^2 & \tau v_{h1} v_{h2} \\ \tau v_{h1} v_{h2} & \tau v_{h2}^2 \end{bmatrix} - \lambda \mathbf{I} \} \mathbf{x} = 0$$

where λ is the eigenvalue of the artificial diffusion matrix and $\mathbf{x}$ is the eigenvector of the matrix. The value λ is related to the amount of artificial diffusion applied in the direction of $\mathbf{x}$. The solution of the eigenproblem is

$$\lambda_1 = 0 \text{ and } \mathbf{x}_1 = \begin{bmatrix} v_{h2} \\ -v_{h1} \end{bmatrix}$$

$$\lambda_2 = \tau(v_{h1}^2 + v_{h2}^2) \text{ and } \mathbf{x}_2 = \begin{bmatrix} v_{h1} \\ v_{h2} \end{bmatrix}$$

The artificial diffusion term gives no diffusion in the $\mathbf{x}_1$ direction, which is perpendicular to the streamline direction and gives an artificial diffusion of magnitude $\lambda_2 = \tau(v_{h1}^2 + v_{h2}^2)$ in the $\mathbf{x}_2$ direction, which is the streamline direction.

For the 9/4c-element, the artificial diffusion term is given by

$$\sum_m \int_{Vol^{(m)}} \overline{\phi}_{h,jj} \; \tau_j |v_{hj}| \; \phi_{h,jj} \; dVol^{(m)}$$

where the value of τ_j is defined as

$$\tau_j = \frac{1}{9}(|\frac{\partial x_j}{\partial \mathbf{r}}|)^3$$

and the characteristic length is defined as

$$|\frac{\partial x_j}{\partial \mathbf{r}}| = \sqrt{(\frac{\partial x_j}{\partial r_1})^2 + (\frac{\partial x_j}{\partial r_2})^2}$$

Now, we want to study the effect of the artificial diffusion on the element level. Let us define

$$\overline{\phi}_h = \mathbf{h}_5 \hat{\overline{\phi}}$$

where $\hat{\overline{\phi}}$ is a vector containing the nodal values of the virtual variable $\overline{\phi}$

$$\hat{\overline{\phi}}^T = [(\overline{\phi})_1, (\overline{\phi})_2, (\overline{\phi})_3, (\overline{\phi})_4, (\overline{\phi})_5]$$

where $(\overline{\phi})_k$ is the nodal value of virtual variable $\overline{\phi}$ at node k and $\mathbf{h}_5$ is a vector of nodal interpolations

$$\mathbf{h}_5 = [h_1, h_2, h_3, h_4, h_5]$$

where h_k is the interpolation function for node k.

Consider v_{hi} and θ_h to be the finite element solution obtained by solving the set of equations (4.2) or (4.3). Consider also the artificial diffusion term for the 5/1-element in the momentum equation in the x_1-direction. For element m, the element nodal forces in the x_1-direction resulting from the artificial diffusion term $\tilde{\mathbf{D}}_5^m$ are

$$\tilde{\mathbf{D}}_5^m = \int_{Vol^{(m)}} \mathbf{h}_{5,k}^T \; (v_{hk} \tau v_{hj}) \; v_{h1,j} \;\; dVol^{(m)}$$

The sum of the forces acting on the element m from the artificial diffusion contribution is obtained by summing all the components of the vector $\tilde{\mathbf{D}}_5^m$, therefore we have

Sum of nodal forces $\tilde{\mathbf{D}}_5^m$ acting on element m

$$
\begin{aligned}
&= [1,1,1,1,1]\,\tilde{\mathbf{D}}_5^m \\
&= [1,1,1,1,1] \int_{Vol^{(m)}} \mathbf{h}_{5,k}^T \left(v_{hk} \tau v_{hj}\right) v_{h1,j} \;\; dVol^{(m)} \\
&= 0
\end{aligned}
$$

This confirms that the artificial diffusion term does not effect the x_1-force equilibrium of each element since the total force contribution from the term is zero. A similar derivation shows that the artificial diffusion does not affect the force equilibrium in the x_2-direction, and also not the moment equilibrium.

For the artificial diffusion term in the energy equation, the nodal heat transfer from the artificial diffusion term $\tilde{\mathbf{Q}}^m$ is

$$
\tilde{\mathbf{Q}}^m = \int_{Vol^{(m)}} \mathbf{h}_{4,k}^T \left(v_{hk} \tau v_{hj}\right) \theta_{h,j} \;\; dVol^{(m)}
$$

where $\mathbf{h}_4 = [h_1, h_2, h_3, h_4]$ is the vector containing the 4-node nodal interpolations (note that the temperature is interpolated bilinearly). Hence

Sum of nodal heat transfer $\tilde{\mathbf{Q}}^m$ in element m

$$
\begin{aligned}
&= [1,1,1,1]\,\tilde{\mathbf{Q}}^m \\
&= [1,1,1,1] \int_{Vol^{(m)}} \mathbf{h}_{4,k}^T \left(v_{hk} \tau v_{hj}\right) \theta_{h,j} \;\; dVol^{(m)} \\
&= 0
\end{aligned}
$$

This confirms that the artificial diffusion term does not affect the total heat transfer equilibrium of each element since the total heat transfer contribution from the term is zero.

A similar proof can be performed for the artificial diffusion term in the 9/4c-element showing that the artificial diffusion term gives zero total force contribution and zero total heat transfer contribution on the element level.

4.4.1 Discussion of an "ideal" solution scheme with upwinding

Finite element methods for incompressible flows can solve any problem of low Reynolds number with sufficient accuracy; however, as the Reynolds number increases, the methods encounter difficulties in terms of iteration convergence and accuracy. The finite element procedure based on the standard Galerkin formulation gives oscillations in the solution of high Reynolds number problems. To stabilize these oscillations, an upwind method is introduced in the formulation by giving more weight to the upstream direction than to the downstream direction which results in a more stable discretization. Further analysis shows that the upwind method is similar to introducing an artificial diffusion in the formulation.

Existing upwind methods, such as the SUPG(Streamline Upwind/Petrov-Galerkin) method, etc., have difficulties in solving very high Reynolds number problems. The methods require many iterations to solve the problems and in some cases the iteration does not converge to a given tolerance. The difficulty of slow iteration convergence for solving high Reynolds number problems is encountered because the matrix corresponding to the finite element discretization increasingly becomes more ill-conditioned as the Reynolds number increases. Another reason is that the methods introduce additional nonlinearities into the formulation which makes the iteration harder to converge. The more iterations are required to solve a problem, the more expensive is the scheme in terms of computational time.

In terms of quality of the flow solution, for some cases, the numerical solutions using an existing upwind method, such as SUPG, contradict physical reasoning. For example, the solution can contain back flow which intuitively should not happen.

Consistency of the upwind method is present if as the mesh is refined, the artificial diffusion term is getting smaller; so as $\Delta x \to 0$, the artificial diffusion $\to 0$. A standard artificial diffusion has a first-order convergence as $\Delta x \to 0$ and we seek for a better artificial diffusion which has a higher order of convergence as the mesh is refined.

In solving a high Reynolds number problem, an "ideal" solution scheme should have the following properties:

1. For any mesh, the method should give a reasonable solution.
2. The method should give the highest possible (optimal) convergence in discretization errors.
3. The method should not be "too sensitive" to the mesh used.
4. For any mesh, the method should converge fast to a small iteration tolerance.
5. For any mesh, an error indicator should be available to evaluate the quality of the solution.
6. If the error indicator indicates too large an error, refining the mesh results into a good solution with an acceptable error.
7. The method converges to the "exact" solution of the mathematical model.

Considering the first property, a reasonable solution means that the solution does not contradict intuition or physical reasoning; for example the direction of the flow should be intuitively correct. The solution should have no oscillation and the overall pictures of the solutions should be similar as the mesh is refined. We want to have

$$\mathbf{U}(\text{coarse mesh}) \subset \mathbf{U}(\text{fine mesh}) \subset \mathbf{U}(\text{finer mesh}) \subset \ldots$$

A method that can solve the laminar flow problems of high Reynolds number is necessary because of two reasons. First, the laminar flow assumption is used to solve any problem in the first iteration. Therefore, if the solution of the first iteration can not be obtained, it is difficult to continue to solve the problem with more complex models, such as a turbulent model. Second, even though the Reynolds number is large, in many cases, the flow in much of the area is laminar and the flow is only turbulent in a small area. Hence, the method should be able to solve any problem with laminar flow assumption and then the solution will be used to indicate where the turbulent model should be used.

When the mesh is very coarse, the method should be able to obtain "a" solution even though the actual physical flow might contain instabilities. With a coarse mesh, the solution will not be able to catch all the physical phenomena, such as boundary layers, backflows, or instabilities but as the mesh is refined, more physical phenomena are revealed in the solution and the overall flow should be similar to the coarse mesh solution. Eventually, when the mesh is fine enough, the solution should pick up the instability behavior of the flow and a transient analysis should be used.

For example, let us consider the driven flow cavity problem, see fig. 4-3. The domain is discreatized into 10×10 elements. The method should be able to solve the problem when the Reynolds number is low, such as 10, 100, without too much difficulties. When the Reynolds number is greater than 1000, the iteration converges slowly and an ideal method should still obtain "a" solution with a reasonable number of iterations. For high Reynolds number flow, circulation flows occur in both lower corners. If the mesh is too coarse, boundary layers on the walls and circulation flows in the lower corners will not be revealed in the solution but the solution should still be reasonable. As the mesh is refined, boundary layers and circulations start to show. Ideally, the method should be able to "solve any problem in this way" with the Reynolds number up to 10^7, where most of the engineering problems lie.

Generally, in solving the problem,

$$\mathbf{K}\mathbf{U} = \mathbf{R}$$

where $\mathbf{U}$ is the solution, the method may modify the problem into

$$(\mathbf{K} + \mathbf{A})\mathbf{U} = \mathbf{R} \tag{4.4}$$

where $\mathbf{A}$ is the artificial diffusion term. As the mesh is refined, $\mathbf{A} \to 0$ and eqn. (4.4) should give a reasonable solution $\mathbf{U}$ and the iteration should converge fast in solving eqn. (4.4) for any reasonable mesh.

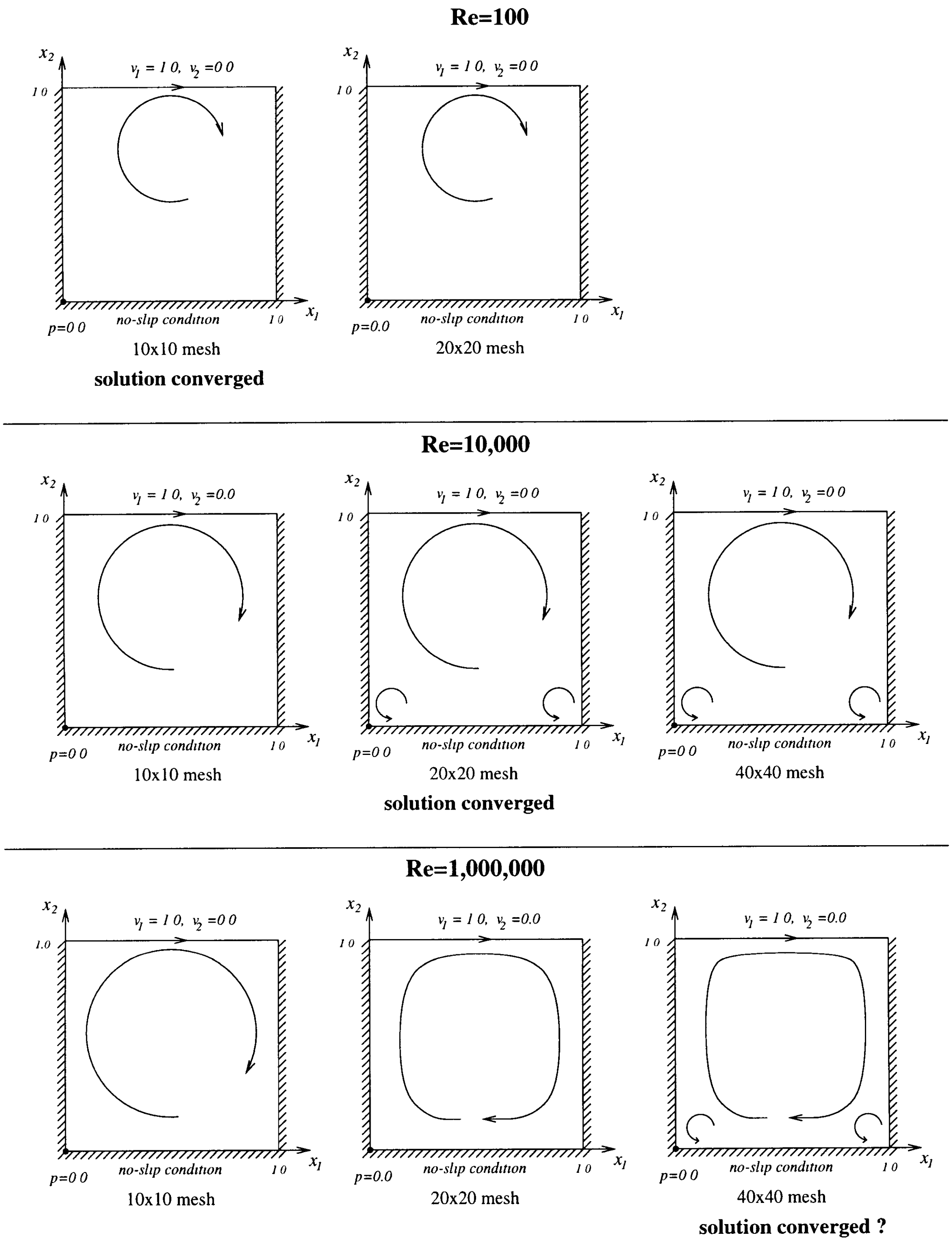

Figure 4-3: Sketches of the solutions of driven flow cavity problem.

4.5 Inf-sup condition

For stability, the finite element for an incompressible formulation should satisfy the inf-sup condition [5, 29] which relates the discretization spaces for the velocity and the pressure. The derivation of the inf-sup condition for the incompressible flow formulation is explained in [5, 28, 29] and we only summarize here the main equations. When a steady-state condition is considered and when the Reynolds number is very small so that we can neglect the convective term, the governing equations of the incompressible flow become

$$\begin{aligned} p_{,i} - \mu(v_{i,j} + v_{j,i})_{,j} - f_i^B &= 0 \\ v_{i,i} &= 0 \end{aligned} \tag{4.5}$$

Eqns. (4.5) are called the steady Stokes' equations. If we define the finite element spaces for velocity V_h, and pressure Q_h,

$$\begin{aligned} V_h &= \{\mathbf{v}_h | \mathbf{v}_h \in L^2(Vol); \frac{\partial(v_h)_i}{\partial x_j} \in L^2(Vol), i,j = 1,2; \mathbf{v}_h|_{S_u} = 0\} \\ Q_h &= \{q_h | q_h \in L^2(Vol)\} \end{aligned}$$

the discrete variational formulation of eqns. (4.5) is :

Find $(v_{h1}, v_{h2}) \in V_h, p_h \in Q_h$ such that for all $(\overline{v}_{h1}, \overline{v}_{h2}) \in V_h, \overline{p}_h \in Q_h$ we have

$$\begin{aligned} \int_{Vol} \{-\overline{v}_{hi,i}\, p_h + (\overline{v}_{hi,j} + \overline{v}_{hj,i})\frac{\mu}{2}(v_{hi,j} + v_{hj,i})\} dVol &= \int_{Vol} \overline{v}_{hi} f_i^B dVol + \int_{S_f} \overline{v}_{hi}^s f_i^s dS \\ -\int_{Vol} \overline{p}_h\, v_{hi,i}\, dVol &= 0 \end{aligned}$$

Rewriting $v_{hi,i} = div\mathbf{v}_h$ where $\mathbf{v}_h^T = [v_{h1} \;\; v_{h2}]$, the inf-sup condition for the Stokes' equations is, see [5, 28, 29]

$$\inf_{p_h \in Q_h} \sup_{\mathbf{v}_h \in V_h} \frac{\int p_h div\mathbf{v}_h dVol}{||p_h||_p ||\mathbf{v}_h||_v} \geq \gamma > 0 \tag{4.6}$$

Let us define $P_h(div\mathbf{w}_h)$ to be the L^2-projection operator onto the space Q_h such that

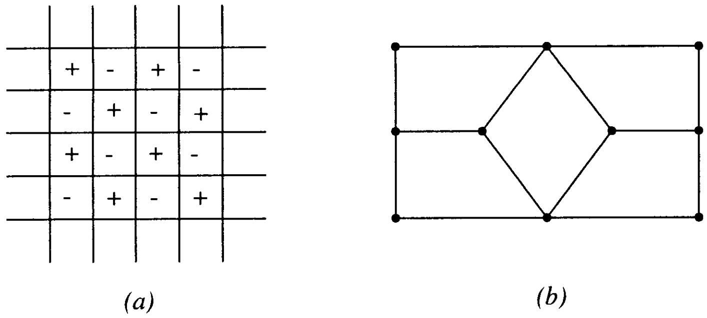

Figure 4-4: (a) Spurious pressure mode in the 4/1-element (b) macroelement of the 4/1-element.

for $\mathbf{w}_h \in V_h$

$$\int_{Vol} \overline{p}_h \ (P_h(div\mathbf{w}_h) - div\mathbf{w}_h)dVol = 0 \qquad \forall \overline{p}_h \in Q_h \tag{4.7}$$

Q_h will always contain $P_h(div\mathbf{w}_h)$ by construction and if Q_h is larger than $P_h(div\mathbf{w}_h)$, Q_h will contain spurious pressure modes p_s such that

$$\int p_s \ div\mathbf{v}_h dVol = 0 \qquad \forall \mathbf{v}_h \in V_h$$

The inf-sup value in the expression (4.6) will be zero if Q_h contains a spurious pressure mode, or if Q_h is larger than $P_h(div\mathbf{w}_h)$ and therefore in this case the inf-sup condition will of course not be satisfied. However, even when there is no spurious pressure mode, we need that eqn. (4.6) holds.

In a regular mesh, the 4/1-element has a spurious pressure mode in the checkerboard pattern shown in fig. 4-4 (a). This spurious pressure arises in the solution of problems containing certain boundary conditions such as specific prescribed velocities on all boundaries. The pressure mode can be eliminated by arranging the elements in the macroelement pattern shown in fig. 4-4 (b), and the macroelement does satisfy the inf-sup condition, see [30]. However, generating such a mesh is cumbersome and rather complicated.

The 5/1-element does not permit the checkerboard pressure pattern, therefore this

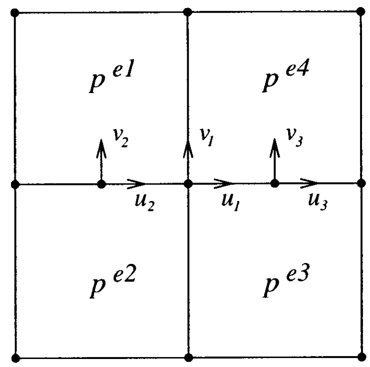

Figure 4-5: Patch of four equal elements.

element does not have a spurious pressure mode. The proof is as follows. Consider a patch of a regular mesh as shown in fig. 4-5. For the velocity u_1 as shown in fig. 4-5, we have

$$\int p_h \; div\mathbf{v}_h \; dVol = [p^{e1} + p^{e2} - p^{e3} - p^{e4}]u_1 = 0$$

and the solution is the checkerboard pattern : $p^{e1} = -p^{e2} = p^{e3} = -p^{e4}$. For the velocity v_1, we have

$$\int p_h \; div\mathbf{v}_h \; dVol = [-\frac{1}{3}p^{e1} + \frac{1}{3}p^{e2} + \frac{1}{3}p^{e3} - \frac{1}{3}p^{e4}]v_1 = 0$$

and the same checkerboard solution : $p^{e1} = -p^{e2} = p^{e3} = -p^{e4}$ holds. However, for the velocity v_2,

$$\int p_h \; div\mathbf{v}_h \; dVol = [-\frac{4}{3}p^{e1} + \frac{4}{3}p^{e2}]v_2 = 0$$

and the velocity v_3,

$$\int p_h \; div\mathbf{v}_h \; dVol = [\frac{4}{3}p^{e3} - \frac{4}{3}p^{e4}]v_3 = 0$$

the solution for the above relations are $p^{e1} = p^{e2}$ and $p^{e3} = p^{e4}$. These eliminate the checkerboard pressure mode. The checkerboard mode is the only spurious pressure mode in a regular mesh of the 4/1-element, hence we can conclude that the 5/1-element does not contain a spurious pressure mode. Therefore we know that

$P_h(div\mathbf{w}_h) \subseteq Q_h$ and the inequality (4.6) becomes

$$\inf_{p_h \in P_h(div\mathbf{w}_h)} \sup_{\mathbf{v}_h \in V_h} \frac{\int p_h div\mathbf{v}_h dVol}{||p_h||_p ||\mathbf{v}_h||_v} \geq \gamma > 0 \tag{4.8}$$

In matrix form, the inf-sup condition (4.8) becomes

$$\inf_{\mathbf{Q}_h} \sup_{\mathbf{V}_h} \frac{\mathbf{Q}_h^T \mathbf{K}_{pu} \mathbf{V}_h}{\sqrt{\mathbf{Q}_h^T \mathbf{K}_{pp} \mathbf{Q}_h} \sqrt{\mathbf{V}_h^T \mathbf{S} \mathbf{V}_h}} \geq \gamma > 0 \tag{4.9}$$

where $\mathbf{K}_{pp}, \mathbf{S}$ are matrices corresponding to the norms $||\cdot||_p$ and $||\cdot||_v$. Here we use the L^2-norm for the pressure and the H^1-seminorm for the velocity. From the L^2-projection (eqn. (4.7)), we have

$$\mathbf{K}_{pp}\mathbf{Q}_h - \mathbf{K}_{pu}\mathbf{W}_h = 0$$

and so

$$\mathbf{Q}_h = \mathbf{K}_{pp}^{-1}\mathbf{K}_{pu}\mathbf{W}_h \tag{4.10}$$

Substituting eqn. (4.10) into (4.9), we have

$$\inf_{\mathbf{W}_h} \sup_{\mathbf{V}_h} \frac{\mathbf{W}_h^T \mathbf{K}_{pu}^T \mathbf{K}_{pp}^{-T} \mathbf{K}_{pu} \mathbf{V}_h}{\sqrt{\mathbf{W}_h^T \mathbf{K}_{pu}^T \mathbf{K}_{pp}^{-T} \mathbf{K}_{pu} \mathbf{W}_h} \sqrt{\mathbf{V}_h^T \mathbf{S} \mathbf{V}_h}} \geq \gamma > 0 \tag{4.11}$$

Consider the eigenproblem

$$\mathbf{G}\phi_h = \lambda \mathbf{S}\phi_h \tag{4.12}$$

where $\mathbf{G} = \mathbf{K}_{pu}^T \mathbf{K}_{pp}^{-T} \mathbf{K}_{pu}$, then the inf-sup value of eqn. (4.9) is the smallest nonzero eigenvalue of the the above eigenproblem [30]. The proof is as follows.

Let us define

$$f(\mathbf{W}_h, \mathbf{V}_h) = \frac{\mathbf{W}_h^T \mathbf{G} \mathbf{V}_h}{(\mathbf{W}_h^T \mathbf{G} \mathbf{W}_h)^{\frac{1}{2}} (\mathbf{V}_h^T \mathbf{S} \mathbf{V}_h)^{\frac{1}{2}}}$$

and

$$\mathbf{S} = \mathbf{L}^T\mathbf{L}, \qquad \mathbf{X}_h = \mathbf{L}\mathbf{V}_h$$

so that

$$f(\mathbf{W}_h, \mathbf{X}_h) = \frac{\mathbf{W}_h^T \mathbf{G} \mathbf{L}^{-1} \mathbf{X}_h}{(\mathbf{W}_h^T \mathbf{G} \mathbf{W}_h)^{\frac{1}{2}} (\mathbf{X}_h^T \mathbf{X}_h)^{\frac{1}{2}}}$$

We use the Cauchy-Schwarz inequality

$$\|\mathbf{W}_h^T \mathbf{G} \mathbf{L}^{-1} \mathbf{X}_h\| \leq \|\mathbf{W}_h^T \mathbf{G} \mathbf{L}^{-1}\| \|\mathbf{X}_h\|$$

and with the Euclidean norm definition

$$\|\mathbf{X}_h\| = (\sum_{i=1}^{N} x_i^2)^{\frac{1}{2}} = (\mathbf{X}_h^T \mathbf{X})^{\frac{1}{2}}$$

Hence,

$$\sup_{\mathbf{L}^{-1}\mathbf{X}_h} f(\mathbf{W}_h, \mathbf{X}_h) = \frac{(\mathbf{W}_h^T \mathbf{G} \mathbf{L}^{-1} \mathbf{L}^{-T} \mathbf{G}^T \mathbf{W}_h)^{\frac{1}{2}}}{(\mathbf{W}_h^T \mathbf{G} \mathbf{W}_h)^{\frac{1}{2}}} \tag{4.13}$$

Note that $\mathbf{G}\mathbf{L}^{-1}\mathbf{L}^{-T}\mathbf{G}^T = \mathbf{G}(\mathbf{L}^T\mathbf{L})^{-1}\mathbf{G}^T = \mathbf{G}\mathbf{S}^{-1}\mathbf{G}^T$. Consider the following eigenproblem

$$\mathbf{G}\mathbf{S}^{-1}\mathbf{G}^T \boldsymbol{\phi}_h = \lambda \mathbf{G} \boldsymbol{\phi}_h \tag{4.14}$$

The infimum of the expression in (4.13) is found by choosing $\mathbf{W}_h$ to be $\boldsymbol{\phi}_h$ corresponding to the smallest eigenvalue of the above eigenproblem, therefore

$$\inf_{\mathbf{W}_h} \sup_{\mathbf{L}^{-1}\mathbf{X}_h} f(\mathbf{W}_h, \mathbf{X}_h) = \lambda_{min}^{\frac{1}{2}}$$

However, the eigenproblem in (4.14) can be rewritten as

$$\mathbf{G}^T \phi_h = \lambda \mathbf{S} \phi_h$$

and since the matrix $\mathbf{G}$ is a symmetric matrix, the above eigenproblem is equivalent to eqn. (4.12).

Let us apply the numerical inf-sup test to our 5/1-element. As a comparison, we also apply the numerical inf-sup test to the 4/1 and 9/1-elements. Note that the 9/4c-element has been proved to satisfy the inf-sup condition analytically [29]. The boundary condition for the test problems are described in fig. 4-6. In problem 1, the

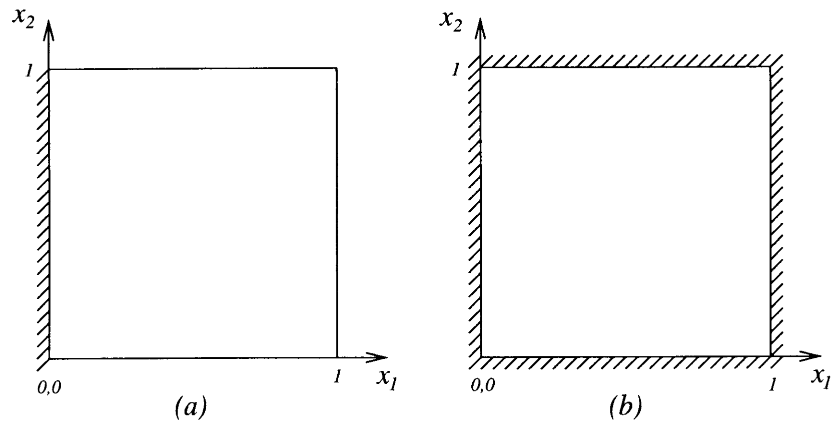

Figure 4-6: Boundary conditions for the inf-sup test, (a) problem 1, (b) problem 2.

velocity is fixed on the left boundary and free on the other sides of the boundary. In problem 2, the velocity is fixed on all sides of the boundary. A sequence of four meshes is considered and successive refinements are obtained by dividing the element side lengths by 2. The results are plotted as a function of the element side lengths h. Fig 4-7 shows the numerical results for both test problems. Fig. 4-7 shows that the 5/1-element passes the inf-sup test since the inf-sup value of this element is bounded from below. Therefore the 5/1-element will most likely satisfy the inf-sup condition. The figure also shows that the 4/1-element does not pass the inf-sup test, and the 9/1-element passes the inf-sup test, as proven in [5].

Let us consider the spurious mode detected by the numerical test for the problem 2. In problem 2, the pressure needs to be prescribed at one point to eliminate the arbitrary constant in the pressure solution. This arbitrary constant corresponds to one zero eigenvalue in the numerical test. For the 4×4 mesh, the 4/1-element contains 16 pressure unknowns (P_m) and the total of 18 velocity unknowns (V_m). Hence, the difference is $V_m - P_m = 2$. The numerical test detects 4 zero eigenvalues. Substracting the difference of the unknowns ($V_m - P_m$) from the number of zero eigenvalues detected by the numerical test, we have still 2 zero eigenvalues to be explained. One eigenvalue corresponds to the physical pressure mode, the arbitrary constant in the pressure solution. The other eigenvalue corresponds to the spurious

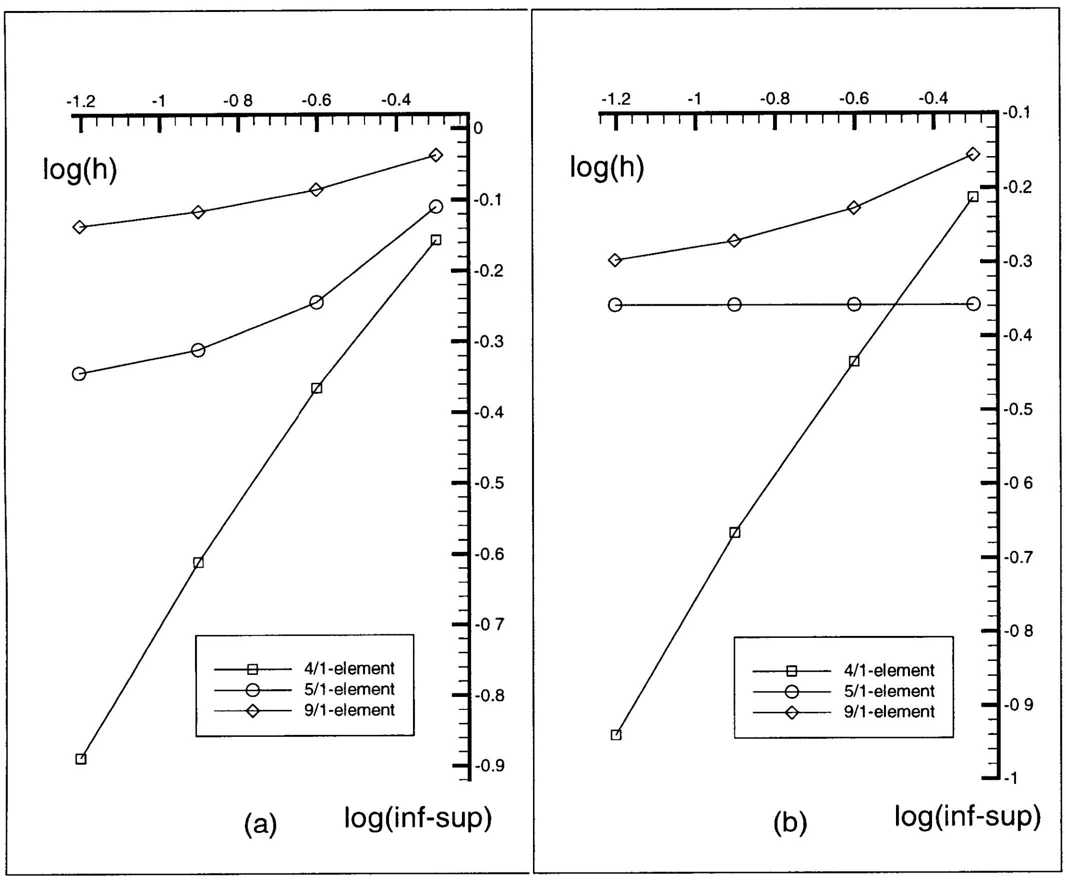

Figure 4-7: Inf-sup test results, (a) problem 1, (b) problem 2.

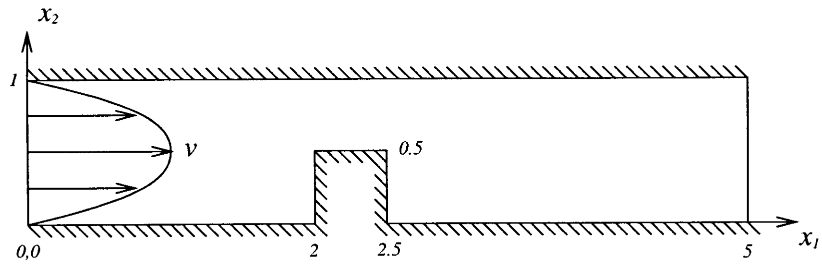

Figure 4-8: Incompressible flow in a channel with a block problem.

pressure mode, the checkerboard pattern.

For the same mesh, the 5/1-element contains 16 nodal pressure unknows and the total of 34 velocity unknowns. Hence, the difference is $34 - 16 = 18$. The numerical test detects 19 zero eigenvalues. Substracting the difference of the unknowns from the number of zero eigenvalues detected by the numerical test, we have 1 zero eigenvalue. This zero eigenvalue corresponds to the physical pressure mode, the arbitrary constant in the pressure solution. This supports our previous analysis that the 5/1-element does not have a spurious pressure mode. The same conclusion is obtained if we consider the 8×8 mesh.

To illustrate the necessity for the element to satisfy the inf-sup condition, let us consider the steady-state problem described in fig. 4-8. In the problem, an incompressible flow is passing a block in a channel. No-slip boundary conditions are imposed on the upper and lower boundaries, and on the left boundary, the velocity is prescribed with a parabolic profile and maximum velocity at the center $= 1$. The Reynolds number of the problem based on the maximum prescribed velocity and the height of the channel at the inlet is 100. The domain is discretized into a total of 324 finite elements as shown in fig. 4-9.

The solution of the problem using the 4/1-element with the SUPG scheme is shown in fig. 4-10. The velocity is predicted quite well using this element and there is no oscillation in the solution; however, the pressure is not well predicted (In fig. 4-10, the pressure plot is obtained by using the element pressure values at the centers of the elements and connecting the values by a line). Significant oscillations occur in the

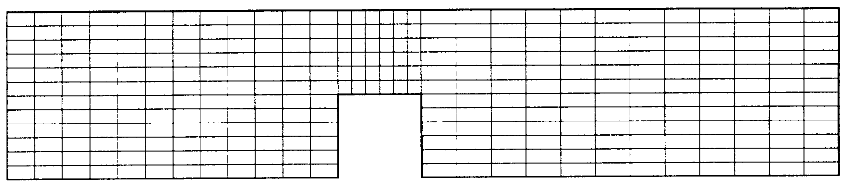

Figure 4-9: Mesh for the incompressible flow in a channel with a block problem.

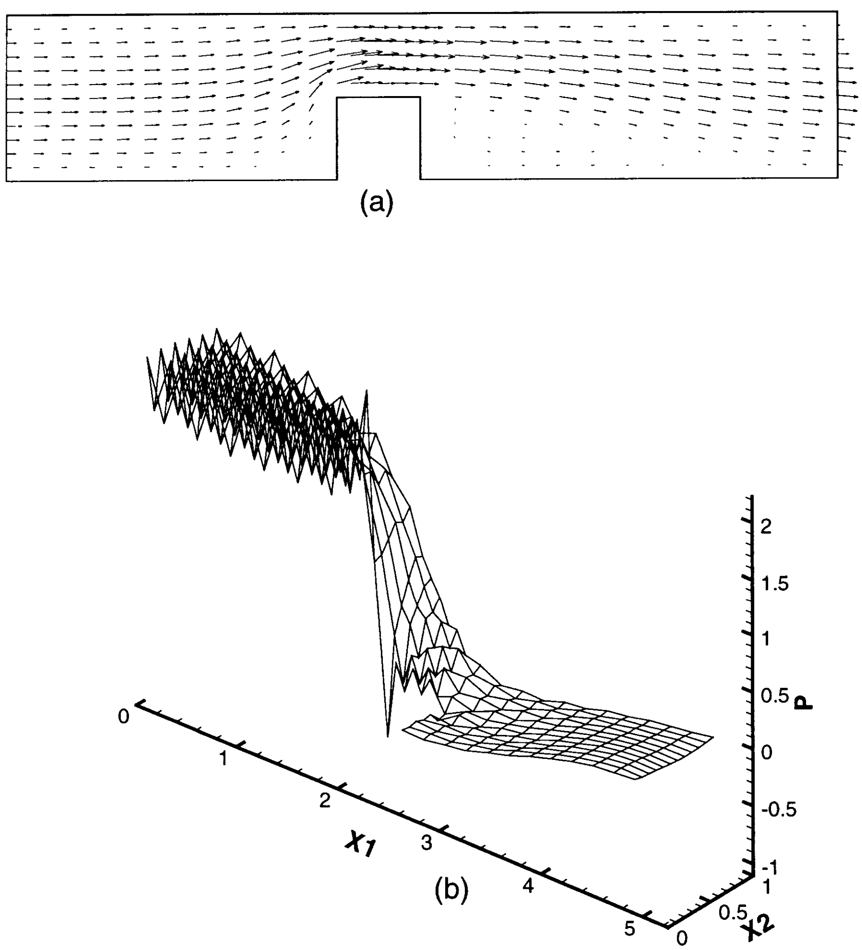

Figure 4-10: Solution of the flow in a channel with a block problem using 4/1-element, (a) velocity, (b) pressure .

pressure solution. Some reseachers [50, 51, 52] modify the mass conservation equation by adding a term that stabilizes the pressure solution so that they can use equal order interpolations for the pressure and velocity. However, the mass conservation will then strictly not be satisfied. These methods with adding a term to the mass conservation equation to stabilize the pressure solution are acceptable as long as the methods still converge.

The solution of the problem using the 5/1-element with the streamline artificial diffusion is shown in fig. 4-11. The same mesh as for the 4/1-element was used. Velocity and pressure solutions with no oscillation are obtained using this element. This confirms the necessity for the element to satisfy the inf-sup condition even for a reasonably high Reynolds number flow.

4.6 Numerical convergence study

The purpose of this numerical convergence study is to see the order of convergence of the schemes proposed in this thesis in some example solutions.

Consider the problem described in fig. 4-12. The problem describes an impinging fluid flow over a slip-wall problem with controlled body force. The body force function is prescribed as

$$f_2^B = 5x_1x_2^8 + 10x_1x_2^3 + 60\mu x_1x_2^2$$

and fluid density is constant, $\rho = 1$. The exact solution for this problem is

$$\begin{aligned} v_1 &= -5x_1x_2^4 \\ v_2 &= -\frac{1}{2} + x_2^5 \\ p &= \frac{1}{2}x_2^5 - \frac{1}{2}x_2^{10} + 5\mu x_2^4 \end{aligned}$$

Two cases are considered. In case 1, we consider a diffusion dominated problem where $\mu = 10$ (Reynolds number, $Re = 0.5025$ based on the maximum velocity and the length of the domain). In case 2, we consider a pure convection problem with

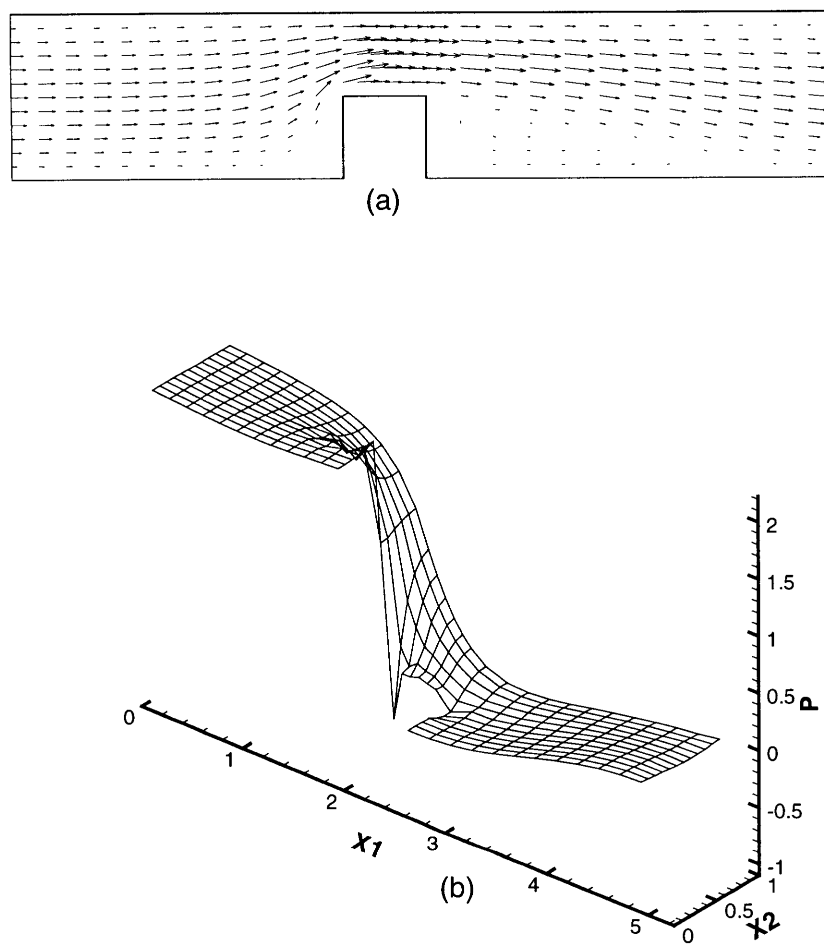

Figure 4-11: Solution of the flow in a channel with a block problem using 5/1-element, (a) velocity, (b) pressure .

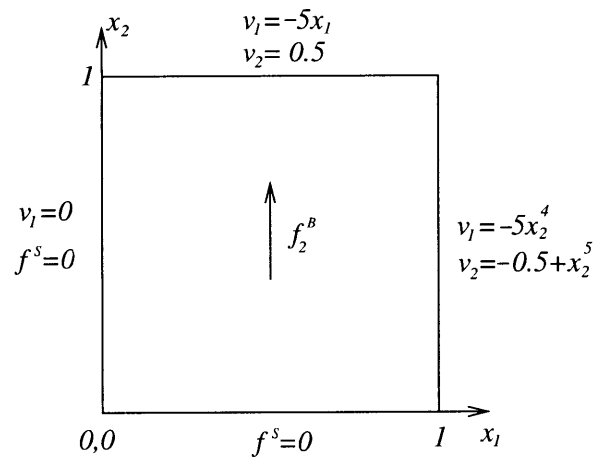

Figure 4-12: Impinging fluid flow over a slip-wall problem.

$\mu = 0$. We perform the convergence study using $8 \times 8, 16 \times 16$ and 32×32 uniform meshes. The errors measured are : pressure error using the L^2-norm ($||p - p_h||_{L^2}$), velocity error using the L^2-norm ($||v_i - v_{hi}||_{L^2}$) and velocity error using the H^1-norm ($||v_i - v_{hi}||_{H^1}$). The solutions of the problems using the 9/4c-element with the finest mesh are shown the fig. 4-13. The results of the convergence study for the case 1 is shown is in fig. 4-14 and for the case 2 in fig. 4-15.

For the diffusion dominated problem, the convergence rates of the elements obtained by this numerical convergence study agree with the results of the theory of interpolation, (see, for example, [31] for the explanation of the theory of interpolation in Sobolev spaces)

$$||p - p_h||_m \leq c_1 ||p - p_I||_m \leq c_2 h^{k+1-m} |p|_{k+1}$$

$$||v_i - v_{hi}||_m \leq c_3 ||v_i - v_{Ii}||_m \leq c_4 h^{k+1-m} |v_i|_{k+1}$$

where p_I, v_{Ii} are the interpolation pressure and velocity. For example, for the 5/1-element, the pressure is interpolated using discontinuos constant functions, hence $(k+1) = 1$ and the pressure error is evaluated using the L^2-norm ($m = 0$) therefore

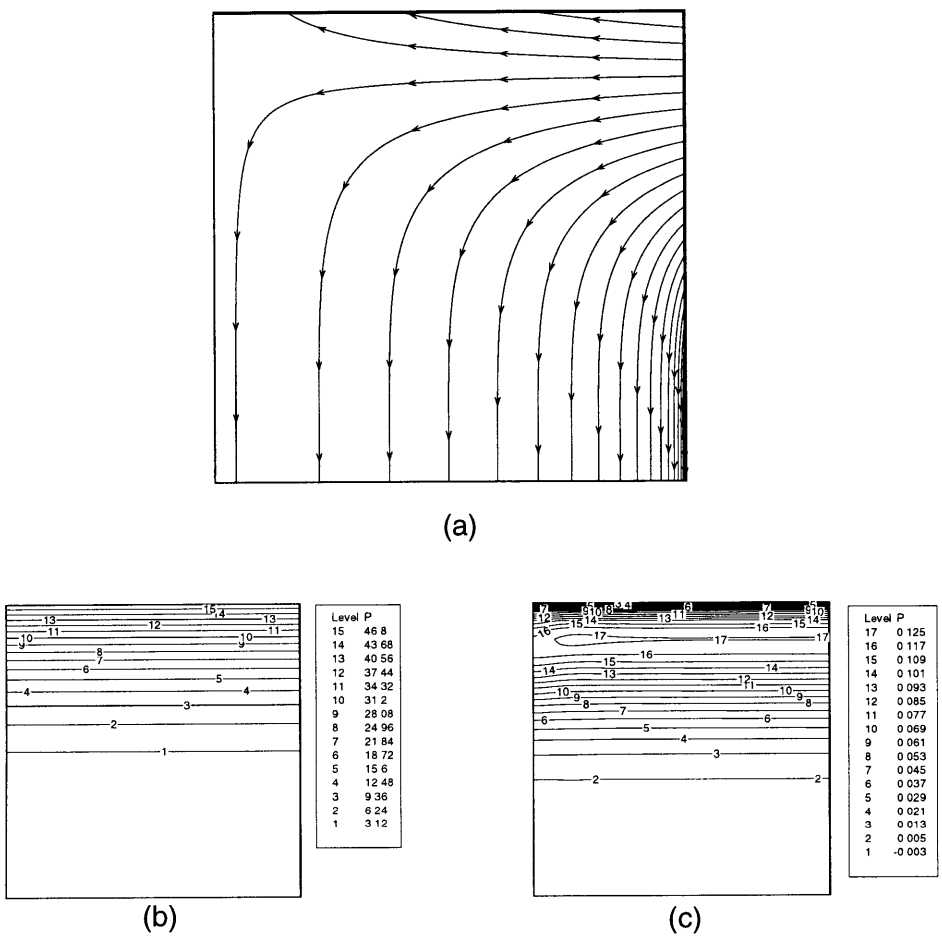

Figure 4-13: Solution of impinging fluid flow over a slip-wall problem using 9/4c-element, (a) streamlines, (b) pressure in case 1, (c) pressure in case 2.

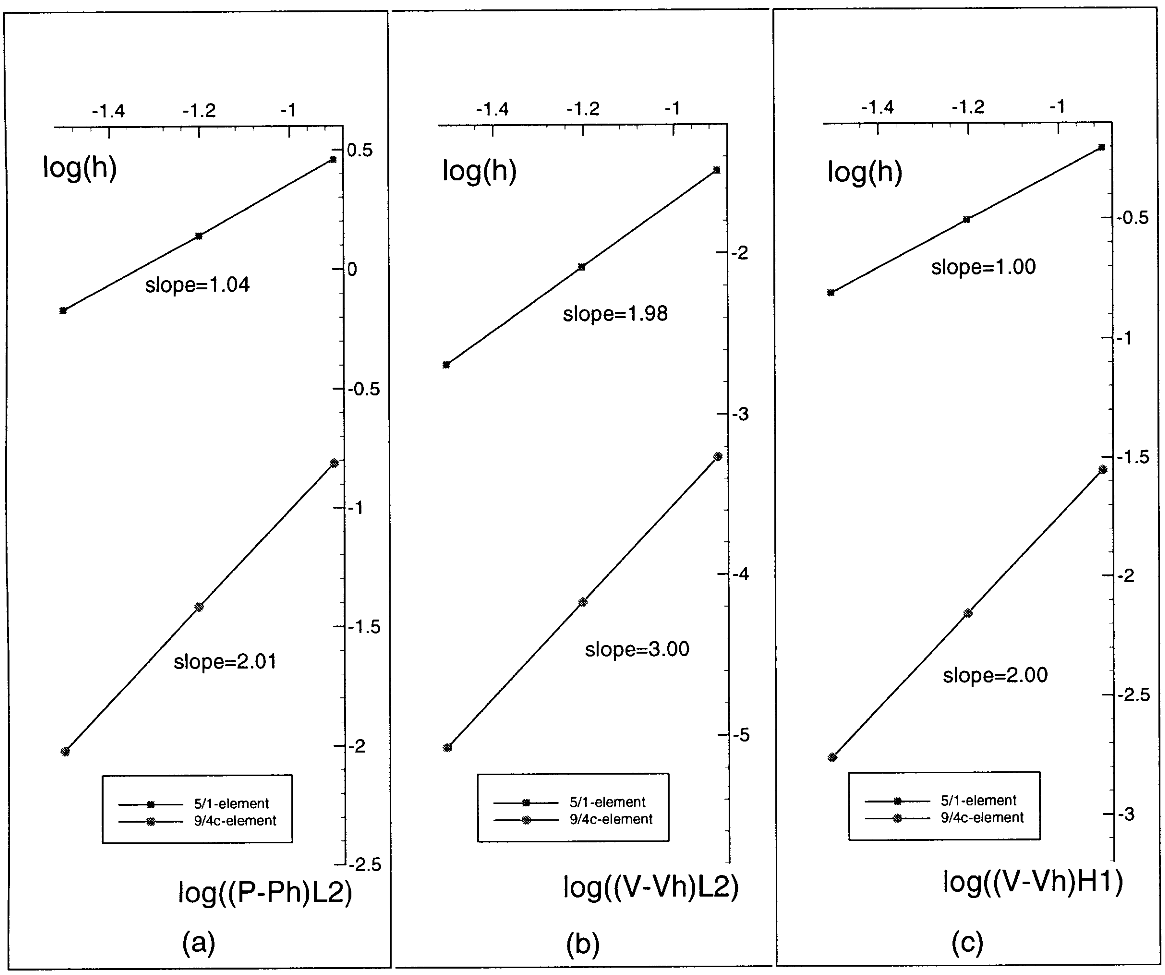

Figure 4-14: Error convergence for impinging fluid flow over a slip-wall problem, case 1, (a) pressure error in L^2-norm, (b) velocity error in L^2-norm, (c) velocity in H^1-norm.

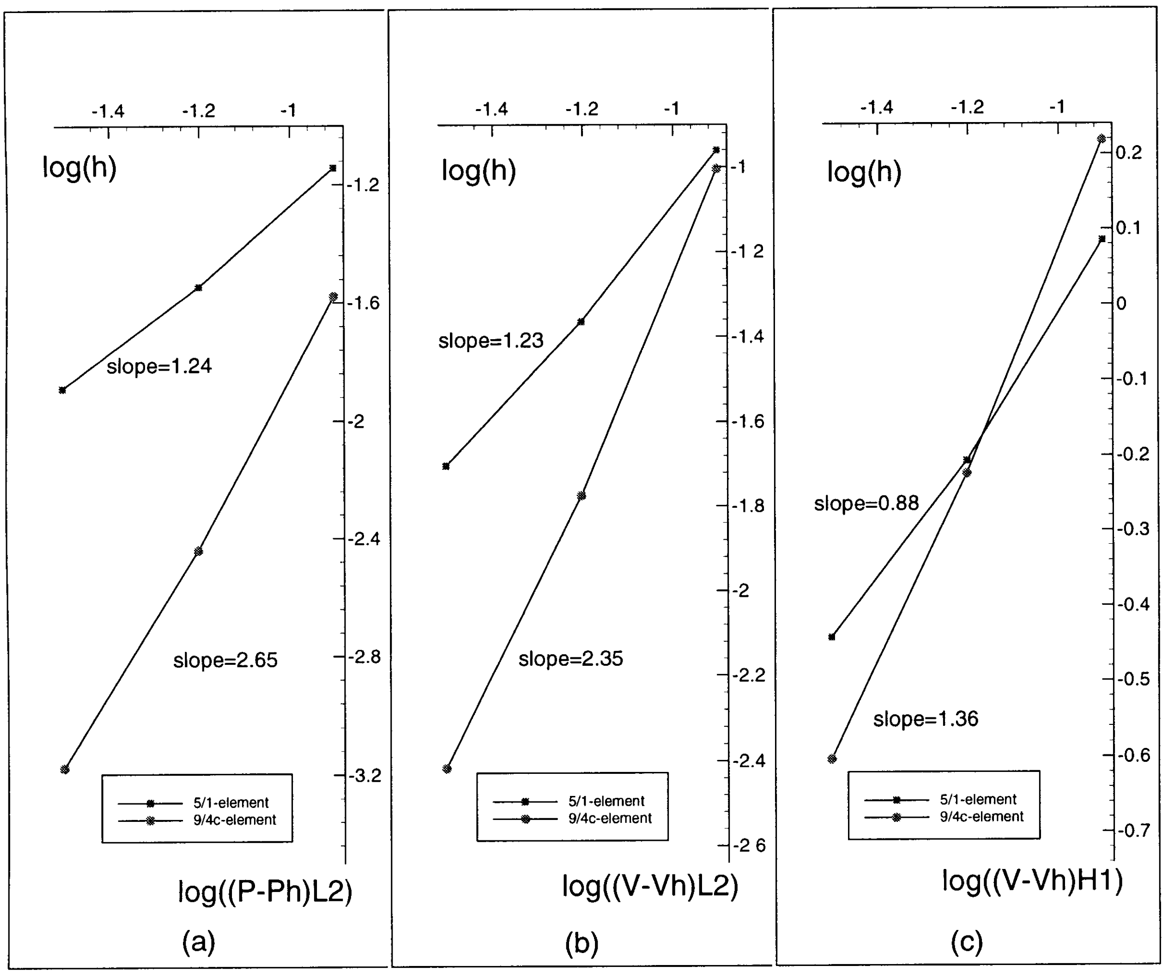

Figure 4-15: Error convergence for impinging fluid flow over a slip-wall problem, case 2, (a) pressure error in L^2-norm, (b) velocity error in L^2-norm, (c) velocity in H^1-norm.

the theory of interpolation gives

$$\|p - p_h\|_0 \leq ch^1 |p|_1$$

which states that the convergence rate is 1.0. Fig. 4-14 shows that the slope is 1.04. Similarly, for the velocity, the 5/1-element uses almost a linear interpolation, hence $(k+1) = 2$ and for the L^2-norm $(m = 0)$, we have

$$\|v_i - v_{hi}\|_0 \leq ch^2 |v_i|_2$$

and for the H^1-norm, we have

$$\|v_i - v_{hi}\|_1 \leq ch^1 |v_i|_2$$

The theory states that for the L^2-norm, the convergence rate is 2.0 and for the H^1-norm, the convergence rate is 1.0. Fig. 4-14 shows that the slope for the velocity error using the L^2-norm is 1.98 and using the H^1-norm is 1.0.

For the 9/4c-element, the theory of interpolation states that the convergence rate of the pressure in the L^2-norm is 2.0, the convergence rate of the velocity in the L^2-norm is 3.0 and in the H^1-norm is 2.0. Fig. 4-14 shows that the slope for the pressure error in the the L^2-norm is 2.01, the velocity error in the L^2-norm is 3.0 and in the H^1-norm is 2.0.

In the pure convection case, the numerical study shows that the convergence rate for the velocity is less than in the diffusion dominated case; however, the convergence rate for the pressure is larger than in the diffusion dominated case. Using the 5/1-element, the convergence rate of the velocity in the L^2-norm is around 1.23 (diffusion dominated, 1.98) and in the H^1-norm is around 0.88 (diffusion dominated, 1.00). For the pressure, the convergence rate in the L^2-norm is around 1.24 (diffusion dominated, 1.04).

Using the 9/4c-element, the convergence rate of the velocity in the L^2-norm is around 2.35 (diffusion dominated, 3.00) and in the H^1-norm is around 1.36 (diffusion

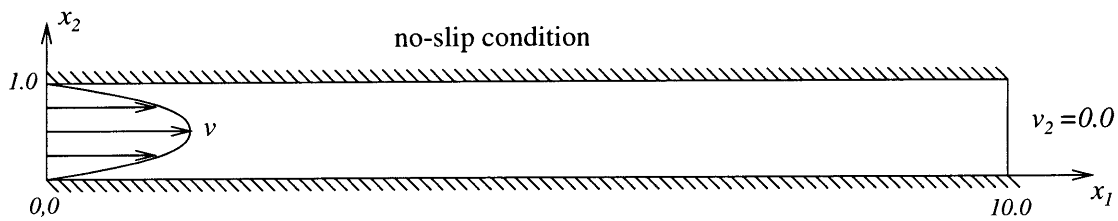

Figure 4-16: Poiseuille flow problem.

dominated, 2.00). For the pressure, the convergence rate in the L^2-norm is around 2.65 (diffusion dominated, 2.01).

A mathematical analysis of the theoretical convergence rate in the pure convection problem for these elements would be valuable.

4.7 Numerical examples

We consider some problems to study the performance of the methods proposed in this thesis.

4.7.1 Poiseuille flow problem

This problem is considered to show the advantage of using the quadratic element over a low order element such as the 5/1-element. The problem considered is described in fig. 4-16. In the problem, the lower and upper boundaries are assumed to be non-slip boundaries. At the left boundary, we prescribe the velocity with a parabolic profile and the maximum velocity at the center = 1. At the right boundary, $v_2 = 0$ is imposed. The Reynolds number for the problem based on the maximum inlet velocity and the height of the channel is 1000. The exact solution for this problem is

$$v_1 = 4x_2(1 - x_2), \qquad v_2 = 0, \qquad p = 0.008(10 - x_1)$$

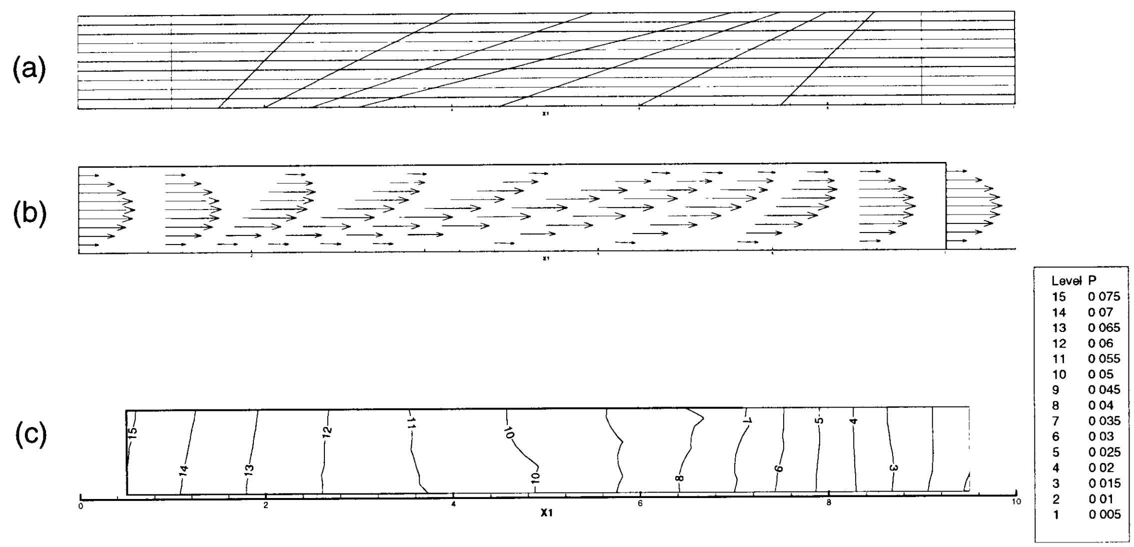

Figure 4-17: Mesh and solution of the Poiseuille flow problem using 5/1-element, (a) the mesh used, (b) velocity, (c) pressure contour.

The domain is discretized into a distorted mesh of 10×10 elements as shown in fig. 4-17 (a).

The solution of the problem using the 5/1-element is shown in fig. 4-17. Note that in plotting the pressure distribution, we use the element pressure values at the centers of the elements and linear interpolation between these values. Fig. 4-17 shows that the velocity is well predicted using this element even though a distorted mesh is used; however, the pressure is not well predicted. A smooth pressure solution is not obtained. However, the total pressure drop across the domain in the solution is close to the pressure drop of the exact solution.

The solution of the problem using the 9/4c-element is shown in fig. 4-18. The same mesh as for the 5/1-element was used. Using this element, the exact solutions for both velocity and pressure are obtained. We can obtain the exact solution of this problem using the 9/4c-element because the finite element spaces of the pressure and velocity for this element can contain the exact solution of the problem. Whereas for the 5/1-element, the finite element spaces of the pressure and velocity do not contain the exact solution of the problem.

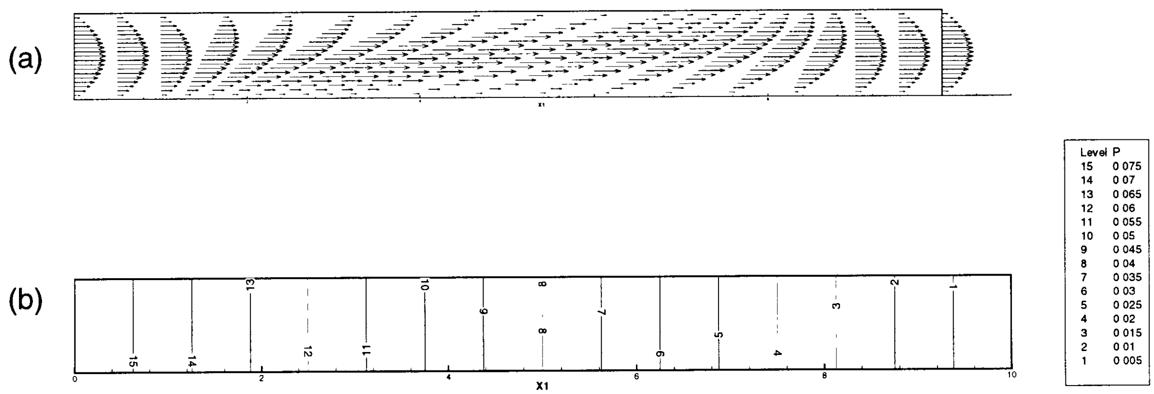

Figure 4-18: Solution of the Poiseuille flow problem using 9/4c-element, (a) velocity, (b) pressure contour.

4.7.2 "S"-shaped channel flow

This problem is considered to study the performance of the 9/4c-element in solving a difficult problem and to discuss the performance of the element in relation to the "ideal" solution scheme described in section 4.4.1. The problem considered is described in fig. 4-19. The no-slip boundary condition is imposed on the walls of the channel. At the inlet, we impose the velocity with a parabolic profile and the maximum velocity at the center = 1. At the outlet, $v_2 = 0$ is imposed. We will show the solutions of the problem with two different Reynolds numbers. The Reynolds number is calculated based on the maximum inlet velocity and the height of the channel at the inlet.

The solutions of the problem with the Reynolds number=100 and with different meshes are shown in fig. 4-20. Fig. 4-20 shows that using the coarse mesh, circulation flows at corners A and D are not well obtained. Using the fine mesh (the total of 384 elements), a reasonable solution is obtained and circulation flows at corners A, D and also close to B are obtained. Using the finest mesh, a similar solution as using the fine mesh is obtained. Therefore we conclude that the fine mesh is sufficient to solve the problem. We can also conclude that using the coarse mesh, the method still gives a reasonable solution (no oscillation). Good pressure solutions are obtained using all

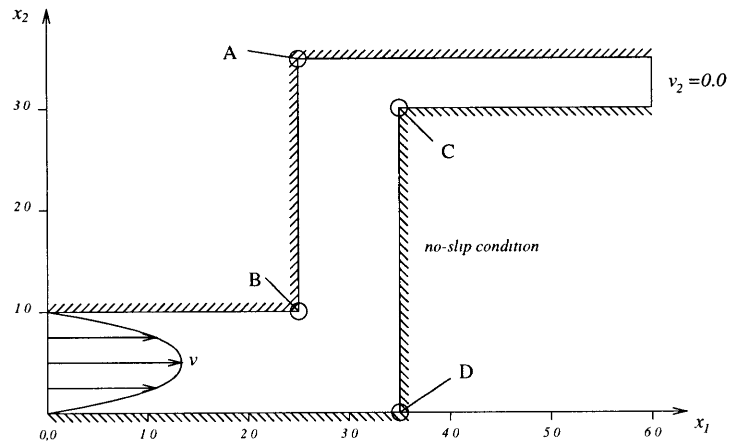

Figure 4-19: "S"-shaped channel flow problem.

the meshes.

The solutions of the problem with the Reynolds number=1,000 and with different meshes are shown in fig. 4-21. Fig. 4-21 shows that using the coarse mesh, circulation flows at corners A, B, C and D are not well obtained. Using the fine mesh (the total of 384 elements), a reasonable solution is calculated and circulation flows at corners A, B, and D are well obtained. However, the backflow at corner C is not well predicted. Using the finest mesh, a similar solution as using the fine mesh is obtained except the backflow at corner C is now well predicted. Therefore we conclude that the fine mesh is not sufficient to solve the problem. A refinement of the mesh around the corner C is necessary to obtain an acceptable solution.

However, when the Reynolds number is increased, the method encounters difficulties in solving the problem. We have experimented that the method can give "a" solution of the problem with Reynolds number up to around 4,500 using a reasonable mesh. Therefore the method does not meet the requirements to be the "ideal" solution scheme since the method can not give "a" solution for a very high Reynolds number flow. More work needs to be done to improve the method.

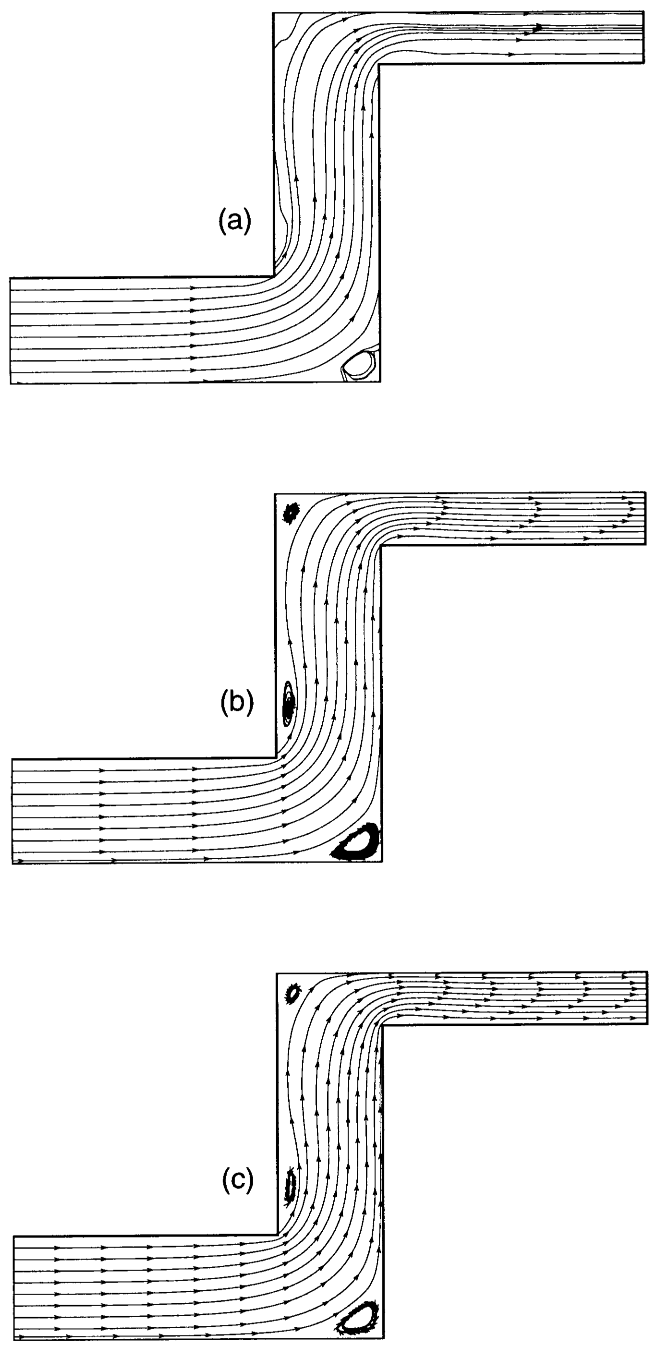

Figure 4-20: Streamline solutions of the "S"-shaped channel flow problem with Reynolds number=100 using the 9/4c-element, (a) with coarse mesh (the total of 96 elements), (b) with fine mesh (the total of 384 elements), (c) with finest mesh (the total of 1536 elements).

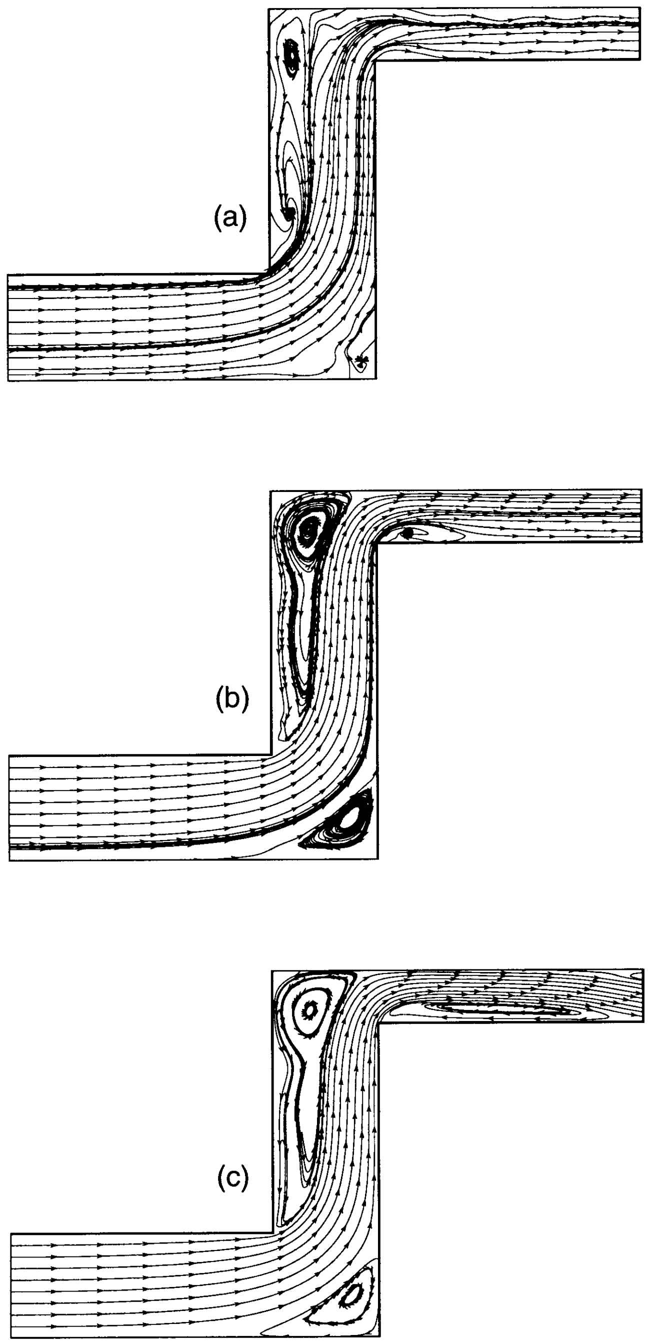

Figure 4-21: Streamline solutions of the "S"-shaped channel flow problem with Reynolds number=1,000 using the 9/4c-element, (a) with coarse mesh (the total of 96 elements), (b) with fine mesh (the total of 384 elements), (c) with finest mesh (the total of 1536 elements).

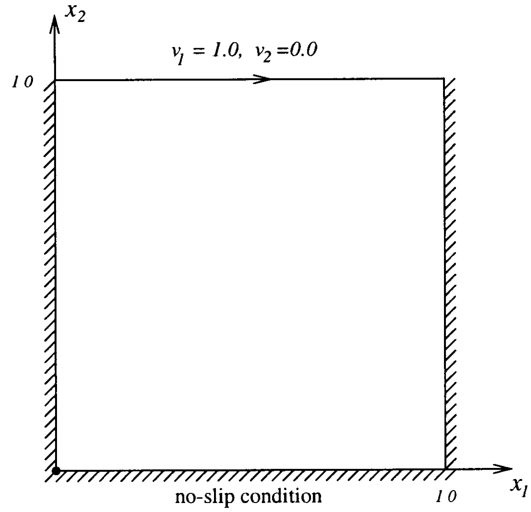

Figure 4-22: Driven flow cavity problem.

4.7.3 Driven flow cavity problem

This problem is considered to compare the solution of the incompressible flow formulation to the solution of the compressible flow formulation in solving a very low Mach number problem. The problem considered is the driven flow cavity problem as described in fig. 4-22. The no-slip boundary condition is imposed on the left, lower and right boundaries. On the upper boundary, we impose the condition: $v_1 = 1, v_2 = 0$ (for the compressible case, we assume the density to be constant, $\rho = 1$, on the upper boundary so that we impose $\rho v_1 = 1, \rho v_2 = 0$ on the upper boundary). The Reynolds number of the problem based on the imposed velocity on the upper boundary and the width of the domain is 1000. For the incompressible flow formulation, the pressure is prescribed at the lower left corner, $p = 10^5$, and a steady-state analysis is used to solve the problem.

For the compressible case, a transient analysis is used to solve the problem with the initial condition

$$p = 10^5, v_1 = v_2 = 0, \theta = 349.65$$

With this initial condition, the average density will be close to one. The solution approximating the steady state condition is obtained once the solution variables no

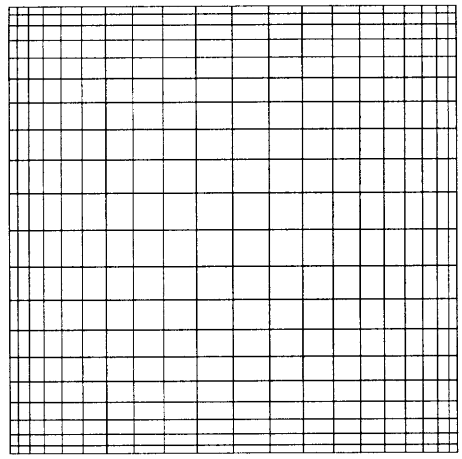

Figure 4-23: The mesh used for the driven flow cavity problem.

longer change with time.

The domain is discretized into a non-uniform mesh with 20×20 elements with smaller elements are close to the boundaries, see fig. 4-23.

The solution of the problem using the incompressible flow formulation with the 9/4c-element is shown in fig. 4-24. The velocity and pressure are well predicted. The pressure singularities at the left and right upper corners are well captured.

The solution of the problem using the compressible flow formulation is shown in fig. 4-25. The velocity and pressure solutions obtained using the compressible flow formulation are similar to the solutions obtained using the incompressible flow formulation. However, the pressure solutions at the singular points are different. This is reasonable since the methods use different basic assumptions regarding the compressibility, and at the singularity points, we do not expect the same pressure solutions.

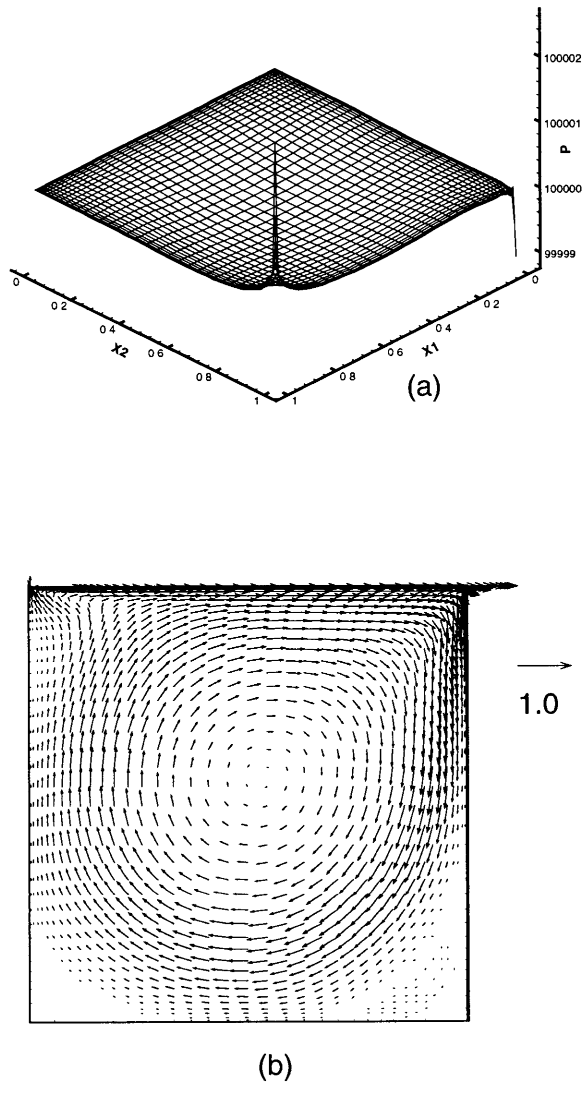

Figure 4-24: Solution of the driven flow cavity problem using the incompressible flow formulation with the 9/4c-element, (a) pressure, (b) velocity.

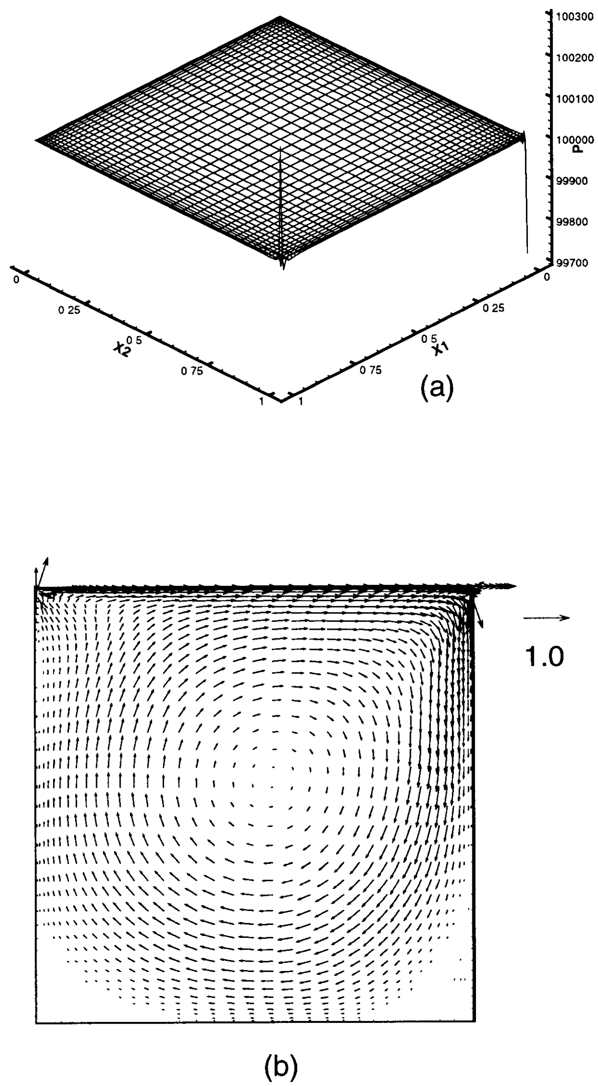

Figure 4-25: Solution of the driven flow cavity problem using the compressible flow formulation, (a) pressure, (b) velocity.

Chapter 5

An inf-sup test for upwind methods

In this chapter, we wish to prove the stability of our proposed artificial diffusion method in the form of eqn. (3.10) using an inf-sup test. In general, finite element formulations should show convergence governed by stability considerations as expressed by an inf-sup condition [5, 29]. The inf-sup condition analysis can be done analytically for simple elements; however, as the element is distorted, the analysis becomes very difficult and a numerical test may become the only available tool for analysis. The inf-sup test for mixed formulations of the incompressible elasticity problem was proposed by Chapelle and Bathe [30] and here we extend this test for upwind methods in solving a convection-diffusion problem. The performance of an upwind method can be evaluated by looking at the result of an example problem and see if the solution contains some oscillations. However, the inf-sup test for convection-diffusion problem provides more insight than just measuring the oscillations in the solutions. The test compactly describes the stability of the upwind methods as the Peclet number and element size are varied.

Other methods will be considered for comparison purposes, namely the standard Galerkin procedure, the full upwind method and the Galerkin least squares method of Hughes et al. [53]. First, we briefly review the inf-sup condition. We choose a test problem, derive appropriate norm definitions for each method and then apply the test to the finite element methods.

5.1 The inf-sup condition

Here, we review the derivation of the inf-sup condition and the numerical inf-sup test for a general linear equation. Consider a general problem in given Hilbert spaces $\overline{W}$ and $\overline{Y}$ with a bilinear form $a(\phi, \psi)$ defined on $\overline{W} \times \overline{Y}$. Note that in general, ϕ does not lie in the same space as ψ. We define the following spaces,

$$\overline{W} = \{u | u \in L^2; \frac{\partial u}{\partial x_i} \in L^2; u = \mathbf{g} \quad \text{on} \quad S_u\}$$

$$\overline{\overline{W}} = \overline{Y} = \{u | u \in L^2; \frac{\partial v}{\partial x_i} \in L^2; u = 0 \quad \text{on} \quad S_u\}$$

where $\mathbf{g}$ is the Dirichlet boundary condition function applied on S_u. Note that $\overline{\overline{W}}$ is introduced to define the space for the variation of the solution function and will be used later. In the continuous space, $\overline{\overline{W}} = \overline{Y}$. Given a linear functional $b(\psi)$ from $\overline{Y}$ to $\mathcal{R}$, we have for the continuous problem:

Find $\phi \in \overline{W}$ such that

$$a(\phi, \psi) = b(\psi) \quad \forall \psi \in \overline{Y} \tag{5.1}$$

An approximate solution is obtained by solving the following finite dimensional problem:

Find $\phi_h \in \overline{W}_h$ such that

$$a(\phi_h, \psi_h) = b(\psi_h) \quad \forall \psi_h \in \overline{Y}_h \tag{5.2}$$

where $\overline{W}_h$ and $\overline{Y}_h$ are finite dimensional subspaces of $\overline{W}$ and $\overline{Y}$ respectively. In this equation, different finite dimensional spaces for ϕ_h and ψ_h are used which might be due to different interpolation functions used for the variables, e.g. ϕ_h is interpolated linearly while ψ_h is interpolated qubically to enhance the upwinding effect.

Brezzi and Bathe have summarized that [28]

$$\|\phi - \phi_h\|_{\overline{W}} \leq (1 + \frac{k_m}{\gamma}) \inf_{\eta_h \in \overline{W}_h} \|\phi - \eta_h\|_{\overline{W}} \tag{5.3}$$

where k_m is obtained from the continuity equation of the continuous space

$$a(\eta, \psi) \leq k_m \|\eta\|_{\overline{W}} \|\psi\|_{\overline{Y}} \quad \forall \eta \in \overline{\overline{W}}, \psi \in \overline{Y} \tag{5.4}$$

Note that the variational solution in the continuous space $\overline{\overline{W}}$ is used in the above inequality. The continuity equation simply states that the bilinear form $a(\eta, \psi)$ behaves normally. Also, γ is obtained from the inf-sup condition of the finite dimensional spaces

$$\inf_{\eta_h \in \overline{\overline{W}}_h} \sup_{\psi_h \in \overline{Y}_h} \frac{a(\eta_h, \psi_h)}{\|\eta_h\|_{\overline{W}} \|\psi_h\|_{\overline{Y}}} \geq \gamma > 0 \tag{5.5}$$

Note that the variational solution space $\overline{\overline{W}}_h$ is used in inequality (5.5) because the difference of two solution functions that is considered. To prove that inequalities (5.4) and (5.5) imply inequality (5.3), consider the following derivation. From inequality (5.5) with $\eta_h = \chi_h - \phi_h$, for all $\chi_h \in \overline{W}$ we have

$$\begin{aligned}
\gamma \|\chi_h - \phi_h\|_{\overline{W}} &\leq \sup_{\psi_h \in \overline{Y}_h} \frac{a(\chi_h - \phi_h, \psi_h)}{\|\psi_h\|_{\overline{Y}}} \\
&= \sup_{\psi_h \in \overline{Y}_h} \frac{a(\chi_h - \phi, \psi_h) + a(\phi - \phi_h, \psi_h)}{\|\psi_h\|_{\overline{Y}}} \\
&= \sup_{\psi_h \in \overline{Y}_h} \frac{a(\chi_h - \phi, \psi_h)}{\|\psi_h\|_{\overline{Y}}} \\
&\leq \sup_{\psi_h \in \overline{Y}_h} \frac{k_m \|\chi_h - \phi\|_{\overline{W}} \|\psi_h\|_{\overline{Y}}}{\|\psi_h\|_{\overline{Y}}} \\
&= k_m \|\chi_h - \phi\|_{\overline{W}}
\end{aligned}$$

and using the triangle inequality,

$$\begin{aligned}
\|\phi_h - \phi\|_{\overline{W}} &\leq \|\phi_h - \chi_h\|_{\overline{W}} + \|\chi_h - \phi\|_{\overline{W}} \\
&\leq \frac{k_m}{\gamma} \|\chi_h - \phi\|_{\overline{W}} + \|\chi_h - \phi\|_{\overline{W}}
\end{aligned}$$

$$= (1+\frac{k_m}{\gamma})||\chi_h - \phi||_{\overline{W}}$$

which proves the inequality (5.3).

Here k_m is given by the problem considered (and has an upper bound by the given physics), and γ should be independent of critical physical constants (that would make $\gamma \to 0$) and the mesh parameter h. If k_m satisfies the inequality (5.4) and γ satisfies the inequality (5.5) (with γ bounded from below), then (5.3) implies optimality of the numerical solution ϕ_h. Note that we generalized the inequality relations given in ref. [28] to use different norms for ϕ and ψ.

The key point is that appropriate $\overline{W}$ and $\overline{Y}$ norms must be selected. The requirement for the $\overline{W}$-norm is that $||\phi - \eta_h||_{\overline{W}}$ should be bounded in order for the inequality (5.3) to make sense. Hence $||\phi||_{\overline{W}}$ should be bounded.

The selection of the norms is dictated by the continuity condition (inequality (5.4)) and we will show later how we proceed.

The value of γ cannot easily be obtained analytically, especially when we consider a sequence of irregular meshes. Here, we evaluate the inf-sup expression (inequality (5.5)) using a numerical method that is similar to the method given in [30]. We now need to consider the non-symmetric bilinear form $a(\phi_h, \psi_h)$.

In matrix form, the general discrete linear equation (equation (5.2)) can be written as

Find $\mathbf{x} \in \mathcal{R}^N$ such that

$$\mathbf{A}\mathbf{x} = \mathbf{b} \tag{5.6}$$

where $\mathbf{A}$ is $N \times N$ non-symmetric matrix in general and $\mathbf{b} \in \mathcal{R}^N$. The inequality (5.5) becomes

$$\inf_{\boldsymbol{\phi} \in \overline{\overline{W}}_h} \sup_{\boldsymbol{\psi} \in \overline{Y}_h} \frac{\boldsymbol{\psi}^T \mathbf{A} \boldsymbol{\phi}}{(\boldsymbol{\phi}^T \mathbf{W} \boldsymbol{\phi})^{\frac{1}{2}} (\boldsymbol{\psi}^T \mathbf{Y} \boldsymbol{\psi})^{\frac{1}{2}}} \geq \gamma > 0 \tag{5.7}$$

where $\mathbf{W}$ and $\mathbf{Y}$ are symmetric matrices of the norm operators $||\cdot||_{\overline{W}}$ and $||\cdot||_{\overline{Y}}$, the $\boldsymbol{\phi}$ and $\boldsymbol{\psi}$ are vectors that contain the nodal values of ϕ_h and ψ_h and the value of γ should be independent of critical physical constants and mesh parameters.

To evaluate the left hand-side of inequality (5.7), let us define

$$f(\boldsymbol{\phi}, \boldsymbol{\psi}) = \frac{\boldsymbol{\psi}^T \mathbf{A} \boldsymbol{\phi}}{(\boldsymbol{\phi}^T \mathbf{W} \boldsymbol{\phi})^{\frac{1}{2}} (\boldsymbol{\psi}^T \mathbf{Y} \boldsymbol{\psi})^{\frac{1}{2}}} \tag{5.8}$$

and

$$\mathbf{Y} = \mathbf{L}^T \mathbf{L} \qquad\qquad \boldsymbol{\xi} = \mathbf{L} \boldsymbol{\psi} \tag{5.9}$$

so,

$$f(\boldsymbol{\phi}, \boldsymbol{\xi}) = \frac{\boldsymbol{\xi}^T \mathbf{L}^{-T} \mathbf{A} \boldsymbol{\phi}}{(\boldsymbol{\phi}^T \mathbf{W} \boldsymbol{\phi})^{\frac{1}{2}} (\boldsymbol{\xi}^T \boldsymbol{\xi})^{\frac{1}{2}}} \tag{5.10}$$

We use the Cauchy-Schwarz inequality

$$||\boldsymbol{\xi}^T \mathbf{L}^{-T} \mathbf{A} \boldsymbol{\phi}||_2 \leq ||\boldsymbol{\xi}||_2 ||\mathbf{L}^{-T} \mathbf{A} \boldsymbol{\phi}||_2 \tag{5.11}$$

with the norm definition:

$$||\mathbf{v}||_2 = (\sum_{i=1}^{N} v_i^2)^{\frac{1}{2}} = (\mathbf{v}^T \mathbf{v})^{\frac{1}{2}}$$

Hence,

$$\sup_{\mathbf{L}^{-1}\boldsymbol{\xi} \in \overline{Y}_h} f(\boldsymbol{\phi}, \boldsymbol{\xi}) = \frac{(\boldsymbol{\phi}^T \mathbf{A}^T \mathbf{L}^{-1} \mathbf{L}^{-T} \mathbf{A} \boldsymbol{\phi})^{\frac{1}{2}}}{(\boldsymbol{\phi}^T \mathbf{W} \boldsymbol{\phi})^{\frac{1}{2}}} \tag{5.12}$$

Note that

$$\mathbf{A}^T \mathbf{L}^{-1} \mathbf{L}^{-T} \mathbf{A} = \mathbf{A}^T (\mathbf{L}^T \mathbf{L})^{-1} \mathbf{A} = \mathbf{A}^T \mathbf{Y}^{-1} \mathbf{A} \tag{5.13}$$

Consider the following eigenproblem

$$(\mathbf{A}^T \mathbf{Y}^{-1} \mathbf{A}) \mathbf{x} = \lambda \mathbf{W} \mathbf{x} \tag{5.14}$$

so,

$$\inf_{\boldsymbol{\phi} \in \overline{W}_h} \sup_{\mathbf{L}^{-1}\boldsymbol{\xi} \in \overline{Y}_h} f(\boldsymbol{\phi}, \boldsymbol{\xi}) = \lambda_{min}^{\frac{1}{2}} \tag{5.15}$$

where λ_{min} is the smallest eigenvalue of the eigenproblem (5.14). Hence, for a given formulation, physical constants and finite dimensional spaces, the value of γ equals to $\lambda_{min}^{\frac{1}{2}}$.

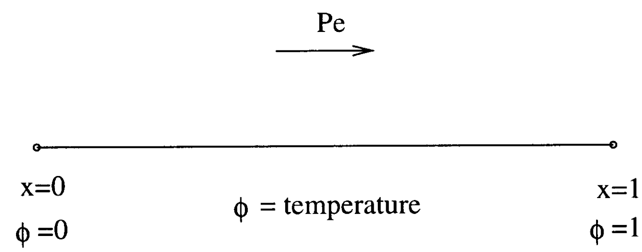

Figure 5-1: Domain and boundary conditions for the test problem

In the inf-sup test, first, given the physical constants, we calculate the values of γ for a sequence of meshes. Then, for a given mesh, we calculate the inf-sup values γ for a series of different values of the physical constants. For both cases, the values of γ should be bounded from below by a positive constant which means that the value of γ is greater than zero and so satisfies the inequality (5.5).

5.2 Model problem

In this section, we apply the inf-sup test derived in the last section on upwind methods for convection-diffusion problem. Selection of the norm definitions used for each upwind methods are described. Consider the nondimensionalized convection diffusion problem in one dimension (described in fig. 5-1) with the governing equation,

$$-\frac{1}{Pe}\frac{d^2\phi}{dx^2} + \frac{d\phi}{dx} = 0 \tag{5.16}$$

where ϕ is the temperature and Pe is the Peclet number. In this specific case, γ should be independent of Pe and the mesh parameter h. Here, we consider the case when the convective term is dominating, $Pe > 1$, and its limit case when $Pe \to \infty$.

The exact solution for the problem is

$$\phi = \frac{\exp(Pe\, x) - 1}{\exp(Pe) - 1}$$

High-order derivative artificial diffusion method

For the high-order derivative artificial diffusion method, we discretize the domain uniformly using quadratic elements. Hence we have the spaces

$$\overline{W}_h = \{u_h | u_h \in L^2; \frac{\partial u}{\partial x} \in L^2; u_h \in Q_2(l^m), u_h = \mathbf{g} \text{ on } S_u\}$$

$$\overline{\overline{W}}_h = \overline{Y}_h = \{u_h | u_h \in L^2; \frac{\partial u}{\partial x} \in L^2; u_h \in Q_2(l^m), u_h = 0 \text{ on } S_u\}$$

where $Q_2(l^m)$ denotes the quadratic function in the element m. The high-order derivative artificial diffusion method for the convection-diffusion equation is :

Find $\phi_h \in \overline{W}_h$ such that

$$\int (\frac{d\psi_h}{dx}\frac{1}{Pe}\frac{d\phi_h}{dx} + \psi_h \frac{d\phi_h}{dx})dx + \sum_m \int_{l^m} \frac{d^2\psi_h}{dx^2}\frac{1}{9}|\frac{dx}{dr}|^3 \frac{d^2\phi_h}{dx^2} dx = 0 \quad \forall \psi_h \in \overline{Y}_h \tag{5.17}$$

For a regular mesh, $|\frac{dx}{dr}| = \frac{h}{2}$, so we have

$$\sum_m \int_{l^m} (\frac{d\psi_h}{dx}\frac{1}{Pe}\frac{d\phi_h}{dx} + \psi_h \frac{d\phi_h}{dx} + \frac{d^2\psi_h}{dx^2}\frac{h^3}{72}\frac{d^2\phi_h}{dx^2})dx = 0 \tag{5.18}$$

The continuity equation of the high-order derivative artificial diffusion method in the continuous space is

$$\begin{aligned}
&\sum_m \int_{l^m} (\psi' \frac{1}{Pe}\phi' + \psi\phi' + \psi'' \frac{h^3}{72}\phi'')dx \\
&\quad \le \sum_m \int_{l^m} (\frac{h^3}{72Pe^3}\phi''^2 + \frac{2}{Pe^3}\phi'^2)^{\frac{1}{2}} (\frac{h^3 Pe^3}{72}\psi''^2 + Pe\psi'^2 + Pe^3\psi^2)^{\frac{1}{2}} dx \\
&\quad \le \left[\sum_m \int_{l^m} (\frac{h^3}{72Pe^3}\phi''^2 + \frac{2}{Pe^3}\phi'^2)dx\right]^{\frac{1}{2}} \left[\sum_m \int_{l^m} (\frac{h^3 Pe^3}{72}\psi''^2 + Pe\psi'^2 + Pe^3\psi^2)dx\right]^{\frac{1}{2}}
\end{aligned}$$

so, we have

$$\begin{aligned}
k_m &= 1 \\
\|\phi\|^2_{\overline{W}} &= \sum_m \int_{l^m} (\frac{h^3}{72Pe^3}\phi''^2 + \frac{2}{Pe^3}\phi'^2)dx
\end{aligned}$$

$$\|\psi\|_{\overline{Y}}^2 = \sum_m \int_{l^m} (\frac{h^3 Pe^3}{72}\psi''^2 + Pe\psi'^2 + Pe^3\psi^2)dx$$

The norm value of the exact solution ϕ in the $\overline{W}$-norm is

$$\begin{aligned}\|\phi\|_{\overline{W}}^2 &= \int_0^1 (\frac{h^3}{72Pe^3}\phi''^2 + \frac{2}{Pe^3}\phi'^2)dx\, dx \\ &= \frac{h^3(\exp(2Pe)-1)}{144(\exp(Pe)-1)^2} + \frac{(\exp(2Pe)-1)}{Pe^2(\exp(Pe)-1)^2}\end{aligned}$$

so, as $Pe \to \infty$,

$$\|\phi\|_{\overline{W}}^2 \to \frac{h^3}{144}$$

which is proved to be bounded for a small element length h.

The matrices of the high-order derivative artificial diffusion method for the inf-sup test are defined as follows

$$\mathbf{A} = \int (\frac{1}{Pe}\mathbf{H}_{,x}^T\mathbf{H}_{,x} + \mathbf{H}^T\mathbf{H}_{,x})dx + \sum_m \int_{l^m} \frac{h^3}{72}\mathbf{H}_{,xx}^T\mathbf{H}_{,xx}\, dx \tag{5.19}$$

$$\mathbf{W} = \int \frac{2}{Pe^3}\mathbf{H}_{,x}^T\mathbf{H}_{,x}\, dx + \sum_m \int_{l^m} \frac{h^3}{72Pe^3}\mathbf{H}_{,xx}^T\mathbf{H}_{,xx}\, dx \tag{5.20}$$

$$\mathbf{Y} = \int (Pe\mathbf{H}_{,x}^T\mathbf{H}_{,x} + Pe^3\, \mathbf{H}^T\mathbf{H})dx + \sum_m \int_{l^m} \frac{h^3 Pe^3}{72}\mathbf{H}_{,xx}^T\mathbf{H}_{,xx}\, dx \tag{5.21}$$

Standard Galerkin method

In the standard Galerkin procedure, we discretize the domain uniformly using linear elements, therefore we have the spaces

$$\overline{W}_h = \{u_h | u_h \in L^2; \frac{\partial u}{\partial x} \in L^2; u_h \in Q_1(l^m), u_h = \mathbf{g} \text{ on } S_u\}$$

$$\overline{\overline{W}}_h = \overline{Y}_h = \{u_h | u_h \in L^2; \frac{\partial u}{\partial x} \in L^2; u_h \in Q_1(l^m), u_h = 0 \text{ on } S_u\}$$

where $Q_1(l^m)$ denotes the linear function in the element m. The standard Galerkin method for the convection-diffusion equation (5.16) is :

Find $\phi_h \in \overline{W}_h$ such that

$$\int (\frac{d\psi_h}{dx}\frac{1}{Pe}\frac{d\phi_h}{dx} + \psi_h \frac{d\phi_h}{dx})dx = 0 \quad \forall \psi_h \in \overline{Y}_h \tag{5.22}$$

The norm definitions are determined by the continuity equation in the continuous space and for the standard Galerkin method, we have

$$\begin{aligned}
\int (\psi' \frac{1}{Pe}\phi' + \psi\phi')dx &\leq \int (\frac{2}{Pe}\phi'^2)^{\frac{1}{2}}(\frac{1}{Pe}\psi'^2 + Pe\,\psi^2)^{\frac{1}{2}}dx \\
&\leq \left[\int \frac{2}{Pe}\phi'^2 dx\right]^{\frac{1}{2}}\left[\int (\frac{1}{Pe}\psi'^2 + Pe\,\psi^2)dx\right]^{\frac{1}{2}}
\end{aligned}$$

so, we have

$$\begin{aligned}
k_m &= 1 \\
\|\phi\|^2_{\overline{W}} &= \int \frac{2}{Pe}\phi'^2 dx \\
\|\psi\|^2_{\overline{Y}} &= \int (\frac{1}{Pe}\psi'^2 + Pe\,\psi^2)dx
\end{aligned}$$

The norm value of the exact solution ϕ in the $\overline{W}$-norm is

$$\begin{aligned}
\|\phi\|^2_{\overline{W}} &= \int_0^1 \frac{2}{Pe}\phi'^2\, dx \\
&= \frac{\exp(2Pe) - 1}{(\exp(Pe) - 1)^2}
\end{aligned}$$

so, as $Pe \to \infty$,

$$\|\phi\|^2_{\overline{W}} \to 1$$

which is proved to be bounded.

The matrices of the standard Galerkin method for the inf-sup test are

$$\mathbf{A} = \int (\frac{1}{Pe}\mathbf{H}^T_{,x}\mathbf{H}_{,x} + \mathbf{H}^T\mathbf{H}_{,x})dx \tag{5.23}$$

$$\mathbf{W} = \int \frac{2}{Pe}\mathbf{H}^T_{,x}\mathbf{H}_{,x}\, dx \tag{5.24}$$

$$\mathbf{Y} = \int (\frac{1}{Pe}\mathbf{H}_{,x}^T\mathbf{H}_{,x} + Pe\ \mathbf{H}^T\mathbf{H})dx \tag{5.25}$$

where $\mathbf{H}$ is the vector containing the interpolation functions.

Full upwind method

Using the same solution and weighting function spaces as for the standard Galerkin method, the full upwind method for the convection-diffusion equation (5.16) is :

Find $\phi_h \in \overline{W}_h$ such that

$$\int \{\frac{d\psi_h}{dx}(\frac{1}{Pe} + \frac{h}{2})\frac{d\phi_h}{dx} + \psi_h\frac{d\phi_h}{dx}\}dx = 0 \quad \forall\psi_h \in \overline{Y}_h \tag{5.26}$$

where h is the element length. The continuity equation of the full upwind method in the continuous space is

$$\begin{aligned}
\int \{\psi'(\frac{1}{Pe} + \frac{h}{2})\phi' + \psi\phi'\}dx \quad &\leq \quad \int \left[\frac{2}{Pe}\phi'^2\right]^{\frac{1}{2}} \left[(\frac{1}{Pe} + \frac{h^2 Pe}{4})\psi'^2 + Pe\ \psi^2\right]^{\frac{1}{2}} dx \\
&\leq \quad \left[\int \frac{2}{Pe}\phi'^2 dx\right]^{\frac{1}{2}} \left[\int \{(\frac{1}{Pe} + \frac{h^2 Pe}{4})\psi'^2 + Pe\ \psi^2\}dx\right]^{\frac{1}{2}}
\end{aligned}$$

so, we have

$$\begin{aligned}
k_m \quad &= \quad 1 \\
\|\phi\|_{\overline{W}}^2 \quad &= \quad \int \frac{2}{Pe}\phi'^2 dx \\
\|\psi\|_{\overline{Y}}^2 \quad &= \quad \int \{(\frac{1}{Pe} + \frac{h^2 Pe}{4})\psi'^2 + Pe\ \psi^2\}dx
\end{aligned}$$

The matrices of the full upwind method for the inf-sup test are

$$\mathbf{A} = \int \{(\frac{1}{Pe} + \frac{h}{2})\mathbf{H}_{,x}^T\mathbf{H}_{,x} + \mathbf{H}^T\mathbf{H}_{,x}\}dx \tag{5.27}$$

$$\mathbf{W} = \int \frac{2}{Pe}\mathbf{H}_{,x}^T\mathbf{H}_{,x}\ dx \tag{5.28}$$

$$\mathbf{Y} = \int \{(\frac{1}{Pe} + \frac{h^2 Pe}{4})\mathbf{H}_{,x}^T\mathbf{H}_{,x} + Pe\ \mathbf{H}^T\mathbf{H}\}dx \tag{5.29}$$

Galerkin least squares method

Using the same solution and weighting function spaces as for the standard Galerkin method, the Galerkin least squares formulation for the convection-diffusion equation is :

Find $\phi_h \in \overline{W}_h$ such that

$$\int \{ \frac{d\psi_h}{dx} (\frac{1}{Pe} + \tau) \frac{d\phi_h}{dx} + \psi_h \frac{d\phi_h}{dx} \} dx = 0 \quad \forall \psi_h \in \overline{Y}_h \tag{5.30}$$

and to obtain nodally exact solution, we have

$$\tau = \frac{h}{2} \coth(\frac{hPe}{2}) - \frac{1}{Pe} \tag{5.31}$$

Substituting eqn. (5.31) to eqn. (5.30), we have

$$\int [\frac{d\psi_h}{dx} \{ \frac{h}{2} \coth(\frac{hPe}{2}) \} \frac{d\phi_h}{dx} + \psi_h \frac{d\phi_h}{dx}] dx = 0 \tag{5.32}$$

The continuity equation of the Galerkin least squares method in the continuous space is

$$\begin{aligned} \int [\psi' \{ \frac{h}{2} \coth(\frac{hPe}{2}) \} \phi' + \psi \phi'] dx &\leq \int \left[\frac{2}{Pe} \phi'^2 \right]^{\frac{1}{2}} \left[\frac{h^2 Pe}{4} \coth^2(\frac{hPe}{2}) \psi'^2 + Pe\, \psi^2 \right]^{\frac{1}{2}} dx \\ &\leq \left[\int \frac{2}{Pe} \phi'^2 dx \right]^{\frac{1}{2}} \left[\int (\frac{h^2 Pe}{4} \coth^2(\frac{hPe}{2})\, \psi'^2 + Pe\, \psi^2) dx \right]^{\frac{1}{2}} \end{aligned}$$

So, we have

$$\begin{aligned} k_m &= 1 \\ ||\phi||_{\overline{W}}^2 &= \int \frac{2}{Pe} \phi'^2 dx \\ ||\psi||_{\overline{Y}}^2 &= \int \{ \frac{h^2 Pe}{4} \coth^2(\frac{hPe}{2})\, \psi'^2 + Pe\, \psi^2 \} dx \end{aligned}$$

The matrices of the Galerkin Least Squares for the inf-sup test are

$$\mathbf{A} = \int \{(\frac{1}{Pe} + \tau)\mathbf{H}^T_{,x}\mathbf{H}_{,x} + \mathbf{H}^T\mathbf{H}_{,x}\}dx \tag{5.33}$$

$$\mathbf{W} = \int \frac{2}{Pe}\mathbf{H}^T_{,x}\mathbf{H}_{,x}dx \tag{5.34}$$

$$\mathbf{Y} = \int \{\frac{h^2 Pe}{4}\coth^2(\frac{hPe}{2})\ \mathbf{H}^T_{,x}\mathbf{H}_{,x} + Pe\ \mathbf{H}^T\mathbf{H}\}dx \tag{5.35}$$

5.3 Results and discussions

The results of the inf-sup test are shown in figs. 5-2 and 5-3. In fig. 5-2, the Peclet number of the problem is 10 and different numbers of elements are used to discretize the domain; $n = 2, 4, 8, 16, 32$ ($h = 0.5, 0.25, 0.125, 0.0625, 0.03125$). In fig. 5-3, the element length h is 0.0625 (number of elements $= 16$) and the Peclet number was increased, $Pe = 1, 10, 100, 1000, 10000$.

Fig. 5-2 shows that as the mesh is made coarser (we follow the curves from left to right), the inf-sup value corresponding to the standard Galerkin method decreases. This trend indicates that the method does not pass the inf-sup test. The method is predicted to be unstable when we use too coarse a mesh. The instability is displayed by oscillations in the solution. Fig. 5-2 also shows that as the mesh is made finer (we follow the curves from right to left), the inf-sup value corresponding to the standard Galerkin method approaches to a fixed value (log(infsup)≈ -0.5). This indicates that, as we already expected, the method becomes stable as the mesh is refined. In terms of accuracy, for low Peclet number, the curve approches the the fixed value rapidly and this indicates that the method converges to the exact solution rapidly. Note that the standard Galerkin method with linear elements has a second order convergence.

Fig. 5-2 shows that as the mesh is refined, the inf-sup value corresponding to the full upwind method is bounded from below. This indicates that the method passes the inf-sup test. The method is predicted to be stable and the stability of the method is displayed by no oscillations in the solution even though the mesh is very coarse.

In terms of the accuracy, fig. 5-2 shows that the inf-sup value corresponding to the full upwind method is higher than other curves. This suggests that the method is stable; however, this also indicates that the method is very diffusive. The rate that the full upwind curve approaches the bounded value is slower than given by the other curves. This indicates that the method converges to the exact solution slower than other methods. Note that the full upwind method with linear elements has a first order convergence.

Fig. 5-2 shows that as the mesh is refined, the inf-sup value corresponding to the Galerkin least squares method is bounded from below. This indicates that the method passes the inf-sup test. The method is stable and no oscillation in the solution is expected. In terms of the accuracy, fig. 5-2 shows that the inf-sup value corresponding to the Galerkin least squares method approaches the bounded value in the moderate way. The curve approaches the bounded value faster than the full upwind method, but slower than the standard Galerkin method. So the convergence rate of this method is more than first order, but less than second order. Even though the Galerkin least squares method gives nodally exact solutions, the convergence of the method that we consider here is not the nodal solution only.

Fig. 5-2 also shows that as the mesh is refined, the inf-sup value corresponding to the high-order derivative artificial diffusion method is bounded from below. This indicates that the method passes the inf-sup test. The method is stable but small oscillations occur in the solution because the method has too little diffusion. This can be seen by comparing the curve corresponding to this method to the one corresponding to the Galerkin least squares method that gives nodally exact solution. The curve corresponding to this method is lower than the one corresponding to the Galerkin least squares method, especially when coarse meshes are used. In terms of the accuracy, fig. 5-2 shows that the inf-sup value corresponding to the high-order derivative artificial diffusion method approaches the bounded value in an excellent way. In the range of h that we consider here, the curve corresponding to this method has already reached the bounded value. This suggest that the method has higher order convergence than the other methods.

We should point out also that as the mesh is refined, all curves corresponding to all the methods approache a single value (log(infsup)≈ -0.5) and that value we expect to be the inf-sup value of the exact solution.

Fig. 5-3 shows that as the Peclet number increases, the inf-sup value of the standard Galerkin method decreases unboundedly. This means that the method does not pass the inf-sup test. The method is unstable and the instability is displayed by unbounded oscillations in the solution as the Peclet number increases. This observation agrees with our earlier conclusion regarding this method.

Fig. 5-3 also shows that as the Peclet number increases, the inf-sup value corresponding to the other methods are bounded from below. This means that those methods pass the inf-sup test and this observation agrees with our earlier conclusion regarding those methods. Note that the curve of the full upwind method approaches the same fixed value as the one of the Galerkin least squares method. This means that those methods behave similarly as the Peclet number increases. As we already know, these methods exhibit no oscillations in the solutions as the Peclet number increases. The curve corresponding to the high-order derivative artificial diffusion method approaches a fixed value which is lower than the one approached by the curves of the full upwind and the Galerkin least squares methods. This indicates that the high-order derivative artificial diffusion method gives smaller artificial diffusion than the Galerkin least squares method for high Peclet number.

In this study, we have used even numbers of elements to discretize the domain to perform the inf-sup test. If odd numbers of element are used, the inf-sup value corresponding to the standard Galerkin method will be bounded from below as we coarsen the mesh, or as the Peclet number increases. The inf-sup value of the standard Galerkin method using odd numbers of elements is bounded from below because the solution converges to a nonphysical solution which is often called a sawtooth solution. However, the idea of this numerical test is that if the method does not pass an inf-sup test, we are sure that the method does not satisfy the inf-sup condition. If the method pass the inf-sup test, it does not mean that the method must satisfy the inf-sup condition. More difficult tests should be carried out and if the method passes

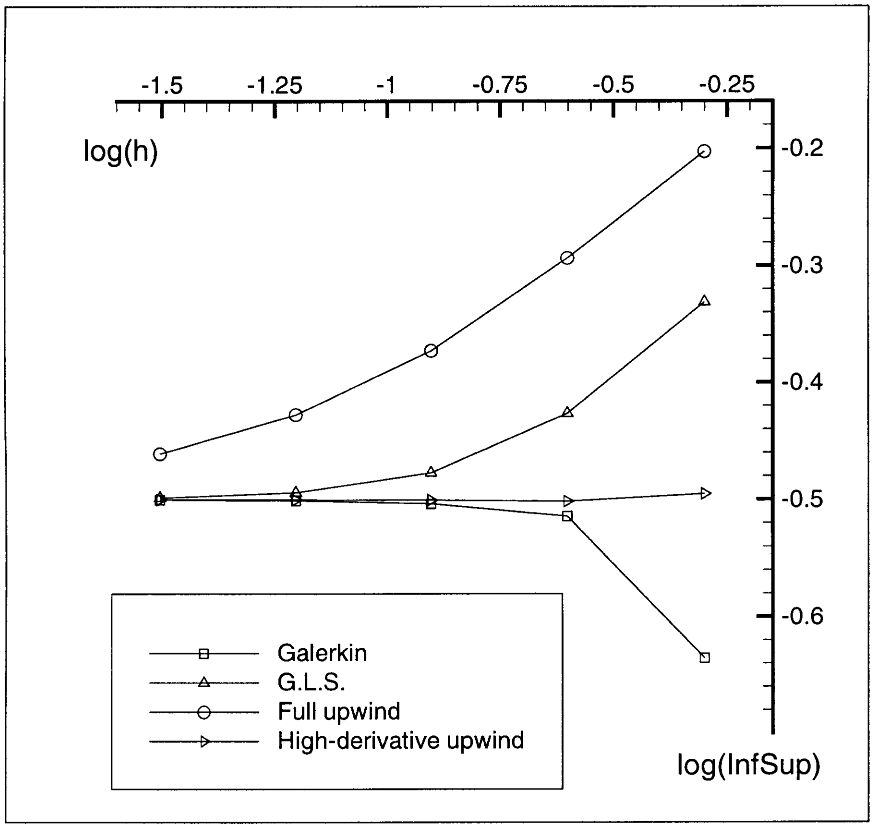

Figure 5-2: Inf-sup value curves as the mesh is coarsened for $Pe = 10$.

all the inf-sup testes with all possible conditions then we are sure that the method will satisfy the inf-sup condition. In our case, the inf-sup test with odd numbers of elements is not a sufficiently severe problem. The inf-sup test with even numbers of elements is more difficult therefore we use the test with even numbers of elements.

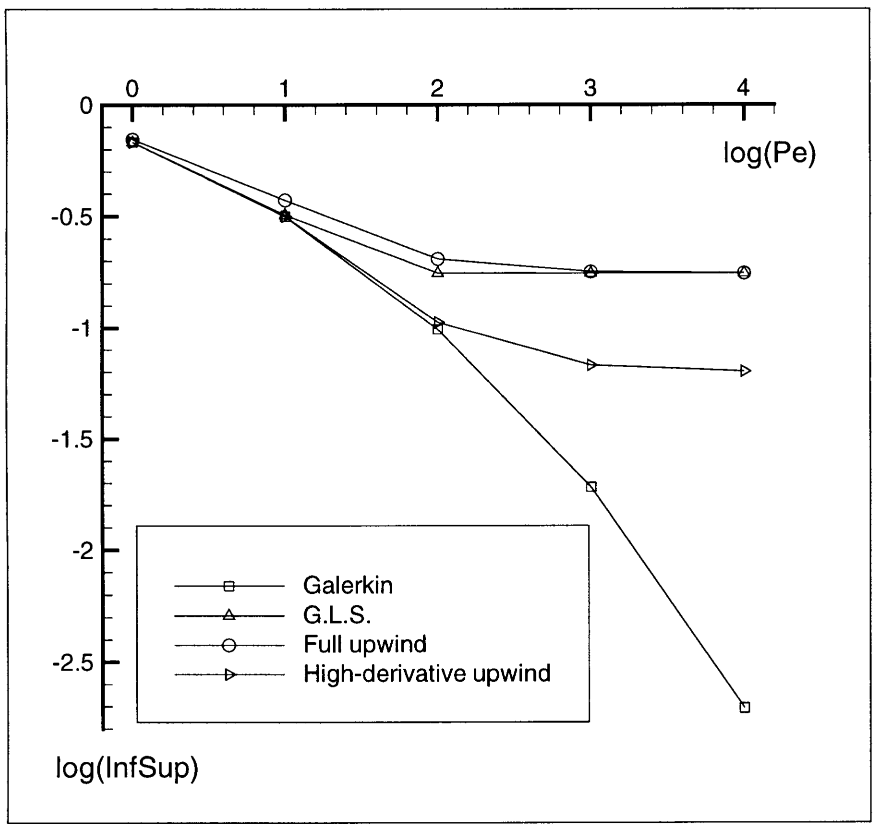

Figure 5-3: Inf-sup value curves as Pe is increased for $h = 0.0625$.

Chapter 6

Conclusions

Our objective in this work was to explore the development of a versatile and computationally effective parabolic quadrilateral finite element for the solution of compressible and incompressible flows. The parabolic quadrilateral element is selected because the element, with a correct combination of the order of interpolations for the working variables, can satisfy the inf-sup condition. We have presented in this thesis an element formulation for compressible flow with new upwinding and shock capturing terms. The new upwinding term is proved to stabilize the formulation by mathematical analysis using a simple model, the 1D convective-diffusive problem, and by numerical analysis using the inf-sup test. The new shock capturing term performs quite well judging from the solutions of the numerical examples presented in this thesis. Highly refined shock solutions are obtained in the numerical solutions. Various flow problems in which the Mach number ranged from about 0.0005 to 6 have been considered. The numerical results indicate that the element can be used to give good solutions and is applicable to a wide range of problems. For the problems considered, the solutions produced using the presented finite element formulation with coarse meshes are comparable to the results produced using other methods with very fine meshes.

For the incompressible flow formulation, we have shown the necessity of the element to satisfy the inf-sup condition. The 9/4c-element which satisfies the inf-sup condition was formulated with a new upwinding term. Some numerical examples were presented to show the effectiveness of the formulation. Although the new upwinding term has a high order accuracy, the term is not strong enough to stabilize the solutions for problems with very high Reynolds number.

When the compressible flow formulation is used to solve low Mach number problems, reasonably good solutions are obtained and the solutions are close to the solutions of the problem using the incompressible flow formulation. However, some small oscillations occur in the pressure solutions of low Mach number problems using the compressible flow formulation.

While the results using the element appear promising, we have not yet considered in our study the details of numerical effectiveness of the element such as the solution of the governing finite element equations. To obtain the solutions of the problems considered in this thesis, we used a successive substitution and relaxation method which resulted into slow convergence. An iterative solver specific for the presented finite element formulation should be developed to obtain faster convergence in the solution of the governing equations. We leave these topics of numerical effectiveness for further research.

Other recommended further research topics are to provide a mathematical analysis of the proposed finite element scheme, especially of the shock capturing term which would include pursuing an error convergence analysis for the proposed formulation, and to improve the performance of the proposed compressible formulation in low Mach number problems. For the incompressible flow formulation, improving the upwind term is required for solving problems with very high Reynolds number; namely an "ideal" numerical scheme as discussed in section 4.4.1 would be very valuable. As the final aim, the development of one unified solution scheme for compressible and incompressible flows should be further pursued.

Appendix A

Convective matrix

The objective in this appendix is to prove by elementary matrix multiplication that the convective vector $\mathbf{F}_j$ in the compressible flow governing equations has the following property

$$\mathbf{F}_j = \mathbf{A}_j \mathbf{U} \tag{A.1}$$

where $\mathbf{A}_j$ is the Jacobian matrix of the convective vector $\mathbf{F}_j$. We also wish to discuss why we have the above property. The definitions of $\mathbf{A}_j$ and $\mathbf{F}_j$ are given in Chapter 3.

Let us define

$$\tilde{\mathbf{F}}_1 = \mathbf{A}_1 \mathbf{U}$$

and f_i^1 is the line i component of the vector $\tilde{\mathbf{F}}_1$. From the definition of $\mathbf{A}_1$ and $\mathbf{U}$, we can calculate f_i^1 as follows

$$\begin{aligned}
f_1^1 &= \rho v_1 \\
f_2^1 &= \rho\{\frac{(\gamma-3)}{2}v_1^2 + \frac{(\gamma-1)}{2}v_2^2\} + \rho v_1(3-\gamma)v_1 + \rho v_2(1-\gamma)v_2 + \rho E\frac{1}{c}(\gamma-1) \\
&= \rho v_1^2 + (\gamma-1)\rho\{\frac{E}{c} - \frac{1}{2}(v_1^2+v_2^2)\} \\
f_3^1 &= \rho(-v_1 v_2) + \rho v_1 v_2 + \rho v_2 v_1 \\
&= \rho v_1 v_2 \\
f_4^1 &= \rho\{-\gamma v_1 E + c(\gamma-1)v_1(v_1^2+v_2^2)\} + \rho v_1\{\gamma E - \frac{c(\gamma-1)}{2}(3v_1^2+v_2^2)\}
\end{aligned}$$

$$
\begin{aligned}
& +\rho v_2 c(1-\gamma)v_1 v_2 + \rho E \gamma v_1 \\
= \; & \gamma \rho E v_1 - (\gamma-1)\rho v_1 \frac{c}{2}(v_1^2 + v_2^2) \\
= \; & \rho E v_1 + (\gamma-1)\rho v_1 \{E - \frac{c}{2}(v_1^2 + v_2^2)\}
\end{aligned}
$$

We see that all the components of the vector $\tilde{\mathbf{F}}_1$ are exactly the same as the components of the convective vector $\mathbf{F}_1$, therefore we can conclude that

$$\tilde{\mathbf{F}}_1 = \mathbf{A}_1\mathbf{U} = \mathbf{F}_1$$

Similarly, let us define

$$\tilde{\mathbf{F}}_2 = \mathbf{A}_2\mathbf{U}$$

and f_i^2 is the line i component of the vector $\tilde{\mathbf{F}}_2$. From the definition of $\mathbf{A}_2$ and $\mathbf{U}$, we can calculate f_i^2 as follows

$$
\begin{aligned}
f_1^2 &= \rho v_2 \\
f_2^2 &= \rho(-v_1 v_2) + \rho v_1 v_2 + \rho v_2 v_1 \\
&= \rho v_1 v_2 \\
f_3^2 &= \rho\{\frac{(\gamma-1)}{2}v_1^2 + \frac{(\gamma-3)}{2}v_2^2\} + \rho v_1(1-\gamma)v_1 + \rho v_2(3-\gamma)v_2 + \rho E\frac{1}{c}(\gamma-1) \\
&= \rho v_2^2 + (\gamma-1)\rho\{\frac{E}{c} - \frac{1}{2}(v_1^2 + v_2^2)\} \\
f_4^2 &= \rho\{-\gamma v_2 E + c(\gamma-1)v_2(v_1^2+v_2^2)\} + \rho v_1 c(1-\gamma)v_1 v_2 \\
& \quad +\rho v_2\{\gamma E - \frac{c(\gamma-1)}{2}(v_1^2 + 3v_2^2)\} + \rho E\gamma v_2 \\
&= \gamma\rho E v_2 - (\gamma-1)\rho v_2 \frac{c}{2}(v_1^2+v_2^2) \\
&= \rho E v_2 + (\gamma-1)\rho v_2\{E - \frac{c}{2}(v_1^2+v_2^2)\}
\end{aligned}
$$

We also see that all the components of the vector $\tilde{\mathbf{F}}_2$ are exactly the same as the components of the convective vector $\mathbf{F}_2$, therefore we have

$$\tilde{\mathbf{F}}_2 = \mathbf{A}_2\mathbf{U} = \mathbf{F}_2$$

Hence, we can conclude that eqn. (A.1) is valid.

We can also conclude from eqn. (A.1) that

$$\mathbf{A}_{j,j}\mathbf{U} = 0 \tag{A.2}$$

The proof is as follows.

We have the definition of the matrix $\mathbf{A}_j$ to be the Jacobian of the convective vector $\mathbf{F}_j$ such that

$$\frac{\partial \mathbf{F}_j}{\partial \mathbf{U}} = \mathbf{A}_j$$

Hence, we have that

$$\mathbf{F}_{j,j} = \frac{\partial \mathbf{F}_j}{\partial \mathbf{U}}\mathbf{U}_{,j} = \mathbf{A}_j\mathbf{U}_{,j} \tag{A.3}$$

From eqn. (A.1), we have the relation

$$\begin{aligned}\mathbf{F}_{j,j} &= (\mathbf{A}_j\mathbf{U})_{,j} \\ &= \mathbf{A}_{j,j}\mathbf{U} + \mathbf{A}_j\mathbf{U}_{,j}\end{aligned}$$

and in order for the above equation and eqn. A.3 to hold, we must have

$$\mathbf{A}_{j,j}\mathbf{U} = 0$$

The above property and the property in eqn. (A.1) are the consequences of the fact that the convective fluxes $\mathbf{F}_j$ are homogeneous functions of degree one of the conservative variable vector $\mathbf{U}$ in the case of a perfect gas. There are two reasons for $\mathbf{F}_j$ to be a homogeneous function of degree one of $\mathbf{U}$. First, the fact that ρ and ρv_j are in the vector $\mathbf{U}$ which leads to the condition v_j to be a function of degree zero of $\mathbf{U}$. For a quantity q (q can be $\rho, \rho v_i, \rho E$), the corresponding convective flux is $(q)v_j$ and since the v_j is a function of degree zero, the convective flux will be a function of degree one.

Second, the fact that the pressure is a function of degree one of the vector $\mathbf{U}$. The convective flux in the momentum equation is $(\rho v_i)v_j + p\delta_{ij}$ and in the energy equation is $(\rho E + p)v_j$. In order for the fluxes to be homogeneous functions of order one of $\mathbf{U}$, the pressure, p, needs to be a function of degree one of $\mathbf{U}$. The ideal gas relation for the pressure

$$p = (\gamma - 1)(\rho E - \frac{1}{2}\rho v_l^2)$$

gives the condition that the pressure is a function of degree one of $\mathbf{U}$.

In conclusion, the fact that v_j is a function of degree zero of $\mathbf{U}$ and the pressure is a function of degree one of $\mathbf{U}$ results the condition $\mathbf{F}_j$ to be homogeneous functions of degree one of $\mathbf{U}$ and the properties in eqns. (A.1) and (A.2) follow.

Appendix B

The upwind term

The objective in this appendix is to analyze the effect of the upwinding in eqn. (3.10) by considering a simple scalar convective-diffusive problem.

Consider the following one-dimensional problem

$$
\begin{aligned}
v^*\theta_{,x} - \alpha^*\theta_{,xx} &= q \qquad \text{in} \qquad 0 < x < 1 \\
\theta(0) = \theta(1) &= 0
\end{aligned}
\tag{B.1}
$$

where θ, α^*, q, v^*, are temperature, diffusivity, heat generation and constant velocity. The variables v^*, α^*, and q are given for the problem and we want to solve for θ. We introduce the space

$$V = \{v | v \in L^2(Vol); \frac{\partial v}{\partial x} \in L^2(Vol); v|_{S_u} = 0\}$$

$$\tilde{V} = \{v | v \in L^2(Vol); \frac{\partial v}{\partial x} \in L^2(Vol); \frac{\partial^2 v}{\partial x^2} \in L^2(Vol^{(m)}); v|_{S_u} = 0\}$$

$$V_h = \{v_h | v_h \in L^2(Vol); \frac{\partial v_h}{\partial x} \in L^2(Vol); v_h \in Q_2(Vol^{(m)}); v_h|_{S_u} = 0\}$$

where $Q_2(Vol^{(m)})$ denotes the quadratic function of element m. $Vol^{(m)}$ is characterized by the element length h.

Introducing the variational formulation for the problem (B.1), the solution $\theta \in V$

is obtained from the following equation

$$\int_{Vol} (wv^*\theta_{,x} + w_{,x}\alpha^*\theta_{,x})\, dVol = \int_{Vol} wq\, dVol \qquad \forall w \in V \tag{B.2}$$

The finite element solution $\theta_h \in V_h$ of the problem (B.1) is obtained by solving the following equation

$$\int_{Vol} (w_h v^*\theta_{h,x} + w_{h,x}\alpha^*\theta_{h,x})\, dVol = \int_{Vol} w_h q\, dVol \qquad \forall w_h \in V_h \tag{B.3}$$

As is well-known, the solution shows oscillations as the Peclet number of the problem increases. To stabilize the solution, in our scheme, we add the high-order derivative artificial diffusion term

$$\sum_m \int_{Vol^{(m)}} w_{h,xx}\, \alpha^t\, \theta_{h,xx}\, dVol^{(m)} \tag{B.4}$$

and obtain

$$\begin{aligned} \int_{Vol} (w_h v^*\theta_{h,x} + w_{h,x}\alpha^*\theta_{h,x})\, dVol + \sum_m \int_{Vol^{(m)}} w_{h,xx}\, \alpha^t\, \theta_{h,xx}\, dVol^{(m)} \\ = \int_{Vol} w_h q\, dVol \qquad \forall w_h \in V_h \end{aligned} \tag{B.5}$$

where α^t is the artificial diffusion, $\alpha^t = o(|v^*|h^3)$, and h is the element length. Note that the upwind term is applied on the element level since the second derivatives $w_{h,xx}$ and $\theta_{h,xx}$ cannot be integrated across the element boundaries.

Adding the high-order derivative artificial diffusion term modifies the original problem considered. Let us consider the consistency of the modified problem with respect to the original problem. The modified problem is to find $\tilde{\theta} \in \tilde{V}$ satisfying

$$\begin{aligned} \int_{Vol} (\tilde{w}v^*\tilde{\theta}_{,x} + \tilde{w}_{,x}\alpha^*\tilde{\theta}_{,x})\, dVol + \sum_m \int_{Vol^{(m)}} \tilde{w}_{,xx}\, \alpha^t\, \tilde{\theta}_{,xx}\, dVol^{(m)} \\ = \int_{Vol} \tilde{w}q\, dVol \qquad \forall \tilde{w} \in \tilde{V} \end{aligned} \tag{B.6}$$

The consistency of the modified problem with respect to the original problem in Eqn.

(B.2) follows because the upwind term vanishes as $h \to 0$ and also the extra constraint in the space definition ($\tilde{V}$) disappears as $h \to 0$. So, we have that $\tilde{\theta} \to \theta$ as $h \to 0$. The consistency of the modified finite element problem in Eq. (B.5) with respect to the original finite element problem in Eq. (B.3) also follows.

To prove that the upwind term stabilizes the solution, we establish an error bound. Consider the consistency condition of the modified problem,

$$\begin{aligned}\int_{Vol}\{w_h v^*(\tilde{\theta}-\theta_h)_{,x} \;&+\; w_{h,x}\alpha^*(\tilde{\theta}-\theta_h)_{,x}\}dVol \\ &+ \sum_m \int_{Vol^{(m)}} w_{h,xx}\;\alpha^t\;(\tilde{\theta}-\theta_h)_{,xx}\;dVol^{(m)} = 0 \qquad \forall w_h \in V_h\end{aligned} \tag{B.7}$$

where $\tilde{\theta}$ is the exact solution of the modified problem.

However, also for any $w_h \in V_h$, we have

$$\begin{aligned}\int_{Vol}(w_h v^* w_{h,x} + w_{h,x}\alpha^* w_{h,x})dVol + \sum_m \int_{Vol^{(m)}} w_{h,xx}\;\alpha^t\;w_{h,xx}\;dVol^{(m)} &= \alpha^*|w_h|_1^2 + \alpha^t|w_h|_2^2 \\ &\geq (\alpha^* + \frac{\alpha^t}{c_1 h^2})|w_h|_1^2\end{aligned} \tag{B.8}$$

where we have used the following inequality

$$|w_h|_1^2 \leq c_1 h^2 |w_h|_2^2$$

with c_1 a constant independent of h. The above inequality holds when $meanvalue((w_h)_x) = 0$. With $w_h = \theta_h - v_h$, $v_h \in V_h$ and $meanvalue((\theta_h)_x - (v_h)_x) = 0$, eqn. (B.8) becomes

$$\begin{aligned}(\alpha^* + \frac{\alpha^t}{c_1 h^2})|\theta_h - v_h|_1^2 \;&\leq\; \int_{Vol}\{(\theta_h - v_h)v^*(\theta_h - v_h)_{,x} + (\theta_h - v_h)_{,x}\;\alpha^*(\theta_h - v_h)_{,x}\}\;dVol \\ &\quad + \sum_m \int_{Vol^{(m)}}(\theta_h - v_h)_{,xx}\;\alpha^t(\theta_h - v_h)_{,xx}\;dVol^{(m)} \\ &= \int_{Vol}\{-(\theta_h - v_h)_{,x}v^*(\tilde{\theta} - v_h) + (\theta_h - v_h)_{,x}\;\alpha^*(\tilde{\theta} - v_h)_{,x}\}\;dVol \\ &\quad + \sum_m \int_{Vol^{(m)}}(\theta_h - v_h)_{,xx}\;\alpha^t(\tilde{\theta} - v_h)_{,xx}\;dVol^{(m)} \qquad \text{(B.9)} \\ &\leq |v^*||\theta_h - v_h|_1\|\tilde{\theta} - v_h\|_{L^2} + \alpha^*|\theta_h - v_h|_1|\tilde{\theta} - v_h|_1\end{aligned}$$

$$+ \alpha^t |\theta_h - v_h|_2 |\tilde{\theta} - v_h|_2$$

where we have used eqn. (B.7) and integration by parts on the convective term. Also, we have the following inequality

$$\|\tilde{\theta} - v_h\|_{L^2} \leq c_2 h |\tilde{\theta} - v_h|_1 \tag{B.10}$$

and the inverse estimates, (see Ciarlet [54], pp. 140-146)

$$\begin{aligned} |\theta_h - v_h|_2 &\leq \frac{c_3}{h} |\theta_h - v_h|_1 \\ |\tilde{\theta} - v_h|_2 &\leq \frac{c_4}{h} |\tilde{\theta} - v_h|_1 \end{aligned} \tag{B.11}$$

where c_2, c_3, c_4 are constants independent of h. Hence we have

$$\begin{aligned} (\alpha^* + \frac{\alpha^t}{c_1 h^2}) |\theta_h - v_h|_1^2 &\leq c_2 |v^*| h |\theta_h - v_h|_1 |\tilde{\theta} - v_h|_1 + \alpha^* |\theta_h - v_h|_1 |\tilde{\theta} - v_h|_1 \\ &+ \frac{c_5 \alpha^t}{h^2} |\theta_h - v_h|_1 |\tilde{\theta} - v_h|_1 \end{aligned} \tag{B.12}$$

where $c_5 = c_3 c_4$. After simplifying the equation, we obtain

$$|\theta_h - v_h|_1 \leq \left[\frac{c_2 |v^*| h + \alpha^* + \frac{c_5 \alpha^t}{h^2}}{\alpha^* + \frac{\alpha^t}{c_1 h^2}} \right] |\tilde{\theta} - v_h|_1 \tag{B.13}$$

Hence we have the following error bound

$$\begin{aligned} |\tilde{\theta} - \theta_h|_1 &= |\tilde{\theta} - v_h + v_h - \theta_h|_1 \\ &\leq |\tilde{\theta} - v_h|_1 + |\theta_h - v_h|_1 \\ &\leq |\tilde{\theta} - v_h|_1 + \left[\frac{c_2 |v^*| h + \alpha^* + \frac{c_5 \alpha^t}{h^2}}{\alpha^* + \frac{\alpha^t}{c_1 h^2}} \right] |\tilde{\theta} - v_h|_1 \\ &\leq \left[1 + \frac{c_2 |v^*| h + \alpha^* + \frac{c_5 \alpha^t}{h^2}}{\alpha^* + \frac{\alpha^t}{c_1 h^2}} \right] |\tilde{\theta} - v_h|_1 \end{aligned} \tag{B.14}$$

When $\alpha^* \to 0$, the Peclet number goes to infinity and the error bound becomes

$$
\begin{aligned}
|\tilde{\theta} - \theta_h|_1 &\leq \left[1 + \frac{c_2|v^*|h + \frac{c_5\alpha^t}{h^2}}{\frac{\alpha^t}{c_1h^2}}\right] |\tilde{\theta} - v_h|_1 \\
&\leq \left[1 + c\frac{|v^*|h^3 + \alpha^t}{\alpha^t}\right] |\tilde{\theta} - v_h|_1
\end{aligned}
\tag{B.15}
$$

where c is a constant independent of h. We see that as the Peclet number increases to infinity, the term in the bracket does not grow to infinity, and the α^t term stabilizes the solution. Also, in order for the term in the bracket to be well-behaved and to have the best convergence for the solution, we must have that $\alpha^t = o(|v^*|h^3)$. The seminorm $|\tilde{\theta} - v_h|_1$ can now be bounded by standard interpolation results.

Finally, as $h \to 0$, $\tilde{\theta} \to \theta$ and from eqn. (B.15) we have that for all $v_h \in V_h$ and $meanvalue((\theta_h)_x - (v_h)_x) = 0$

$$
|\theta - \theta_h|_1 \leq \left[1 + c\frac{|v^*|h^3 + \alpha^t}{\alpha^t}\right] |\theta - v_h|_1 \tag{B.16}
$$

which bounds the finite element solution to the exact solution of the original problem as the Peclet number goes to infinity. The constraint condition for the weighting function v_h such that $meanvalue((\theta_h)_x - (v_h)_x) = 0$ is due to the high-order derivative in the stabilizer term, the upwinding term.

Appendix C

Lagrange multiplier method to impose temperature

The purpose of this appendix is to study the use of the Lagrange multiplier method in imposing the temperature constraint on the wall. Assume S_w is the boundary where the wall with prescribed temperature is applied. From the constitutive relation, we have the temperature relation to be imposed at node k in S_w

$$\begin{aligned} c_v \theta &= E - \frac{1}{2} v_l^2 \\ &= \frac{\rho E}{\rho} - \frac{1}{2} \frac{(\rho v_l)^2}{\rho^2} \end{aligned}$$

At the wall, we have $v_l = 0$ so that the constraint equation to impose the temperature θ_c is

$$c_v \theta_c (\rho) - (\rho E) = 0$$

In the matrix form, the constraint equation can be written as

$$\mathbf{B} \mathbf{U}_k = 0$$

where $\mathbf{B} = [c_v \theta_c, 0, 0, -1]$ and $\mathbf{U}_k^T = [\rho, \rho v_1, \rho v_2, \rho E]$ is the nodal solution at node k. The Lagrange multiplier method to impose the temperature constraint is formulated as

$$\begin{bmatrix} \mathbf{K}_k & \mathbf{B}^T \\ \mathbf{B} & 0 \end{bmatrix} \begin{bmatrix} \mathbf{U}_k \\ \lambda_k \end{bmatrix} = \begin{bmatrix} \mathbf{R}_k \\ 0 \end{bmatrix} \tag{C.1}$$

where $\mathbf{K}_k$ is the original coefficient matrix corresponding to $\mathbf{U}_k$, and $\mathbf{R}_k$ is the original loading vector corresponding to $\mathbf{U}_k$. The variable λ is the Lagrange multiplier variable. Let's study closely the construction of the matrix $\mathbf{K}_k$. The first line in the matrix $\mathbf{K}_k$ is corresponding to the coefficients obtained from the mass conservation equation. The modified equation with the Lagrange multiplier corresponding to the first line of the matrix $\mathbf{K}_k$ is

$$\mathbf{K}_k(\text{first line})\ \mathbf{U}_k + c_v \theta_c \lambda_k = \mathbf{R}_k(\text{first line})$$

We see that the Lagrange multiplier contributes to the mass conservation equation as a negative mass source at node k. Therefore, prescribing the temperature using a Lagrange multiplier is not desirable since it effects the mass conservation equation.

On the other hand, the fourth line of the matrix $\mathbf{K}_k$ corresponds to the coefficients obtained from the energy conservation equation. We have

$$\mathbf{K}_k(\text{fourth line})\ \mathbf{U}_k - \lambda_k = \mathbf{R}_k(\text{fourth line})$$

where we see that the Lagrange multiplier variable contributes to the energy conservation equation as an energy source at node k. This is physically reasonable since when we impose the temperature at node k, we need to put some energy into the node and λ_k is the magnitude of the energy needed to obtain the prescribed temperature.

Appendix D

A factor in the upwind term

The objective in this appendix is to show how we determine the value of the factor in the upwinding in eqn. (3.10).

Consider the following one-dimensional problem

$$\begin{aligned} v^*\theta_{h,x} - \alpha^*\theta_{h,xx} &= 0 \qquad\qquad \text{in} \qquad 0 < x < 1 \\ \theta_h(0) = \theta_h(1) &= 0 \end{aligned} \tag{D.1}$$

where θ, α^*, v^*, are temperature, diffusivity and constant velocity. The variables v^* and α^* are given for the problem and we want to solve for θ. We introduce the finite element space for quadratic element

$$V_h = \{v_h | v_h \in L^2(Vol); \frac{\partial v_h}{\partial x} \in L^2(Vol); v_h \in Q_2(Vol^{(m)}); v_h|_{S_u} = 0\}$$

where $Q_2(Vol^{(m)})$ denotes the quadratic function of element m. $Vol^{(m)}$ is characterized by the element length h.

Introducing the variational formulation for the problem (D.1) and adding the high-order derivative artificial diffusion in the same form as in eqn. (3.10), the solution

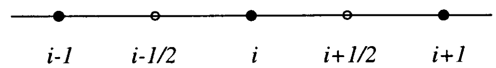

Figure D-1: Nodal numbering in a uniform mesh.

$\theta_h \in V_h$ is obtained from the following equation

$$\int_{Vol} (w_h v^* \theta_{h,x} + w_{h,x} \alpha^* \theta_{h,x})\, dVol + \sum_m \int_{Vol^{(m)}} w_{h,xx}\, \alpha^t\, \theta_{h,xx}\, dVol^{(m)} = 0 \qquad \forall w_h \in V_h \tag{D.2}$$

where α^t is the artificial diffusion, $\alpha^t = o(|v^*|h^3)$, and h is the element length. Note that the upwind term is applied on the element level since the second derivatives $w_{h,xx}$ and $\theta_{h,xx}$ cannot be integrated across the element boundaries.

Considering the extreme condition such that $\alpha^* \to 0$ (Peclet number $\to \infty$), we have

$$\int_{Vol} w_h v^* \theta_{h,x}\, dVol + \sum_m \int_{Vol^{(m)}} w_{h,xx}\, \alpha^t\, \theta_{h,xx}\, dVol^{(m)} = 0 \qquad \forall w_h \in V_h \tag{D.3}$$

For a uniform mesh as shown in fig. D-1, we have the stencil equations

for node i:

$$(\frac{1}{6}v^* + 16\frac{\alpha^t}{h^3})\theta_{i-1} + (-\frac{2}{3}v^* - 32\frac{\alpha^t}{h^3})\theta_{i-\frac{1}{2}} + (32\frac{\alpha^t}{h^3})\theta_i + (\frac{2}{3}v^* - 32\frac{\alpha^t}{h^3})\theta_{i+\frac{1}{2}} + (-\frac{1}{6}v^* + 16\frac{\alpha^t}{h^3})\theta_{i+1} = 0 \tag{D.4}$$

for node $i - \frac{1}{2}$:

$$(-\frac{2}{3}v^* - 32\frac{\alpha^t}{h^3})\theta_{i-1} + (64\frac{\alpha^t}{h^3})\theta_{i-\frac{1}{2}} + (\frac{2}{3}v^* - 32\frac{\alpha^t}{h^3})\theta_i = 0 \tag{D.5}$$

for node $i + \frac{1}{2}$:

$$(-\frac{2}{3}v^* - 32\frac{\alpha^t}{h^3})\theta_i + (64\frac{\alpha^t}{h^3})\theta_{i+\frac{1}{2}} + (\frac{2}{3}v^* - 32\frac{\alpha^t}{h^3})\theta_{i+1} = 0 \tag{D.6}$$

where θ_i denotes the value of θ at node i, etc.

Eliminating the $\theta_{i-\frac{1}{2}}$ and $\theta_{i+\frac{1}{2}}$ terms in eqn. (D.4) by using eqns. (D.5) and (D.6), we have

$$
\begin{aligned}
\{(64\frac{\alpha^t}{h^3})(\frac{1}{6}v^* + 16\frac{\alpha^t}{h^3}) - (-\frac{2}{3}v^* - 32\frac{\alpha^t}{h^3})^2\}\theta_{i-1} & \\
+\{(32\frac{\alpha^t}{h^3})(64\frac{\alpha^t}{h^3}) - 2(\frac{2}{3}v^* - 32\frac{\alpha^t}{h^3})(-\frac{2}{3}v^* - 32\frac{\alpha^t}{h^3})\}\theta_i & \\
+\{(64\frac{\alpha^t}{h^3})(-\frac{1}{6}v^* + 16\frac{\alpha^t}{h^3}) - (\frac{2}{3}v^* - 32\frac{\alpha^t}{h^3})^2\}\theta_{i+1} &= 0 \qquad \text{(D.7)}
\end{aligned}
$$

Using the same form of the artificial diffusion definition as in eqn. (3.11), we have

$$\alpha^t = c(|\frac{\partial x}{\partial r}|)^3|v^*|$$

and for a uniform mesh, $|\frac{\partial x}{\partial r}| = \frac{h}{2}$, therefore we have

$$\alpha^t = c(\frac{h}{2})^3|v^*|$$

To determine the value of c, we impose full upwinding to eqn. (D.7) so that when $v^* > 0$ ($\alpha^t = c(\frac{h}{2})^3 v^*$), the coefficient in front of θ_{i+1} should be zero,

$$\{(64\frac{\alpha^t}{h^3})(-\frac{1}{6}v^* + 16\frac{\alpha^t}{h^3}) - (\frac{2}{3}v^* - 32\frac{\alpha^t}{h^3})^2\} = 0$$

$$\{(8cv^*)(-\frac{1}{6}v^* + 2cv^*) - (\frac{2}{3}v^* - 4cv^*)^2\} = 0$$

$$v^{*2}(-\frac{8}{6}c + 16c^2 - \frac{4}{9} + \frac{16}{3}c - 16c^2) = 0$$

solving for c, we have

$$c = \frac{1}{9}$$

Similarly, when $v^* < 0$ ($\alpha^t = -c(\frac{h}{2})^3 v^*$), the coefficient in front of θ_{i-1} should be zero,

$$\{(64\frac{\alpha^t}{h^3})(\frac{1}{6}v^* + 16\frac{\alpha^t}{h^3}) - (-\frac{2}{3}v^* - 32\frac{\alpha^t}{h^3})^2\} = 0$$

$$\{(-8cv^*)(\frac{1}{6}v^* - 2cv^*) - (-\frac{2}{3}v^* + 4cv^*)^2\} = 0$$

$$v^{*2}(-\frac{8}{6}c + 16c^2 - \frac{4}{9} + \frac{16}{3}c - 16c^2) = 0$$

solving for c, we have

$$c = \frac{1}{9}$$

Therefore we use $c = \frac{1}{9}$ in eqn. (3.11).

Bibliography

[1] Hirsch C. *Numerical Computation of Internal and External Flows Vol. 1* . John Wiley and Sons, 1988.

[2] Hirsch C. *Numerical Computation of Internal and External Flows Vol. 2* . John Wiley and Sons, 1990.

[3] Idelsohn S.R. and Onate E. Finite volumes and finite elements: two 'good friends'. *Inter. J. for Num. Methods in Engrg*, 37:3323–3341, 1994.

[4] Zhu J. On the higher-order bounded discretization schemes for finite volume computations of incompressible flows. *Comput. Methods Appl. Mech. Engrg*, 98:345–360, 1992.

[5] Bathe K.J. *Finite element procedures.* Prentice Hall, 1996.

[6] Bathe K.J., Zhang H. and Zhang X. Some advances in the analysis of fluid flows. *Computers and Structures*, 64:909–930, 1997.

[7] Bathe K.J., Zhang H. and Wang M.H. Finite element analysis of incompressible and compressible fluid flows with free surfaces and structural interations. *Computers and Structures*, 56:193–213, 1995.

[8] Lyra P.R.M., Morgan K., Peraire J. and Peiro J. TVD algorithms for the solution of the compressible Euler equations on unstructured meshes. *Inter. J. for Num. Methods in Fluids*, 19:827–847, 1994.

[9] Fortin M., Manouzi H. and Soulaimani A. On finite element approximation and stabilization methods for compressible viscous flows. *Inter. J. for Num. Methods in Fluids*, 17:477–499, 1993.

[10] Soulaimani A. and Fortin M. Finite element solution of compressible viscous flows using conservative variables. *Comput. Methods Appl. Mech. Engrg*, 118:319–350, 1994.

[11] Almeida R.C. and Galeao A.C. An adaptive Petrov-Galerkin formulation for the compressible Euler and Navier-Stokes equations. *Comput. Methods Appl. Mech. Engrg*, 129:157–176, 1996.

[12] Luo H., Baum J.D., Löhner R. and Cabello J. Implicit schemes and boundary conditions for compressible flows on unstructured grids. *AIAA paper 94-0816*, 1994.

[13] Beau G.J.L., Ray S.E., Aliabadi S.K. and Tezduyar T.E. SUPG finite element computation of compressible flows with the entropy and conservation variables formulations. *Comput. Methods Appl. Mech. Engrg*, 104:397–422, 1993.

[14] Shapiro R.A. *Adaptive finite element solution algorithm for the Euler equations.* Notes on numerical fluid mechanics v.32, Vieweg, 1991.

[15] Chakravarthy S.R. Euler equations - Implicit schemes and boundary conditions. *AIAA journal*, 21:699–706, 1983.

[16] Demkowicz L., Oden J.T., Rachowicz W. and Hardy O. An h-p Taylor-Galerkin finite element method for compressible Euler equations. *Comput. Methods Appl. Mech. Engrg*, 88:363–396, 1991.

[17] Demkowicz L., Oden J.T., Rachowicz W. and Hardy O. Toward a universal $h-p$ adaptive finite element strategy, part 1. Constrained approximation and data structure. *Comput. Methods Appl. Mech. Engrg*, 77:79–112, 1989.

[18] Oden J.T., Demkowicz L., Rachowicz W. and Westermann L. A posteriori error analysis in finite elements: The element residual method for symmetrizable problems with applications to compressible Euler and Navier-Stokes equations. *Comput. Methods Appl. Mech. Engrg*, 82:183–203, 1990.

[19] Tworzydlo W.W., Oden J.T. and Thornton E.A. Adaptive implicit/explicit finite element method for compressible viscous flows. *Comput. Methods Appl. Mech. Engrg*, 95:397–440, 1992.

[20] Brooks A.N. and Hughes T.J.R. Streamline upwind/Petrov-Galerkin formulations for convection dominated flows with particular emphasis on the incompressible Navier-Stokes equations. *Comput. Methods Appl. Mech. Engrg*, 32:199–259, 1982.

[21] Hughes T.J.R. and Mallet M. A new finite element formulation for computational fluid dynamics: III. The generalized streamline operator for multidimensional advective-diffusive systems. *Comput. Methods Appl. Mech. Engrg*, 58:305–328, 1986.

[22] Donea J. A generalized Galerkin method for steady convection-diffusion problems with application to quadratic shape function elements. *Comput. Methods Appl. Mech. Engrg*, 48:25–43, 1985.

[23] Codina R., Oñate E. and Cervera M. The intrinsic time for the streamline upwind/Petrov-Galerkin formulation using quadratic elements. *Comput. Methods Appl. Mech. Engrg*, 94:239–262, 1992.

[24] Hill D.L. and Baskharone E.A. A monotone streamline upwind method for quadratic finite elements. *Inter. J. Num. Methods in Fluids*, 17:463–475, 1993.

[25] DeBlois B.M. Quadratic, streamline upwinding for finite element method solution to 2-D convective transport problems. *Comput. Methods Appl. Mech. Engrg*, 134:107–115, 1996.

[26] Jiang B.N. and Carey G.F. Least-squares finite element methods for compressible Euler equations. *Inter. J. for Num. Methods in fluids*, 10:557–568, 1990.

[27] Leonard B.P. The ULTIMATE conservative difference scheme applied to unsteady one-dimensional advection. *Comput. Methods Appl. Mech. Engrg*, 88:17–74, 1991.

[28] Brezzi F. and Bathe K.J. A discourse on the stability conditions for mixed finite element formulations. *Comput. Methods Appl. Mech. Engrg*, 82:27–57, 1990.

[29] Brezzi F. and Fortin M. *Mixed and hybrid finite element methods.* Springer, Berlin, 1995.

[30] Chapelle D. and Bathe K.J. The Inf-sup Test. *Computers and Structures*, 47:537–545, 1993.

[31] Oden J.T. and Carey G.F. *Finite elements mathematical aspects.* Prentice-Hall, New Jersey, 1983.

[32] Mills A. F. *Heat Transfer* . Irwin, 1992.

[33] Hendriana D. and Bathe K.J. On a parabolic quadrilateral finite element for compressible flows. *submitted.*

[34] Warming R.F., Beam R.M. and Hyett B.J. Diagonalization and Simultaneous Symmetrization of Gas-Dynamics Matrices. *Mathematics of Computation*, 29:1037–1045, 1975.

[35] Hughes T.J.R. and Mallet M. A new finite element formulation for computational fluid dynamics: IV. A discontinuity-capturing operator for multidimensional advective-diffusive systems. *Comput. Methods Appl. Mech. Engrg*, 58:329–336, 1986.

[36] Shakib F., Hughes T.J.R. and Johan Z. A new finite element formulation for computational fluid dynamics: X. The compressible Euler and Navier-Stokes equations. *Comput. Methods Appl. Mech. Engrg*, 89:141–219, 1991.

[37] Chakravarthy S.K. Euler Equation-Implicit Schemes and Boundary Conditions. *AIAA Journal*, 21:699–706, 1983.

[38] Wang X. and Bathe K.J. Displacement/pressure based mixed finite element formulations for acoustic fluid-structure interaction problems. *Inter. J. for Num. Methods in Engrg*, 40:2001–2017, 1997.

[39] Roe P.L. Approximate Riemann Solvers, Parameter Vectors, and Difference Schemes. *Journal of Computational Physics*, 43:357–372, 1981.

[40] Glaister P. An approximate linearised Riemann solver for the three-dimensional Euler equations for real gases using operator splitting. *Journal of Computational Physics*, 77:361–383, 1988.

[41] Hassan O., Morgan K. and Peraire J. An Implicit Finite-Element Method for High-Speed Flows. *Internat. J. Numer. Methods Engrg.*, 32:183–205, 1991.

[42] Tworzydlo W.W., Oden J.T. and Thornton E.A. Adaptive Implicit/Explicit Finite Element Method for Compressible Viscous Flows. *Comput. Methods Appl. Mech. Engrg*, 95:397–440, 1992.

[43] Demkowicz L., Oden J.T., Rachowicz W. and Hardy O. An h-p Taylor-Galerkin Finite Element Method for Compressible Euler Equations. *Comput. Methods Appl. Mech. Engrg*, 88:363–396, 1991.

[44] Lindquist D.R. A comparison of numerical schemes on triangular and quadrilateral meshes. technical report, CFDL-TR-88-6, Computational fluid dynamics laboratory MIT, 1988.

[45] Hughes T.J.R., Franca L.P., Hulbert G.M., Johan Z. and Shakib F. The Galerkin/least-squares method for advective-diffusive equations. *Comput. Methods Appl. Mech. Engrg*, 73:173–189, 1989.

[46] Chapelle D. and Bathe K.J. Fundamental considerations for the finite element analysis of shell structures. *Computers and Structures*, 66:19–36, 1998.

[47] ADINA R&D, Inc., ADINA-F user manuals, Watertown, Massachusetts, 1996

[48] Lewis J.E., Kubota T. and Lees L. Experimental investigation of supersonic laminar, two-dimensional boundary-layer separation on a compression corner with and without cooling. *AIAA journal*, 6:7–14, 1968.

[49] Gyftopoulos E.P. and Beretta G.P. *Thermodynamics: Foundations and applications.* Macmillan, 1991.

[50] Droux J.J. and Hughes T.J.R. A boundary integral modification of the Galerkin least squares formulation for the Stokes problem. *Comput. Methods Appl. Mech. Engrg*, 113:173–182, 1994.

[51] Storti M., Nigro N. and Idelsohn S. Equal-order interpolations: a unified approach to stabilize the incompressible and advective affects. *Comput. Methods Appl. Mech. Engrg*, 143:317–331, 1997.

[52] Codina R. and Blasco J. A finite element formulation for the Stokes problem allowing equal velocity-pressure interpolation. *Comput. Methods Appl. Mech. Engrg*, 143:373–391, 1997.

[53] Hughes T.J.R., Franca L.P., and Hulbert G.M. A new finite element formulation for computational fluid dynamics: VIII. the Galerkin/least-squares method for advective-diffusive equations. *Comput. Methods Appl. Mech. Engrg*, 73:173–189, 1989.

[54] Ciarlet P.G. *The finite element method for elliptic problems.* North-Holland, Amsterdam, 1978.